Surface chemistry of colloidal semiconductor nanoparticles on graphitic substrates

A dissertation submitted to the University Autonoma of Madrid for the degree of physics science doctor

Fabiola Iacono

Thesis diretors:

Beatriz Hernández Juárez

Roberto Otero Martín

May 2013

To my family

Index

Summary 8

Chapter 1 10

General Introduction 10

1.1 Nanoparticles, carbon nanotubes and hybrid systems 10

Nanoparticles (NPs) 10

Carbon nanotubes (CNT) and Hybrid systems (HS) 12

1.2 The “Hot injection” method 13

CdSe NPs 14

CdSe-CNT hybrid system (CdSe-CNT HS) 14

1.3 Intra-particle and inter-particle ripening 16

Ripening in solution 16

Ripening on surface 17

1.4 Aim of this work 18

1.5 Content of this thesis 18

References 19

Chapter 2 21

Nanoparticle deposition techniques 21

2.1 Introduction 21

2.2 Langmuir Blodgett; theory and results 21

2.3 Convective assembly; theory and results 24

2.4 Electrospray; theory and results 29

2.4.1 Deposition of pyramidal CdSe NPs dispersed in chloroform 32

2.4.2 Deposition of CdSe/ZnS NPs dispersed in chloroform 36

2.4.3 Deposition of Au NPs dispersed in water 41

2.4.4 Comparison between the three samples 42
2.5 Pot-deposition of CdSe pyramidal NPs 43
2.6 Comparison between the four deposition methods 48
References 50
Chapter 3 51
Surface chemical characterization of rod-like and pyramidal CdSe NPs by means of XPS 51
3.1 Introduction 51
3.2 X-ray Photoelectron Spectroscopy (XPS) 52
3.3 Pyramids vs rod-like CdSe NPs 56
3.3.1 XPS results: photon energy of 1486,6 eV 58
Changes in elements composing the core: Se and Cd 59
Cl analysis 62
Changes in elements composing organic shell C, P and O 63
3.3.2. Synchrotron results: photon energy of 620 eV 68
Core elements analysis; Se and Cd 69
Cl analysis 70
Discussion 74
3.5 Conclusions 76
References 78
Chapter 4 79
Adhesion of pyramidal CdSe NPs to carbonaceous surfaces and heating treatments 79
4.1 Introduction 79
4.2 Cl per NPs versus coverage 79
SEM characterization 79
Comparison between a high and a low coverage sample 83
Role of polydispersity 87

The excess of Cl with respect to P 88
4.3 Heating treatments; STM and XPS results 89
STM measurements: a brief introduction 90
STM results 92
Discussion 97
High resolution XPS annealing analysis 98
Conclusions 102
References 104
Chapter 5 105
General conclusions 105
Chapter 6 107
Experimental part 107
6.1 Synthesis of nanoparticles and Hybrid System 107
Synthesis of CdSe rod-like NPs 108
Synthesis of CdSe pyramidal NPs 108
Synthesis of pyramidal CdSe NPs attached to CNTs hybrid system (CdSe-CNTs HS) 108
Synthesis of CdSe/ZnS colloidal nanoparticles 109
Langmuir Blodgett (LB) films 109
6.2 Sample characterization 109
Transmission electron microscopy (TEM) 109
Scanning electron microscopy (SEM) 109
Atomic force microscopy (AFM): 109
Ultra High Vacuum system (UHV): XPS and STM 110
6.3 Electrospray set-up 113
Electrospray allignment 115
Electrospray calibration 117

Annexes..... 118

1 Calculation of CdSe dispersion concentration used in convective assembling 118

2 Comparison between convective assembling of CdSe NPs using different dispersion concentrations..... 118

3 Electrospray experiment details 119

Pyramid CdSe NPs in chloroform..... 119

CdSe/ZnS NPs dispersed in chloroform 120

Deposition of Au NPs dispersed in water 120

Drops-jet operating regime 121

Spray-jet operating regime..... 121

List of publication 123

Acknowledgment..... 124

Summary

In the search of promising synergetic effects for future technological applications such as the generation of photocurrent in photovoltaics, the combination of semiconductor nanoparticles (or colloidal quantum dots) and graphitic surfaces such as those of carbon nanotubes has attracted considerable attention. The experimental results shown in this thesis are the outcome of combined work that includes both synthesis of nanomaterials (CdSe semiconductor nanoparticles, NPs) and surface chemical characterization when they are in contact to graphitic surfaces. The work has been carried out in chemical laboratories belonging to IMDEA Nanoscience and Universidad Autónoma of Madrid and in the Surface Science Laboratory at the Universidad Autónoma of Madrid (LASUAM).

From the synthetic point of view it has been confirmed that little variations in the amount of a chlorinated co-solvent added during the synthesis of CdSe NPs lead to chemical and morphological changes on the NPs, modifying their shape from rod-like to pyramidal. Furthermore, if a graphitic surface is added to the synthetic mixture (such as highly oriented pyrolytic graphite (HOPG) or carbon nanotubes, once the NPs acquire the pyramidal shape they are prone to decorate graphitic surfaces in contrast to rod-like NPs, which do not show this tendency.

The main part of this work has focused on the elucidation of the CdSe NPs surface in contact to graphitic surfaces, in particular to HOPG. CdSe NPs composed of an inorganic core covered by organic molecules (the so-called ligand shell) have been analyzed mainly by X-ray photoelectron spectroscopy (XPS). XPS analysis confirms the presence of two different phosphorous chemical environments on the NPs surface, which have been assigned to two different organic ligands (molecules) capping the NPs surface. It has been elucidated that the final morphology of the NPs depends not only on the concentration of these molecules but also on the ratio between them and the presence of chlorine on the surface. Correlated Scanning Electron Microscopy and XPS studies allow extracting information about the role of the chlorinated co-solvent during the synthesis of the NPs and their effect in the interaction to graphitic surfaces. In particular, if the synthetic process takes place in the absence chlorinated co-solvents, both P-containing species co-exists on the surface leading to the production of rod-like NPs. If the process takes place in the presence of the chlorinated co-solvent partial and selective displacement of one of the P-environments occurs, boosting the shape transformation and further interaction to the graphitic surfaces. This knowledge allows obtaining control over the coverage and monodispersity of CdSe NPs monolayer arrangements on graphitic surfaces.

Other methods to produce monolayer arrangements of NPs on surfaces have been studied and compared with the above mentioned approach. Among them, NP depositions by means Langmuir Blodgett, convective assembling and electrospray in high-vacuum conditions have been carried out.

Finally, morphological changes of pyramidal CdSe NPs on HOPG upon annealing treatments have been characterized by means of Scanning Tunneling Microscopy (STM) along with correlated high resolution XPS analysis. These studies point to several mechanisms taking place either in individual NPs (intra-particle ripening) or among NPs (inter-particle ripening) depending on the temperature. The former mechanism taking place at relatively low temperature yields a shape relaxation of the NPs while mass transfer occurs during the second one taking place at temperatures above 150°C. A correlation between the desorpted species from the NPs surface and the subsequent ripening process has been established.

Chapter 1

General Introduction

During the last decades the emerging area of nanoscience has attracted great attention from researchers all over the world. With contributions from Chemistry, Physics, Biology and Material science, this area of research offers very interesting challenges in many fields for modern technological applications like solar energy conversion, optoelectronic devices, molecular and cellular imaging as well as ultrasensitive detection.

In particular, nanoparticle research has developed into one of the major fields in modern science. Efforts in synthetic activities during the last two decades have allowed gaining knowledge on the reactivity and spectroscopic features of these fascinating materials. A deep knowledge of the properties of nano-objects like semiconductor nanoparticles, carbon nanotubes and hybrid systems composed by combinations of such nano-sized material yields control over synergetic effects that turn to be promising for future technological applications.

1.1 Nanoparticles, carbon nanotubes and hybrid systems

Nanoparticles (NPs)

The basis of nanoparticle research was established by studies of photocatalysis and artificial water splitting in the early 1980´s (Ref 1). Almost at the same time, one of the first determinant steps of the history of nanoscience was published in the work of L. Brus (Ref 2) and A. Efros (Ref 3 and 4). In these works the optical properties of semiconductor crystals of a few nanometers in size was investigated either in colloidal suspension or embedded in a dielectric matrix. Two extremely interesting results were found that must be interpreted as a consequence of the quantum confinement effect: the shift to smaller wavelengths of the semiconductor optical absorption edge with decreasing particle size, and the generation of discrete peaks in the absorption spectra. These two phenomena can be explained trough the model of a “particle in a box” where the confinement of a particle with mass m leads to discrete energy levels E_n such as

$$E_n = \frac{\hbar^2 \pi^2}{2mL^2} n^2$$

equation 1

where L is the length of the box. Hence, these nanocrystals or nanoparticles (NPs) with typical sizes is in the range of 1-100 nm, represent the perfect link between isolated atoms and/or small molecules and bulk materials, reason why they are often called artificial atoms. Note that equation 1 shows that as L decreases, the energy of the first level increases as well as the difference between adjacent levels E_{n+1} and E_n. This leads to a higher separation between the energy levels for minor sizes. In the case of spherical semiconductor NPs a similar expression is used, the so-called Brus equation, which describes the dependency of the band-gap with the radius R of the NP (Ref 2)

$$E = E_g + \frac{\hbar^2\pi^2}{2\mu_{ex}R^2} - \frac{1.786\ e^2}{\varepsilon R}$$

equation 2

where μ_{ex} is the effective mass of the exciton, that is the quantum particle describing the interaction between a state of an excited electron in the conduction band and the empty electron state left in the valence band (hole), ε is the dielectric constant and the last term is the Coulomb energy included to take into account the electron-hole interaction. The dependency of the energy band gap with the NPs radius R allows tuning the optical properties, absorption and luminescence, over a wide spectral range by simply varying the size of the NPs. An example of colloidal cadmium selenide (CdSe) spherical NPs of different sizes under UV excitation is shown in figure 1.

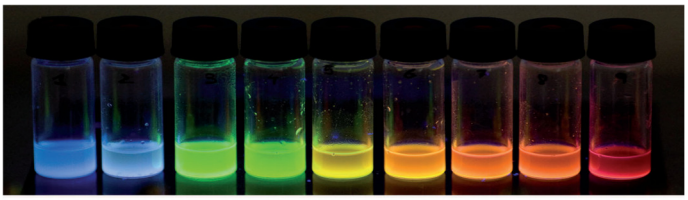

Fig 1. Colloidal suspensions of luminescent CdSe NPs with sizes from approximately 2 to 7 nm (from left to right) under UV excitation (Ref 5).

The optical properties, however, are not determined only by the size of the NPs, in fact, shape and surface composition also play a role. Researchers have investigated the properties of NPs with shapes different from spherical such as nanorods and nanotetrapods (Ref 6). Furthermore, the chemical surface composition also determines the optical and electronic properties of semiconductor NPs in a great extent. In the case of colloidal NPs it is possible to cover the core (i.e CdSe) with a shell of atomic layers of other semiconducting material. Covering the CdSe NPs with a shell of a higher band-gap material (such as CdS or ZnS) generates a so-called type I structure (Ref 7), where the wave-function of electrons and holes are both localized in the core material. It was found that the presence of this shell improves the efficiency of these NPs as light emitters (see Ref 5 and 8). This strategy minimizes traps in the interface, which are

electronic states generated by reticular defects where the periodic potential of the crystal is perturbed. The removal of the traps decreases the non-radiative paths for relaxation, increasing the probability of exciton recombination in the core, thus increasing the optical efficiency - quantum yield - (Ref 9 and 10) The coverage of the core material with semiconductor materials in which, either the valence band edge or the conduction band edge lies within the band gap of the core, results in a staggered band alignment that leads to a spatial separation of electron and hole upon excitation in the different regions (core or shell). In these so-called type II structure NPs, charge carriers must cross the core-shell interface for radiative recombination, what leads to a relatively long carrier lifetimes compared to type I structures (Ref 11 and 12).

Carbon nanotubes (CNT) and Hybrid systems (HS)

CNTs consist of layers of graphene rolled up forming tube like structures. These cylindrical carbon structures have novel properties that make them potentially useful in many applications in optoelectronics (Ref 13). They exhibit extraordinary strength, efficient thermal conductance and unique electrical properties. In fact, thanks to the overlapping of the π orbitals conjugated structure of carbon-sp^2, electrons can travel through the CNTs without scattering (balistically) (Ref 14). Figure 2 schematizes this geometry.

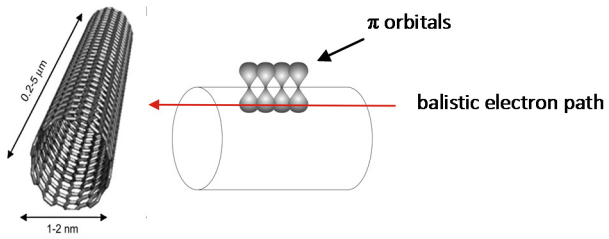

Fig 2. Single walled carbon nanotube and a scheme of its π orbitals symmetry that allows for the ballistic electron path.

CNTs can be produced in different geometries such as in multi - or single - layers depending on the number of concentric graphene layers rolled up (multiwalled MWCNTs or singlewalled SWCNTs respectively). MWCNTs exhibit a metallic behavior while SWCNTs can show either metallic or semiconducting behavior depending on the diameter of the tube and the "helicity", that is, the angle between the direction of the axis of the tube and a defined direction of the honeycomb graphene atomic structure (Ref 15).

A great challenge for the emergent nanotechnology is represented by hybrid nano-architectures based on the assembly of various types of NPs on CNTs. The synergistic properties derived from the possibility to combine CNTs and NPs (semiconducting,

metallic, magnetic, etc.) are of interest for several applications from field emission displays to energy conversion and storage devices, artificial muscles, molecular recognition (gas and vapour sensors for environmental) and also for specific medical applications *in vivo* imaging, drug delivery, and magnetic hyperthermia (Ref 16-22). In the case of semiconductor NPs, the generation of photocurrent by the injection of excited electrons into CNTs is possible. The key for the synergistic effects of NP-CNT combinations is expected to be dependent on the interactions between the components through the interface. Several physical and chemical methods to produce such kinds of hybrid systems have been developed including covalent and non-covalent assembly approaches (Ref 23, 24–28). Approaches including covalent functionalization (Ref 29 and 30) comprise aggressive methods (strong acid oxidization or plasma etching) that inevitably cause the damage of the CNTs structure affecting their electronic and mechanical properties. Thus, non-covalent functionalization is desirable.

In the following the synthetic method called "hot injection" that permits the growth of highly monodisperse semiconductor NPs will be introduced, making especial emphasis on the synthetic methodology that allows the simultaneous production of CdSe NPs suspension and CdSe NPs attached to CNTs non-covalently. The main effort of this thesis has been dedicated to the understanding of the surface and the interface chemistry of CdSe NPs interacting with Carbon-sp^2 (C-sp^2) lattices.

1.2 The "Hot injection" method

The so-called "hot injection" synthesis was introduced for the first time in 1993 by C. Murray, D. Norris and M. Bawendi with the publication of the organometallic synthesis of colloidal cadmium chalcogenide NPs (Ref 31). This method is based on the injection of an organometallic precursor into a hot coordinating organic solvent. According to the theory proposed by Lamer (Ref 32), under high monomer concentration conditions, a strong nucleation event produces small nuclei followed by a process of crystal growth. In the hot injection synthesis, the crystal growth can be stopped at any time allowing for the generation of NPs with the desired size (Ref 33). The separation between nucleation and growth is the main feature of this method and has been used to produce a huge variety of semiconductor NPs such as II-VI (CdSe, CdS, CdTe, ZnSe, ZnS, ZnO14), III-V (InP, AsGa, InAs) and IV-VI (PbS, PbSe, PbTe) (Ref 34).

In this chemical route organic molecules or surfactants that bind the surface of NPs are used. Hence, the resulting NPs are composed of an inorganic core covered by organic molecules forming the so-called ligand shell. The binding of the different surfactants to the NP surface occurs selectively to the different crystalline facets of the NPs depending on the chemical affinity between surfactants and the chemical composition of the facets (Ref 35). This favored binding generates preferential

crystalline growth directions allowing for the production of different NPs shapes. Furthermore, the role of these molecules also include the stabilization of the NPs in certain organic solvents avoiding agglomeration and the reduction of surface defects that generates localized states as surface traps cited above.

CdSe NPs

The synthesis of rod-shaped CdSe NPs was reported for the first time in 2000 (Ref 36) by using dimethyl cadmium, a dangerous organometallic compound, and a coordinating solvent composed by trioctylphosphine oxide (TOPO) and hexylphosphonic acid (HPA). In 2002 the synthesis of rod-shaped CdSe NPs using a less expensive and toxic compound, cadmium oxide (CdO), was reported (Ref 37). In this synthesis, a mixture of CdO and octadecylphosphonic acid (ODPA) in TOPO, the coordinating solvent is heated up before Se dissolved in trioctylphosphine (TOP) is injected. Upon Se in TOP injection, the nucleation starts followed by crystal growth and shape stabilization. By adding 1,2-dichloroethane (DCE) before injecting Se in TOP the result of the synthesis after 15-18 hours for shape stabilization leads to a different shaped NPs; pyramids instead of rods, as shown in figure 3. The presence of the chlorinated co-solvent changes the chemical composition of the surface and it is responsible for the shape change, as it will be discussed along the next chapters.

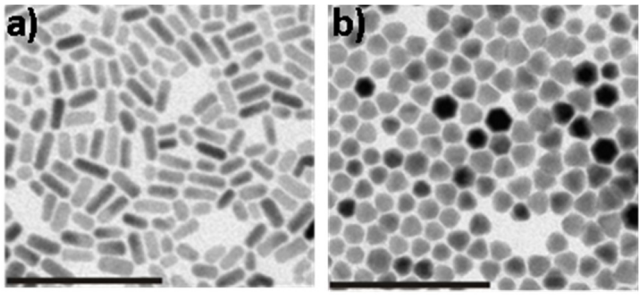

Fig 3. TEM images of rods-like CdSe NPs (a) and pyramidal CdSe NPs (b). Size reference bar 100 nm.

CdSe-CNT hybrid system (CdSe-CNT HS)

If during the synthesis described above a toluene dispersion of CNTs is added before injecting the Se in TOP solution, the process leads to a very interesting result; an hybrid system composed of pyramidal CdSe NPs attached to the surface of CNTs. Figure 4 (a) shows a TEM image of a bundle of pyramidal CdSe NPs–CNTs hybrid system (CdSe–CNT HS) and figure 4 (b) an individual SWCNT in which is possible to distinguish the NPs attached on its surface.

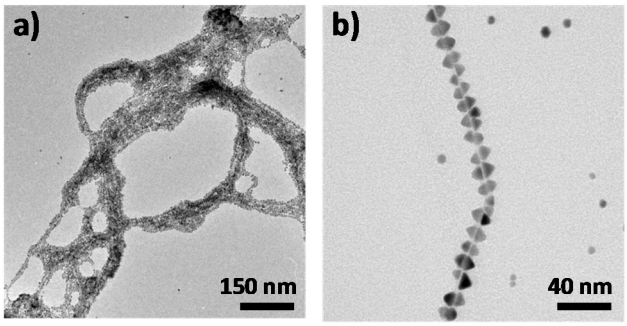

Fig 4. TEM image of a bundle of CdSe-CNTs HS (a). Individual CdSe-CNTs HS (b).

By means of Raman spectroscopy it was previously demonstrated that the C-sp^2 lattice of CNTs is not affected by this type of synthesis, that is, CNTs preserve their structural properties excluding oxidation of the CNT surface (Ref 38). It was also found that NPs are in close contact to the C-sp^2 lattice through the basal (000-1) Cd-rich facet of the NPs. As it was described in a previous work, the HS can work as a donor-acceptor (NP-CNT) couple in photovoltaic devices (Ref 39). Figure 5 depicts the change in the electrical response of the HS when it is exposed to visible light indicating a strong electronic coupling between the NPs and the CNTs.

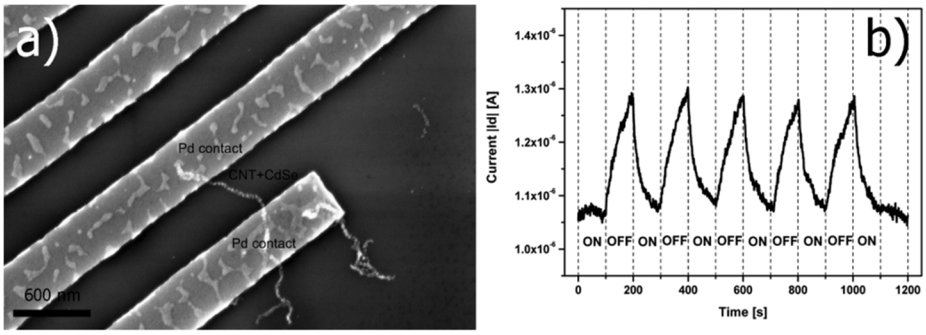

Fig 5. (a) SEM image of a CNT-CdSe HS placed in between two electrodes and (b) photoelectric response of the HS under visible radiation (Ref 39).

It is Important to mention that the attachment to the CNT walls, visible after approximately 18 hours of reaction, is not observed in the case of rods which are produced in absence of chlorine (Cl). Hence the presence of Cl may be related to the adhesion of NPs and CNTs (see Ref 39). Several questions remain opened, namely, whether Cl is incorporated in the C-sp^2 lattice or NPs surface or just triggering the interaction by a shape modification. These are questions that will be addressed during the course of this work. In order to understand the influence of Cl during the synthesis, one should take into account different phenomena taking place during the nucleation

and growth of NPs. In particular, the phenomena of intra-particle and inter-particle ripening have a crucial role in the production of NPs.

1.3 Intra-particle and inter-particle ripening

The term intra-particle ripening refers to the shape modification by atomic diffusion and surface reorganization of a given NP. In contrast, the term inter-particle ripening refers to a mechanism involving mass diffusion among several NPs. In general, the intra-particle ripening is responsible for the NP shape evolution and stabilization while, the inter-particle ripening may be responsible for both shape evolution and mainly polydispersity (the NP size distribution) within a NP sample. Both phenomena take place in solution during the synthesis of the NPs, and under certain conditions, on solid surfaces, that is, when the NPs are arranged on a substrate.

Ripening in solution

The resulting shape of CdSe NPs at the end of the growth process is related to the dynamic equilibrium between the species in solution and those in the vicinity of the NP, the so-called diffusion sphere shown in figure 6 (Ref 40). Such species include Cd and Se monomers, atoms, etc. When the concentration of species is high, the most reactive facets grow faster. In the case of CdSe NPs this growth yields to elongate NPs as a result of a 1D growth. When the concentration of species decreases, the diffusion of species on the NPs surface may take place, what modifies the shape from elongated to spherical. This process is called intra-particle ripening.

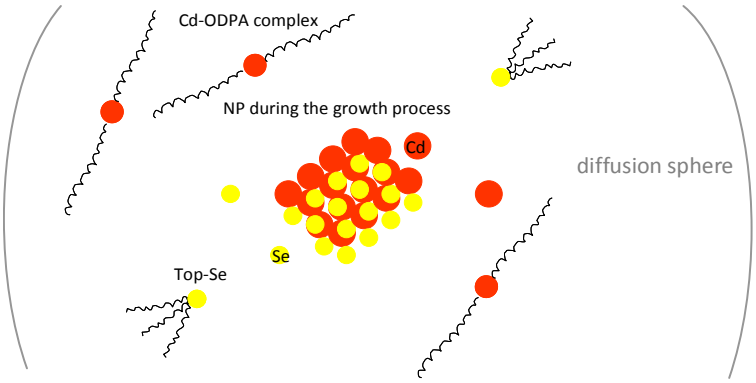

Fig 6. Scheme of NP and species within the diffusion sphere.

In those cases in which the concentration of species in solution is very low, the inter-particles ripening, also known as *Ostwald ripening* (Ref 41) is activated. By this mechanism smaller particles in solution dissolve and deposit on larger particles in order to reach a more thermodynamically stable state increasing the polydispersity. In

general, the polydispersity of a NP sample depends on how strongly the inter-particle ripening influences the growth of NPs. Hence, in order to produce highly monodisperse NP samples, the undesired effect caused by the inter-particle ripening should be minimized (Ref 42).

As it will be demonstrated along this work, the presence of Cl in the synthesis of CdSe rod-like NP produces those chemical modifications that activate an intra-particle ripening stage that leads to the pyramidal shape stabilization and, in some cases, it leads to the activation of the inter-particle ripening.

Ripening on surface

The results concerning the last part of this thesis show that, under certain annealing treatments, a modification in the morphology of NPs deposited on a surface takes place. In the same way it was referred to intra- and inter-particle ripening in solution, related phenomena can be found when studying NPs grown by approaches such as molecular beam epitaxy (MBE) and chemical vapor deposition (CVD). In these cases and, as schematized in figure 8, the growth of films composed by adsorbed gas phase atoms on a substrate can be classified in three modes: Frank-van der Merwe or 2D growth, Volmer-Weber or 3D growth and Stranski-Krastanov mode that is the intermediate case where a 2D layer reaches a critical thickness for which a transition from 2D to 3D growth occurs (Ref 43). Volmer-Weber and Stranski-Krastanov modes are largely used to nucleate metal and semiconductor NPs directly on a substrate. In the case of Stranski-Krastanov mode, a 2D layer of adsorbed atoms, the so-called wetting layer (WL), remains after NPs nucleation as indicated in figure 8.

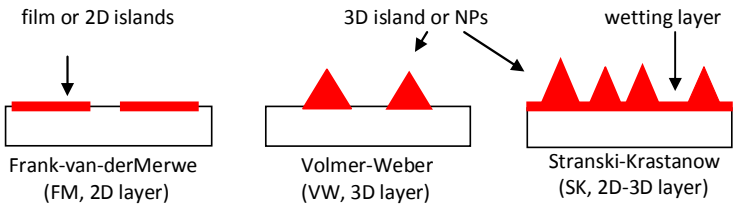

Fig 8. Scheme of the three modes for metal and semiconductor islands growth.

Ripening has been observed mainly for the 2D case (Ref 44) and scarcely for the 3D case. A phenomenon that was attributed to surface ripening was observed for post-nucleated Ge NPs on Si (VW mode) upon annealing treatments; atoms composing the NPs detach and diffuse along the substrate leading the NP shape to evolve toward a more stable configuration (shape relaxation) and to an increase in the polydispersion (Ref 45). Regarding NPs grown by SK modes (presence of WL), a post-nucleation Ostwald ripening have been reported for semiconductor InAs NPs grown on GeAs (001).

The changes in the WL morphology indicate a NP-NPs mass transport via WL providing the direct prove of the NP ripening process (Ref 46).

Considering what have been said above, the phenomena observed in this work can be actually ascribed to similar cases of surface ripening previously observed.

1.4 Aim of this work

The principal aim of this thesis is to study the surface chemistry of CdSe NPs attached to C-sp^2 lattices by surface science techniques. For this purpose, a suitable arrangement of the sample on a conductive substrate is mandatory. Hence, to obtain a suitable system to perform XPS and STM characterization, special emphasis has been given to the deposition method of NPs on C-sp^2 surfaces. For this purpose, various NPs deposition techniques (such as Langmuir-Blodgett, controlled solvent evaporation, etc.) attracting great interest for the preparation of NPs films have been examined and compared. As a result of this work a model system was found. This system, composed of monolayers of CdSe pyramidal NPs tightly arranged on HOPG substrates with controlled coverage degrees, allows acquiring information not only from the interaction of the NPs to the C-sp^2 but also from the surface chemistry of the NPs.

1.5 Content of this thesis

Chapter 2 is dedicated to the different deposition techniques employed to obtain homogeneous NPs arrangements and the comparison among them in terms of coverage.

In chapter 3 the XPS characterization of pyramidal and rod-like CdSe NPs will be introduced, where differences in the chemical surface of the NPs produced by adding DCE into the reaction will be elucidated.

A SEM and XPS study of several samples of pyramidal CdSe NPs on HOPG presenting different coverage and polydispersity will be presented in the first part of chapter 4 where the role of Cl will be further clarified. Finally, a STM study on pyramidal CdSe NPs on HOPG exposed to heating treatments will be reported in the second part of chapter 4. The effects of the heating treatments on the NP surface will be compared by means of HR XPS.

After a brief general conclusion reported in chapter 5, the experimental section and some experimental and analysis details are reported in the chapter 6 and in the appendix respectively.

References

1) Z. Alfassi, D. Bahnemann, A. Henglein, *J. Phys. Chem*., **86**, 4656 (1982); A. Henglein, *J. Phys. Chem*., **86**, 2291 (1982)
2) a)L. E. Brus, *J. Chem. Phys.*, **80**, 4403 (1984). b) L. Brus *J. Phys. Chem* **90**, 3393 (1986)
3) L. Efros and A. L. Efros, *Sov. Phys. Semicond.*, **16**, 772 (1982)
4) I. Ekimov, A. L. Efros and A. A. Onushchenko, *Solid State Commun*, **56**, 921 (1985)
5) Beatriz H. Juárez, *Anales de Química*, **107**, 229 (2011)
6) a) Y. Yin and A. P. Alivisatos, *Nature*, **437**, 664 (2005). b) D. V. Talapin et al, *Nano Letters*, **7**, 2951 (2007)
7) S. Doose, *Small*, **3**, 1858 (2007)
8) D. Schooss, A. Mews, A. Eychmuller, H. Weller, Phys. Rev. B, 49, 17072 (1994)
9) S. Kim, B. Fisher, H. J. Eisler, M. Bawendi, *J. Am. Chem. Soc.*, **125**, 11466 (2003)
10) J. M. Pietryga et al, *J. Am. Chem. Soc.,* **130**, 4879 (2008)
11) K. L. Jansens, B. Partoens and F. M. Peeters, *Phys. Rev. B*, **66**, 075314 (2002)
12) S. Kim at al, *Nature Biotechnology*, **22**, 93 (2004)
13) S. Gullapalli, M.S. Wong, *Chemical Engineering Progress*, **107**, 28 (2011)
14) C. Charlier, X. Blase, and S. Roche, *Rev. Mod. Phys.*, **79**, 677 (2007)
15) X. Lu, Z. Chen, *Chemical Reviews*, **105**, 3643 (2005)
16) L. Marty, A.M. Bonnot, A. Bonhomme, A. Iaia, C. Naud, E. Andre and V. Bouchiat, *Small*, **2**, 110 (2006)
17) V. H. Ebron et al, *Science*, **311**, 1580 (2006)
18) a) P. V. Kamat, *J. Phys. Chem. C*, **111**, 2834 (2007). (b) A. Kongkanand, R. M. Dominguez and P. V. Kamat, *Nano Lett*., **7**, 676 (2007)
19) W. Zhang, B. Xu and L. Jiang, *J. Mater. Chem*., **20**, 6383 (2010)
20) J. Guerra and M. A. Herrero, *Nanoscale*, **2**, 1390 (2010)
21) D. R. Kauffman and A. Star, *Angew. Chem*. *Int. Ed*., **47**, 6550 (2008)
22) D. Shi et al *Appl. Phys. Lett.*, **95**, 223702 (2009)
23) J. Guerra and M. A. Herrero, *Nanoscal*, **2**, 1390 (2010)
24) G. Wildgoose, C. E. Banks and R. G. Compton, *Small*, **2**, 182 (2006)
25) V. Georgakilas, D. Gournis, V. Tzitzios, L. Pasquato, D. M. Guldi and M. Prato, J. *Mater. Chem*, **17**, 2679 (2007)
26) X. Peng, J. Chen, J. A. Misewich and S. S. Wong, *Chem. Soc. Rev.*, **38**, 1076 (2009)
27) D. Eder, *Chem. Rev*., **110**, 1348 (2010)
28) N. Karousis and N. Tagmatarchis, *Chem. Rev*., **110**, 5366 (2010)

29) a) S. Banerjee, T. Hemraj-Benny and S. S. Wong, *Adv. Mater*., **77**, 17 (2005). b) J. L. Bahr and J. M. Tour, *J. Mater. Chem*., **12**, 1952 (2002)
30) D. Tasis, N. Tagmatarchis, A. Bianco and M. Prato, *Chem. Rev.*, **12**, 1952 (2006)
31) C. B. Murray, D. J. Norris and M. G. Bawendi, *J. Am. Chem. Soc*., **106**, 1105 (1993)
32) V. K. Lamer, R. H. Dinegar, *J. Am. Chem. Soc.*, **72**, 4847 (1950)
33) J. Park, J. Joo, S. G. Kwon, Y. Jang, T. Hyeon, *Angew. Chem. Int. Ed.*, **46**, 4630 (2007)
34) a) A.G. Roca, M.P. Morales, K. O'Grady, C.J. Serna, *Nanotechnology*, **17**, 2783 (2006). b) N.O. Nunez et al, *Chem. Mater.*, **15**, 3558 (2003). c) S.G. Kwon et al, *J. Am. Chem. Soc.*, **129**, 12571 (2007)
35) X. H. Ji, D. Copenhaver, C. Sichmeller, X. G. Peng, *J. Am. Chem. Soc.*, **130**, 5726 (2008)
36) X.G. Peng, et al, *Nature*, **404**, 59 (2000)
37) Z.A. Peng and X. Peng, *J. Am. Chem. Soc*.,**124**, 13, 3345 (2002)
38) A. Hungría et al, *Nano Res*., **1**, 89 (2008).
39) B.H. Juárez, C. Klinke, A. Kornowski, H. Weller, *Nano Letters*, **7**, (12) 3564 (2007)
40) Z. A. Peng, X. Peng, *J. Am. Chem. Soc*., **123**, 1389 (2001)
41) A. D. McNaught and A. Wilkinson: Compendium of Chemical Terminology 2nd ed, Blackwell Scientific Publications, Oxford (1997).
42) D.V. Talapin, A.L. Rogach, M. Haase, and H. Weller, *J. Phys. Chem. B*, **105**, 12278 (2001)
43) H. Brune, *Surface Science Reports*, **31** 121 (1998)
44) C.Wagner, *Z. Elektrochem*, **65**, 581 (1961)
45) G. Medeiros-Ribeiro, T.I. Kamins, D.A.A. Ohlberg, R.S. Williams, *Phys. Rev. B*, **58**, 3533 (1998)
46) T. J. Krzyzewski and T. S. Jones, *J. Appl. Phys*, **69**, 668 (2004)

Chapter 2

Nanoparticle deposition techniques

2.1 Introduction

In this chapter results concerning the deposition of pyramidal CdSe NPs, and other semiconductor and metallic NPs using several methods such as Langmuir Blodgett, convective assembly, electrospray and the so-called pot-deposition method will be shown and properly compared. One of the goals of this part of the work was to obtain a film of CdSe NPs on HOPG suitable to study the physical and chemical properties of the NPs surface and the interface between CdSe NPs and the C-sp2 lattice by means of XPS and STM. The possibility to control the growth of NPs, to obtain ordered arrangements and to get a deep knowledge of their physical and chemical properties are, indeed, strategic instruments not only for our specific purpose but, in general, for the development of a wide range of potential applications in opto-electronics, magnetic storage devices, and catalysis (Ref 1).

2.2 Langmuir Blodgett; theory and results

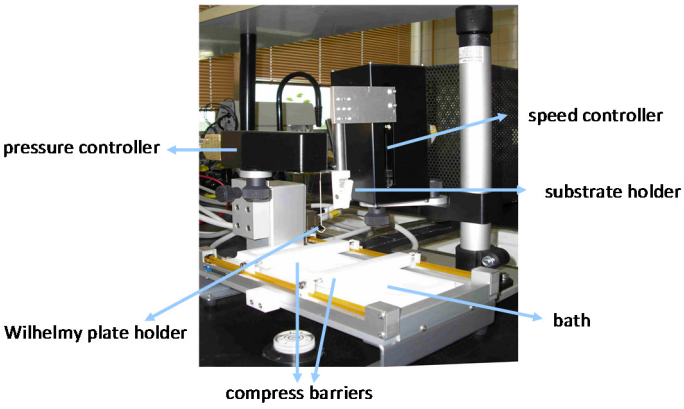

Fig 1. The Langmuir Blodgett set-up used in this work.

The Langmuir Blodgett (LB) technique (named because of the American scientists Irving Langmuir (Ref 2) and Katherine Blodgett (Ref 3)) is a method used to create a molecular films, typically surfactants, at the air-water interface and to transfer it on a solid substrate. The employed set-up can be seen in figure 1, which is equipped with a teflon bath with compress barriers, a pressure sensor and a stepper motor. To produce a molecular film, the molecules dissolved in highly volatile solvents are spread on the so-called sub-phase, generally a water bath. After solvent evaporation the molecules start to organize in the available surface. The two barriers placed in contact with the sub-phase compress the surface occupied by the molecules and a metallic plate of some cm^2 in size, the so-called Wilhelmy plate, registers the variation of surface pressure. Previous to any deposition, the behavior of the surface pressure versus the area occupied by the molecules on the sub-phase should be studied to obtain information about the stability of the film (isotherm). A scheme of an isotherm in the case of surfactants is shown in figure 2.

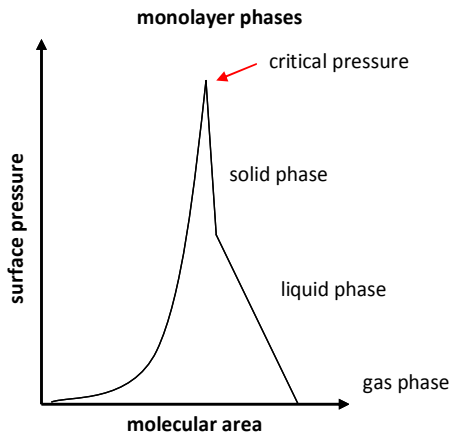

The isotherm generally describes three phases namely, the gas phase, the liquid phase and the solid phase. In the gas phase the surface pressure is constant. When molecules start to interact to each other (liquid phase), the pressure starts to increase till molecules are packed in a sort of solid surface phase. This phase is accompanied by an increase in the isotherm slope. The pressure reaches a maximum value after which the layer collapses, meaning that the molecular packing is no longer stable due to the progressive area compression. This pressure value is called critical pressure.

Fig 2. Scheme of LB isotherm where the three typical phases are described.

At the critical pressure, the deposition on a solid substrate can be performed. There are several parameters influencing the quality of a LB films like the surface pressure during the deposition (measured with the Wilhelmy plate), the speed, and the angle of deposition, as shown in figure 3.

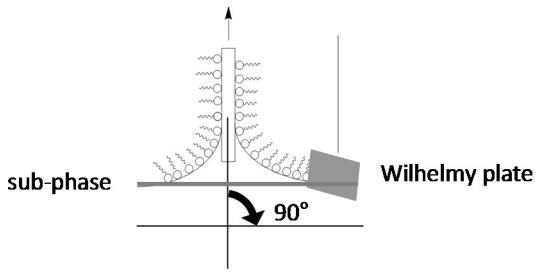

Fig 3. Scheme of LB film deposition where the angle between the substrate and the sub-phase is 90°.

In this section the results of LB deposition in which the molecules are replaced by pyramidal CdSe NPs of about 8 nm in size using a HOPG as a substrate are presented. 30 µL of a saturated dispersion of pyramidal CdSe NPs in toluene was spread on a diethyleneglycol sub-phase. The use of diethyleneglycol as sub-phase (instead of water) is due to the fact that the surface tension of water is not suitable for NPs LB deposition. The angle of deposition was fixed to 105°. For smaller angles a poor coverage was observed, probably due to the excessive weight of NPs islands (Ref 4). Figure 5 (a) shows a SEM image of a typical NPs LB film. Large areas of the HOPG substrate are covered by a compact NPs monolayer. Some defects such as cracks (due to the weight of the NPs during the transfer process) and/or stacked layers (figure 5 (b)) are apparent.

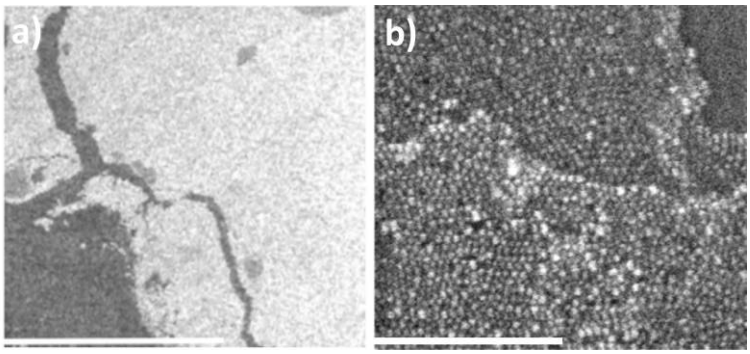

Fig 5. (a) SEM image of the CdSe NPs LB film deposited on HOPG, 500 µm reference bar. (b) Magnification c the NP monolayer, 200 nm reference bar.

NPs films produced by means of LB presents a very high NPs coverage which is suitable to perform XPS and STM measurements. On the other hand, this method does not exclude the co-adsorption of diethylenglycol (the sub-phase) on the HOPG substrate during the film transfer which would modify the CdSe NP-C-sp^2 interface.

2.3 Convective assembly; theory and results

Dimitrov and Nagayama developed a method that allows the formation of periodic arrangements of spherical particles on a substrate from a colloid by controlling the evaporation of the solvent (Ref 5). The periodic arrays can be formed by dipping a substrate into the particles dispersion and then, withdraw it at a control rate under fixed conditions of pressure, temperature, and concentration. This process is shown in figure 6, where a positive meniscus is depicted in this case (like that formed at water-hydrophilic substrates interfaces).

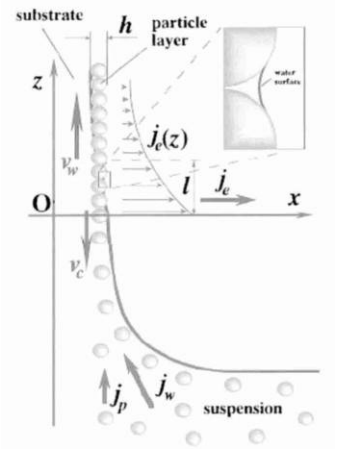

Fig 6. Particles and solvent fluxes at the beginning of 2D array growth. The inset shows the menisci shape between particles. Vw is the substrate withdrawal rate, Vc is the array growth rate, Jw is the solvent influx, Jp is the particle influx, Je is the solvent evaporation flux and h is the thickness of the array. (Ref 5).

The formation of periodic particle arrays can be described by the following scheme:

(1) convective transfer of particles from the dispersion to the substrate due to solvent evaporation and,

(2) interactions between particles that lead to specific arrangements of the particles on the substrate.

The thickness of the solvent-substrate meniscus, indicated as h_o in figure 7, decreases as the relative distance between the bulk-dispersion and the wet-dried substrate frontier increases. According to Dimitrov and Nagayama the solvent-substrate interaction in the region of the meniscus may cause a capillary force that pushes the particles out of those solvent-substrate meniscus regions presenting h_o thinner than the diameter of the particles. The particles with diameters d smaller than h_o will be packed irregularly, while particles with d much bigger than h_o will be not transferred to the substrate. The authors conclude that the ideal balance between d and h_o (depicted in figure 7) is reached when the particle diameter is slightly larger than the thickness h_o.

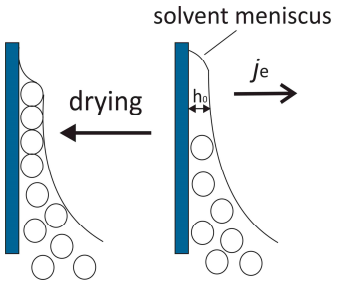

Fig 7. Ideal balance between the particle diameter *d* and the water-substrate meniscus thickness h_o. J indicates the solvent evaporation flux.

Convective assembly experiments with polystyrene spheres show that not only the particle diameter, but also the polydisperisty of the particles strongly influence the quality of particle packing. Large uniformly oriented domains of highly aligned particles can only be obtained with low polydisperse samples (Ref 5).

Prevo and Velev used the convective assembly method to produce films of Au NPs of about 12 nm in diameter, by dragging a small volume of NPs suspension confined in a meniscus between two plates. The process is performed at a controlled constant velocity by using a stepper motor. They observed that the convective assembly with NPs requires a low substrate withdrawal rate optimized at 10 µm/s. They also noted that NPs tend to aggregate as they become concentrated at the meniscus forming disordered structures. Hence, also in the case of NPs, the solvent-substrate meniscus plays a crucial rule (Ref 6).

Considering that the preparation of good quality films requires the right combination between the meniscus size, the concentration of NP dispersion, and the substrate withdrawal rate, the work developed in this study was focused on the effects produced by variations of these parameters. In this work no stepper motor to control the withdrawal rate was used. Instead, ambient conditions for the solvent evaporation were fixed.

In order to investigate the role of the meniscus size, two representative films with different deposition angles were prepared. A dispersion of pyramidal CdSe NPs in toluene (which average size of 8 ± 1 nm was obtained from TEM analysis) was used. Details about the estimation of the dispersion concentration are reported in annex 1 and in reference 7. Representative convective assembly films were prepared with 1,5 mL of 3,2 µmol/L dispersion of pyramidal CdSe NPs. Two glass vials containing fresh cleaved HOPGs immersed in the NP dispersion were kept during one day at room temperature and atmospheric pressure and positioned such that the angle between the substrate and the dispersion was fixed to 16° and 35° respectively, as shown in figure

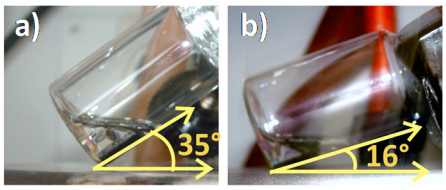

Fig 8. Pictures of HOPG substrates dipped in 1,5 mL of the dispersion of 3,2 µmol/L of pyramidal CdSe NPs. The angle between the HOPGs and the surface dispersion was 35° in (a) and 16° in (b).

Figure 9 shows SEM images of the obtained films. Figure 9 (a) shows a SEM image of the film generated at a deposition angle of 35°. The light gray background makes difficult, at a first sight, to distinguish NPs from the organic residues laying on the substrate. Once a first layer of organic residues is removed due to the heating effect generated by focusing the electron beam of the microscope (see the different marks left by the electron beam in figure 9 (a)), a layer of NPs starts to be visible. The direction of solvent evaporation is discernible and marked with a blue arrow. The organic residues present in the film might come both from the synthesis of the NPs and from toluene (the solvent) that are also transferred on the HOPG. Figure 9 (b) shows a SEM image of the film generated at a deposition angle of 16°. White spots in figure 9 (b) are NPs agglomerations and light grey zones are thinner NPs aggregates randomly distributed on the surface. As a general trend, the morphology of the film obtained with deposition angle of 16° looks much more disordered compared to that generated at 35°. This result proves that, for similar concentrations, the angle and hence, the shape of the meniscus, is a crucial parameter in this type of depositions.

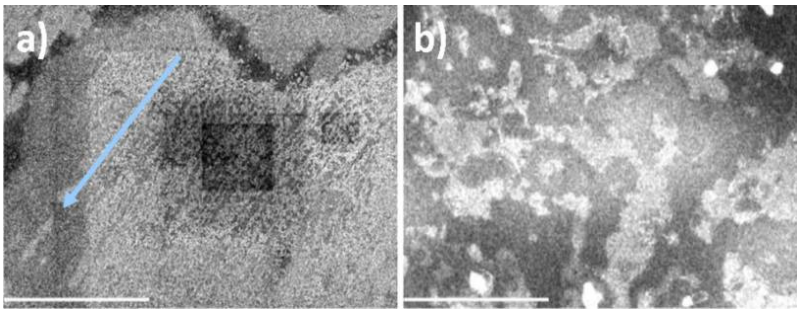

Fig 9. SEM images showing a comparison between convective assembly films of 3,2 µmol/L dispersion of pyramidal CdSe NPs with different deposition angles; 35° (a) and 16° (b). 5 µm reference bar.

Figure 10 shows the shape of the meniscus formed by toluene and HOPG, that is, a hydrophobic-hydrophobic (positive) meniscus, and the comparison between the two deposition angles. In the case of 16° deposition angle, toluene-substrate meniscus presents h_o thinner than in the case of 35°. The meniscus region presenting h_o thinner than the diameter of the particles is more extended for 16°. Thus, the effect caused by

the capillary force, which pushes the particles out of those regions is stronger than in the case of 35°. Thus, at 16° the transfer of NPs on the substrate occurs in a more disorderly way.

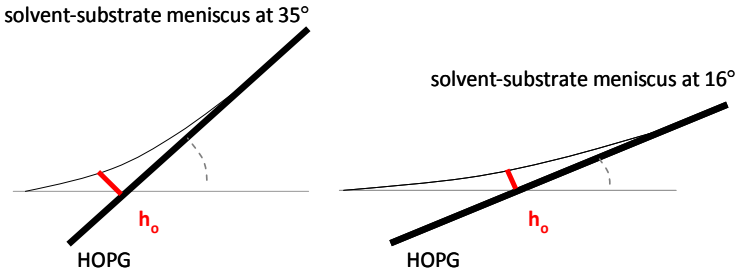

Fig 9. Solvent- substrate menisci shapes at 35° and 16° deposition angle.

With the aim of increasing the NPs coverage obtained in convective assembled films generated at 35°, several experiment using higher NP concentrations were performed. Figure 11 shows HOPG substrates at the initial stage of the experiment in which the concentration of NP dispersion was varied. The glass vials containing the HOPG substrates dipped in 1,5 mL of pyramidal CdSe NPs dispersions with concentrations of 320 µmol/L and 3,2 µmol/L ((a) and (b) respectively) were kept at room temperature and atmospheric pressure during one day.

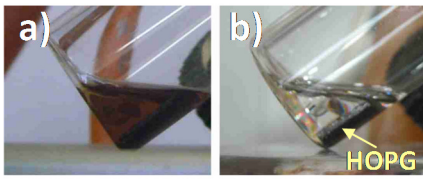

Fig 11. (a) Pictures of HOPG substrates dipped in a dispersion of 320 µmol/L (a) and 3,2 µmol/L of pyramidal CdSe NPs (b) at the beginning of the NPs convective assembly experiments.

In both cases the deposition angle was fixed at 35°.It was observed that the time required to completely evaporate the diluted dispersion is longer. This can be due to a decrease in the vapor pressure for the highly concentrated sample in agreement with the colligative properties of the colloid (properties depending exclusively on the amount of solute particles). This makes this dispersion to evaporate faster.

Figure 12 (a) and (b) illustrates SEM pictures showing the general aspect of the films generated by the evaporation of 320 µmol/L and 3,2 µmol/L dispersions respectively. In figure 12 (a) white strips on the darker background, the HOPG substrate, indicate quite clearly the direction of the solvent evaporation, marked with a blue arrow. In

figure 12 (b) the lighter and homogeneous background makes hard, at this magnification, to distinguish a direction of solvent evaporation due to the higher density of NPs and organic residues on the HOPG. According to this result increasing the concentration of the dispersion does not generate a higher NP coverage. This fact is confirmed by observing figure 12 (c) and (d) that show higher magnifications of SEM images (a) and (b) respectively. In (c) NPs islands and large free areas of the substrate are visible. Notice that the height of the islands is not homogeneous. In fact, the brighter spots marked with red circles are NP multilayers. In (b), ordered islands connected to each other forming an extended net of NPs along vast areas of the substrate are visible. The film generated by 3,2 µmol/L dispersion looks much more homogeneous with respect to the film generated by a dispersion concentration of 320 µmol/L. The same experiment was performed using an intermediate concentration of 32 µmol/L and the resulting film presents, as in the case of 320 µmol/L, a lower NP coverage with respect to 3,2 µmol/L dispersion. These data are available in annex 3.

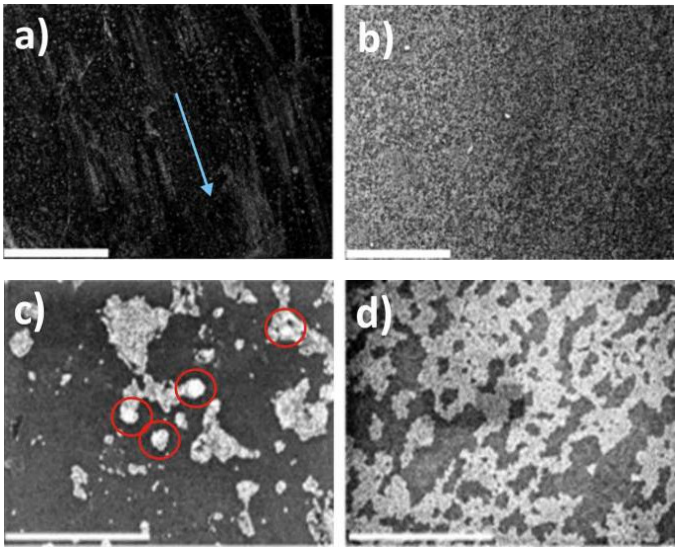

Fig 12. SEM images of convective assembling films generated by the evaporation of of 320 µmol/L (a) and 3,2 µmol/L (b) dispersions. 500 µm reference bar. (c) and (d) are magnifications of (a) and (b) respectively. 500 nm reference bar.

Having fixed the value of the deposition angle at 35°, the diversity in the morphology of the obtained films is a consequence of the different solvent evaporation rate. In fact, even if the relative number of NPs (available to be transferred to the HOPG) is minor when the dispersion of 3,2 µmol/L is used instead of higher concentrations, being the process of toluene evaporation slower, the probability to find NPs equally distributed around the region of the meniscus increases. If the evaporation rate increases, NPs

condense and are chaotically transferred at the meniscus forming disordered structures. With the same meniscus shape, the lower the toluene evaporation rate, the higher the density of NPs deposited on the substrate.

The possibility to control the arrangement of NPs using convective assembly is very promising considering the several interesting works found in the literature. For example, using a very similar method, highly ordered structures as binary super-lattices of CdSe-PbS and PbSe-Pd NPs were generated by controlling the temperature of evaporation of the solvent. This allows for the NPs self-assembly into different single and binary structures (Ref 8). In another work, a binary NPs structure composed by CdSe and Au NPs on silicon substrate for optical properties investigations was produced (Ref 9).

From the point of view of the NP disposition on the HOPG, convective assembly film generated by the evaporation of 3,2 µmol/L with a deposition angle of 35° could be a good candidate for the study of pyramidal CdSe NPs – C-sp^2 lattice interaction. However, as it was found, the presence of organic residues on the substrate is quite high for that purpose.

In the next section a novel technique that allows the deposition of samples in solution directly on a substrate placed into a high vacuum (HV) chamber will be introduced.

2.4 Electrospray; theory and results

Since liquids are generally not compatible with vacuum because of their high vapor pressures, the deposition in situ of NPs dispersions is an experimental hurdle for a full ultra high vacuum (UHV) preparation. Electrospray ionization, a technique used in mass spectrometry to produce ions, gives a solution for this problem. It became extensively used as ionization source for mass spectrometry after the Fenn group demonstrated its employ for the analysis of large biomolecules (Ref 10).

In this part of the section the operating principle and the process known as Coulomb fission responsible for the conversion from liquid-phase to gas-phase molecules will be reported. The experimental set-up, including the calibration of the instrument will be described in the experimental part (chapter 5).

The electrospray set-up can be seen as an electric circuit where a liquid emitter, at which a positive voltage is applied, represents the electrode and a vacuum system connected to a grounded UHV main chamber represents the counter electrode. For electrospray experiments, a syringe containing the bulk liquid, whose compression rate can be mechanically controlled, is connected to a metallic capillary. The metallic

capillary is connected by a coupling system to a metallic hollow needle, the high voltage tip or emitter, schematized in figure 13.

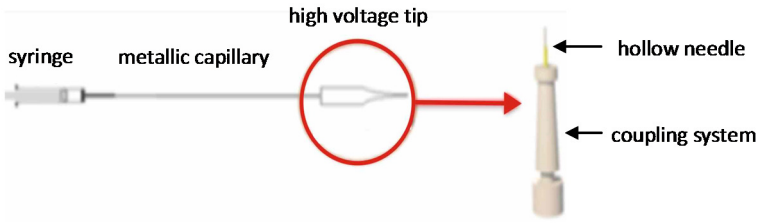

Fig 13. Scheme of the connection from the syringe containing the liquid to the high voltage tip.

Figure 13 depicts a scheme of the system. At a distance *d* there is a first entrance to the system, the entrance capillary, which leads to the first vacuum chamber or first stage. The 1° and the 2° flanges lead to the second and to third stages, respectively. The stages are differentially pumped chambers in such a way that from the first to the third stage the pressure decreases. All the entrances are connected to the ground and their diameters increase toward a HV preparation chamber (0,4 mm, 0,6 mm, and 1mm respectively) where the substrate for samples depositions is placed. In this manner the charged jet travels from the high voltage tip to the substrate, passes through the differentially pumped chambers, stages 1, 2, and 3, previous to the entrance to the HV environment of the preparation chamber.

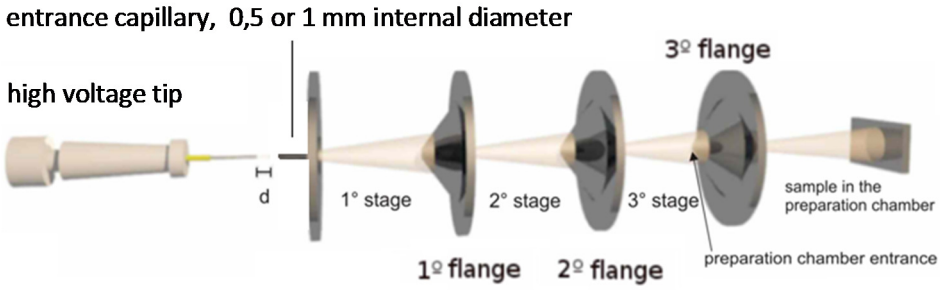

Fig 14. Scheme of the differentially pumped chambers.

Figure 15 schematizes the steps of electrospray operation principle. Under the effect of surface tension, the liquid meniscus adopts a semi-spherical shape (15 (a)). The application of a positive voltage Vc induces an electric field Ec such as

$$E_c = \frac{2V_C}{r_c \ln\left(\frac{4d}{r_c}\right)}$$

equation 2

where r_C is the capillary outer radius. The polarization field induced by E_C causes a distortion of the spherical meniscus into a cone pointing to the direction of the field E_C. This is called *Taylor cone* as indicated in figure 15 (b) (see Ref 11). When the applied field reaches a certain value, the tip of the cone becomes unstable and the jet composed by charged liquid droplets and positive ions emerges from the cone toward the grounded entrance capillary (figure 15 (c)) while the charge loss at the metal-liquid interface is balanced electrochemically. Imbalances between the amount of charge generated electrochemically and the amount of charge lost at the cone apex can lead to different electrospray operating regimes (Ref 12). In our experiments two distinct operating regimes were individuated and tested namely, *spray-jet* and *drops-jet* regime. In the drops-jet regime the jet generated at the cone apex is composed by visible drops while in the spray-jet regime the jet is composed by smaller droplets composing by a continuous suspension flux.

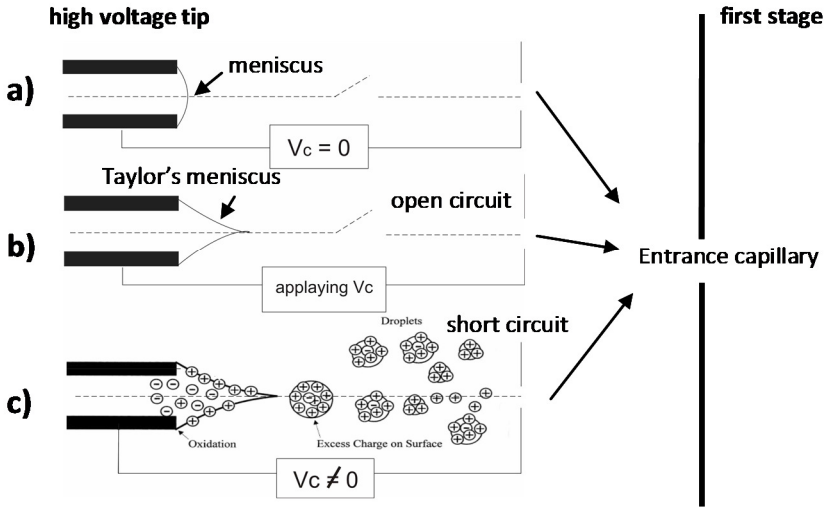

Fig 15. (a) The meniscus at the emitter assumes a semi-spherical shape due to surface tension (the shape of the meniscus is convex or concave depending on the solvent). (b) Open circuit regime: a positive voltage Vc is applied and the shape of the meniscus starts to deform from spherical to a cone–shape due to the exposition of the induced electric field. (c) Short circuit regime: when the applied field reaches a certain value, a jet of liquid formed by charged droplets and positive ions is driven out from the cone apex to the counter electrode, that is, to the first stage through the entrance capillary.

Figure 16 shows the process known as Coulomb fission. Once the jet is generated, the charged droplets solvent evaporates and the charge density on the droplets surface increases. When the Rayleigh limit is reached, that is, when the maximum amount of charge that a liquid droplet could carry is reached, the surface of the droplet becomes unstable with the consequent desorption of ions to balance the excess of charge (the Rayleigh breakup indicated in figure 16). It has been estimated that for a small loss of its mass, 1,0 – 2,3%, a droplet loses a large percentage of its charge, 10 - 18%, (Ref 13).

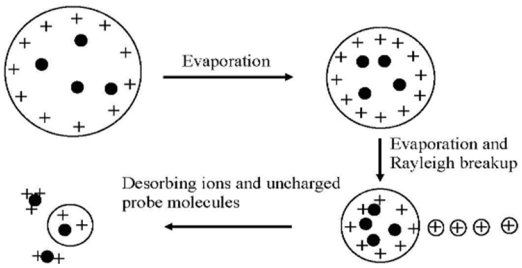

Fig 16. Scheme of Coulomb fission process (Ref 13).

The process would takes place indefinitely until the excess of charge is balanced, so that those gas-phase molecules originally dispersed in the solvent will be neutrally charged. This process is helped by the use of polar solvent. Thus, such kinds of solvents are ideal in electrospray depositions.

Electrospray has been successfully used for the deposition of nanometer objects such as fullerenes and CNTs (Ref 14 and 15). In this part of the work the results of the deposition by electrospray of three types of NPs on a HOPG substrates will be reported; pyramidal CdSe NPs, CdSe/ZnS NPs and Au NPs.

2.4.1 Deposition of pyramidal CdSe NPs dispersed in chloroform

In the synthesis of pyramidal CdSe NPs the organic molecules used are trioctylphosphine oxide (TOPO), octadecylphosphonic acid (ODPA) and trioctylphosphine (TOP). These molecules contain metal coordinating groups on one side and alkyl chains on the other. The metal coordinating groups bind to electron-poor metal atoms providing electrons at the NPs core surface. The alkyl chains extend to the solvent determining the solubility of NPs. In this case, they provide the NPs with a hydrophobic character (Ref 16) and actually toluene turns out to be an appropriate solvent. It has been observed that chloroform, a solvent showing a non zero dipole moment (1,04 Debye) can be also used to disperse this type of NPs, even if the resultant dispersion is quite instable (in some case it has been noticed that NPs precipitate after some hours). Hence, pyramidal CdSe NPs dispersed in chloroform were used for

electrospray depositions after having tested a toluene NPs dispersion and having verified that it is not a suitable solvent for electrospray depositions due probably to its non-polar character.

During the deposition of all NP samples employed, pressure and flux of elements entering to the preparation chamber were constantly checked by pressure controllers and a mass spectrometer. This gives the possibility to control the flux regime conditions. However, a very common technical problem found in these experiments is the obstruction of the entrance capillary. To illustrate this problem Figure 17 shows the pressure values and mass spectra in three steps of the experiment: (a) initial experimental conditions, just before the generation of the NP dispersion flux, (b) at maximum flux and (c) when the entrance capillary is obstructed.

In order to overcome this problem, several pressure and flux conditions were tested.

Mass spectrometer spectra	**Preparation chamber pressure**
Initial condition 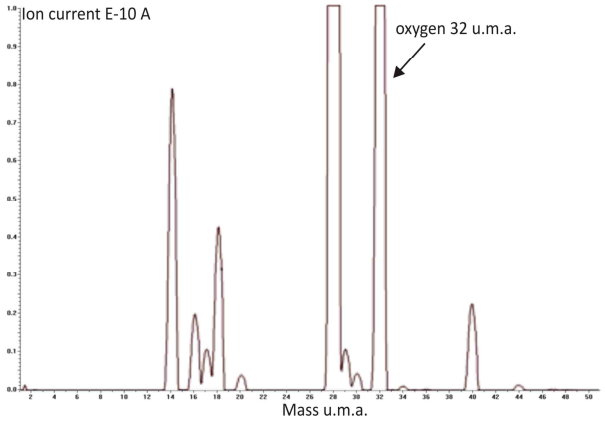	$3{,}0 \cdot 10^{-6}$mbar Standard pressure before the generation of the flux. The peak related to oxygen is at its maximum value.

maximum flux 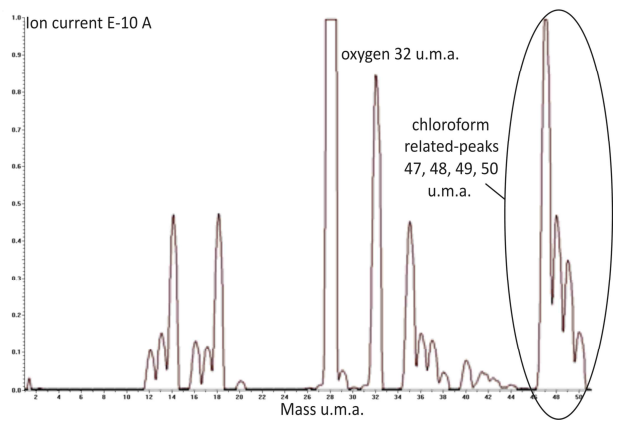	$8{,}3\cdot10^{-6}$mbar The pressure increases while the oxygen peak decreases. The intensity of chloroform peaks increases; the flux of the NP dispersion entering to the chamber reaches its maximum value.
Obstruction 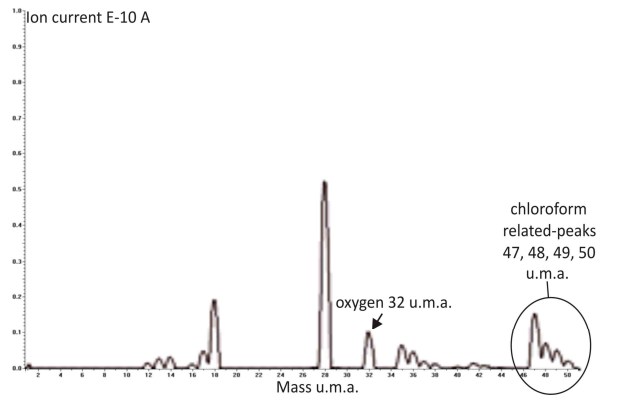	$5{,}6\cdot10^{-7}$mbar The pressure decreases as well as oxygen and chloroform peaks. An obstruction at the entrance capillary isolates the preparation chamber. At this step, the flux is interrupted and an accumulation of liquid at the entrance capillary is observed.

Fig 17. Mass spectra and pressure values in three different moment of pyramidal CdSe electrospray deposition.

When the obstruction of the entrance capillary occurs, the experiment has to be interrupted. The entrance capillary has to be profusely washed to eliminate NP agglomerations. The clearance of the entrance capillary is a tedious procedure that involves the ventilation of the differentially pumped stages. To avoid this inconvenient, when both pressure and oxygen flux start to decrease, fresh chloroform can be electrosprayed to clean the line. This implies the substitution of the syringe containing the dispersion of NPs to another one containing fresh chloroform.

The timing of flux regime condition, that is, the time between the generation of the flux and the entrance capillary obstruction were varied by slightly changing the voltage Vc, the distance d (see figure 14), and the syringe rate compression. Once this problem is solved the optimized conditions allows for the right deposition of the NP suspensions. The majority of the experiments were performed under drop-jet regime.

Figure 18 shows the result of the electrospray deposition of 3 mL of CdSe pyramidal NPs dispersed in chloroform. The film generated after the deposition presents circular spots of about 300 nm in diameter, indicated with red squares, and regions of ordered layers, two of them indicated with blue squares. The circular spots are the marks left by the droplets of the dispersion after solvent evaporation which, for the sake of simplicity, will be called simply droplets along this chapter. The white borders of the droplets are composed by NPs accumulations, and the darker centers are free spaces left by the evaporation of chloroform.

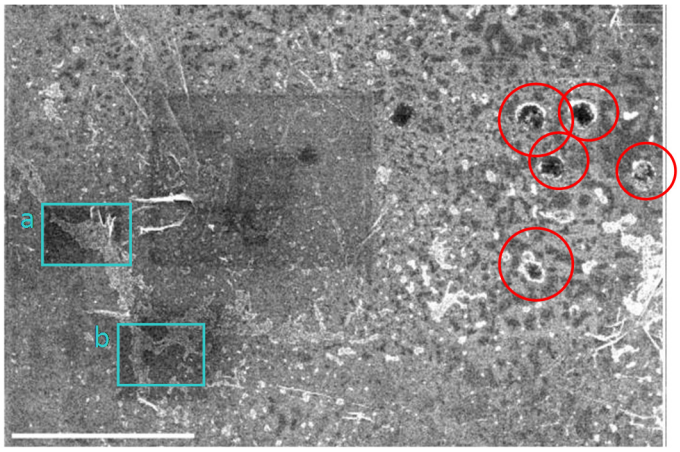

Fig 18. SEM picture of CdSe pyramidal NPs deposited on HOPG by means of electrospray. Blue squares (a) and (b) indicate two regions presenting NPs layers and red circles point out some droplets. 2 µm reference bar.

Figure 19 are SEM images corresponding to magnified areas from figure 18 in the region of NP layers (blue squares (a) and (b)). Notice that the layer is composed by self-assembled NPs and that no darker traces, as in the case of the red spots in figure 18, are apparent. This kind of arrangements may be due to a complete evaporation of the solvent before the NP reach the HOPG surface. However, following this hypothesis, the way in which NPs can self-assemble turns out to be hard to explain. In fact, NPs need a certain mobility to self-organize on the substrate.

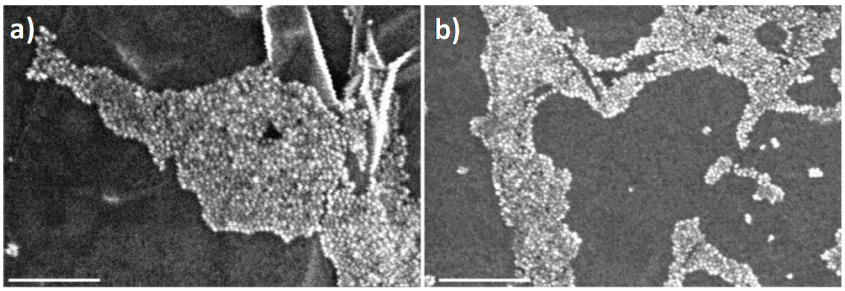

Fig 19. Magnifications of SEM picture of figure 18 (blue squares "a" and "b"). 200 nm reference bar.

An alternative hypothesis might be that various droplets have reached the substrate in the same region forming a single expanded drop, so that NPs originally carried by the different droplets, could diffuse, interact to each other and self-assemble before the complete solvent evaporation. A graphical simulation is depicted in figure 20. If the hypothesis is correct, the ordering and self-assembly of the NPs on the HOPG would improve with the solubility of the NPs in chloroform. As already said, pyramidal CdSe NPs show a higher solubility in toluene rather than in chloroform, hence another kind of NPs that are highly stable in chloroform were tested for comparison.

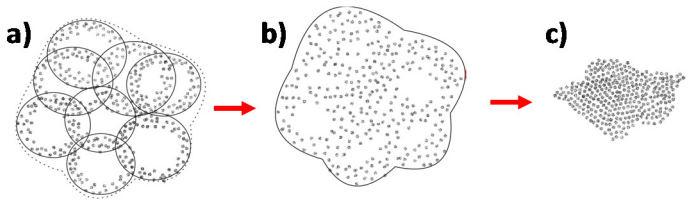

Fig 20. (a) Various droplets reach the substrate in the same region. (b) Droplets form a bigger drop and NPs start to diffuse. (c) NPs self-assemble while chloroform desorbs.

2.4.2 Deposition of CdSe/ZnS NPs dispersed in chloroform

The organic molecules used in the CdSe/ZnS NPs synthesis are TOP and oleic acid (OA). The nucleation of NPs is triggered by injecting Se and S dissolved in TOP. Therefore, OA is supposed to bind to Zn and Cd and TOP to Se and S (see chapter 6 for details). These NPs show a very high solubility in chloroform. Figure 21 shows SEM images giving a general view of the film obtained by depositing 1,5 mL of a highly diluted dispersion of CdSe/ZnS NPs in chloroform (not measurable by standard optical means). In these images droplets and little NP islands are visible. NPs are quite homogeneously distributed on the HOPG substrate following circular patterns with a low density.

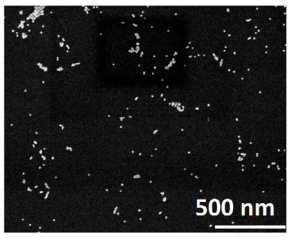

Fig 21 SEM images of the HOPG substrate after CdSe/ZnS NPs electrospray deposition where circular deposits are discernible.

SEM images 22 (a) and (b) reveal the existence of circular islands of densely packed NPs. The enhanced solubility of CdSe/ZnS NPs in chloroform actually allows for a uniform coverage of NPs in the interior of the droplets. Figure 22 (c) shows a NPs arrangement composed by a circular compact island of about 1 µm in diameter inside the circular perimeter of a bigger droplet of about 3 µm in diameter. A detail of the highly dense area is shown in 22 (d). The conclusion to these observable deposits is that there are droplets that probably reach the HOPG during the Coulomb fission process ongoing. In fact the bigger perimeter seems to mark the volume in which solvent ions and the uncharged NPs were expanding during desorption for Coulomb fission (see figure 16) while the majority of NPs were kept concentrated in a smaller volume. Thus, depending on the moment in which drops reach the surface, several types of deposits can be observed.

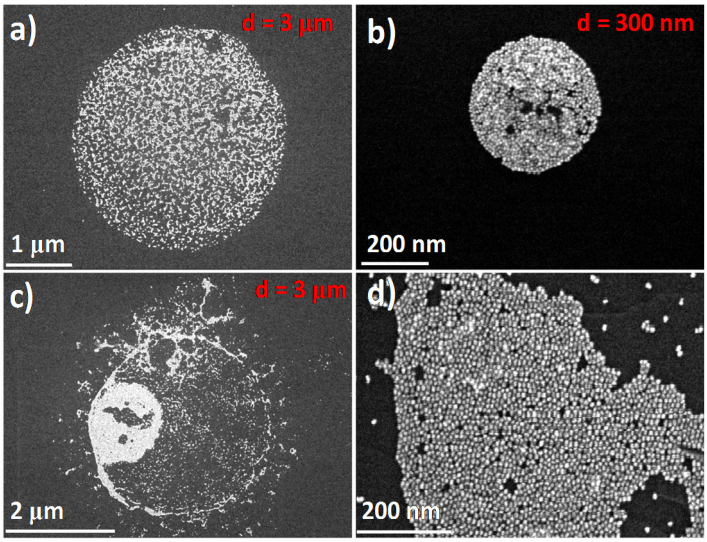

Fig 22. (a) and (b) droplets of CdSe/ZnS NPs. (c) A droplets reaching the substrate during Coulomb fission process ongoing. (d) Magnification of droplet (c).

After every electrospray deposition process, XPS measurements were performed to check whether the signals related to the NPs composition could be detected. Even if Zn, Cd and Se were not present after the first XPS measurements, these spectra provide an interesting clue to understand which kind of mechanisms may occur during the electrospray depositions.

Figure 23 shows a high resolution (HR) XPS spectra of elements composing the inorganic core of NPs. Figure 23 (a) depicts the Zn 2p signal centered to 1022 eV (the lowest BE peak). Figure 23 (b) and (c) show Cd 3d and Se 3d peaks centered to about 406 eV (the lowest BE peak) and about 54.7 eV respectively. No signal of S was detected, what does not exclude its presence. (see discussion of figure 25).

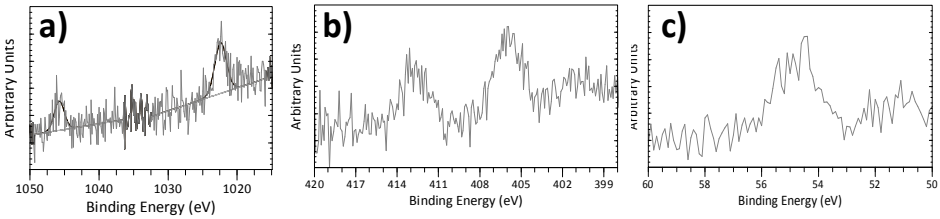

Fig 23. HR XPS spectra of Zn 2p (a), Cd 3d (b) and Se 3d (c). Spectra were performed with a photon energy of 1486,6 eV and an energy pass of 20 eV.

Figure 24 (a) and (b) show a comparison between XPS measurements taken from the survey spectra of the HOPG under three different conditions: clean HOPG prior to any electrospray deposition (down spectrum), HOPG after electrospray deposition before getting NP core signals (middle) and HOPG after electrospray deposition where NPs core signals were finally detected (top). Figure 24 (a) shows the C 1s BE region of the three survey spectra where the C 1s signals were fitted with similar functions. The resulting parameter of the fitting are reported in the inset of the figure. The fact that the fits of C 1s after NPs deposition present a higher FWHM and a shift in the BE position indicates the presence of another contribution related to C. Figure 24 (b) shows the BE regions of O 1s and Cd 3d for the same spectra where the Cd 3d signal is visible in the top grey line proving that NPs were deposited. The O 1s intensity signal after NPs deposition increases, what suggests an additional contribution also to O. The additional contributions probably arise from the organic ligands carried by those NPs deposited on the HOPG, in particular from oleic acids containing both C and O. Interestingly the intensity of O 1s signal of the electrosprayed HOPG before detecting NP is higher than that of the clean HOPG and BE position and FWHM of the fitted C 1s change similarly to

that of HOPG after NPs deposition. This might indicate that an amount of molecules arising from the NP organic shell reach the substrate before depositing NPs.

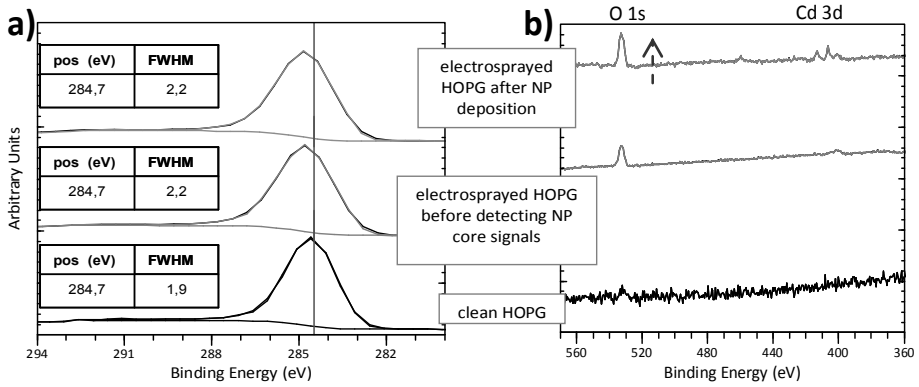

Fig 24. (a) C 1s BE region taken from survey spectra of clean HOPG (black line) and electrosprayed HOPG before and after depositing NPs (middle and top grey lines respectively). BE positions and FHWM resulting from the C 1s signals fits are reported in the tables. (b) O 1s and Cd 3d BE regions of the same survey spectra. The top grey line shows the signal of Cd 3d proving that NPs were deposited. Spectra were acquired by using a photon energy of 1486,6 eV and an energy pass of 50 eV.

To prove this hypothesis a comparison between the sample before and after NPs deposition was performed. Figure 25 shows the survey spectra relative to Cl 2p, Se LMM augers, Se 3p and P 2p BE regions. As expected Se 3p (which 3p 3/2 peak is centered to 162 eV) and Se auger signals are visible in HOPG after NP deposition and Cl 2p peak coming from chloroform and centered to 200 eV is present in both spectra. The interesting thing is that also P is detected in both spectra (P 2s at 190 eV and P 2p at 133 eV). P may arise from TOP, the organic ligand capping Se and S sites (see also reference 18). The fact that P is detected before NP deposition means that TOP molecules may be detached from the surface of the NPs and deposited on the substrate during the electrospray process. The results shown in figure 24 would confirm that oleic acid molecules are probably also detached and deposited on the HOPG. NPs deprived of their ligands tent to agglomerate easier. The formation of NPs agglomeration and the simultaneous evaporation of the solvent explain the obstruction of the entrance capillary under the experimental conditions described above.

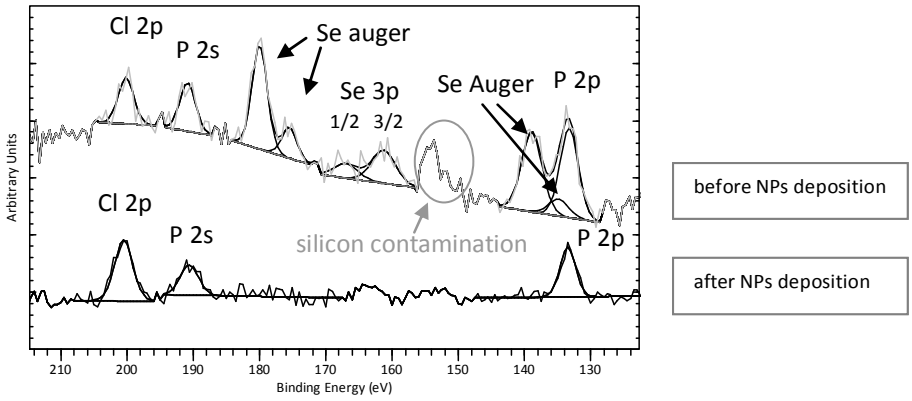

Fig 25. BE region relative to Cl 2p, P 2s and P 2p, and Se 3p. Silicon contaminations are also visible.

Figure 26 shows the XPS spectra of P 2p BE region of the sample before and after NPs deposition. Deconvoluted HR XPS P 2p spectrum of the sample before NPs deposition (taken in the same measurement) is also reported. The correct proportion between P 2p 3/2 and 1/2 components were found in literature (Ref 17). The BE position of P 2p 3/2 component is 132.86 eV.

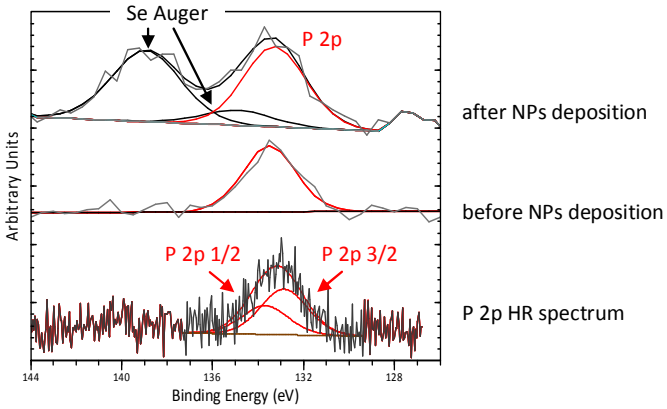

Fig 26. P 2p BE region the sample after and before NPs deposition and HR XPS spectra of the same region of the sample before NPs deposition. (10 eV energy pass)

Some interesting considerations arise from these data. The S 2p signal whose BE position is around 163 eV is not distinguishable as long as Se 3p signal is dominant in that BE range. In the case of the here reported samples of CdSe/ZnS NPs, the fact that the Se 3p is the dominant signal between Se and S suggests that rather than a distinct ZnS shell, this kind of NPs present a chemical composition gradient core, in good

agreement with previous reports (Ref 18). The Se 3p signal has been fitted using the same parameters from previous XPS measurements on pyramidal CdSe NPs (same proportion between 3p 1/2 and 3p 3/2 peaks in absence of S contribution). Therefore, within the limits of the experimental and analytical errors, one concludes that, even if the presence of S cannot be discarded, the shape of the Se 3p peak suggests that both core and interface of these CdSe/ZnS NPs is probably richer in Se than in S. Hence, the P detected signal may be related to the TOP molecules detached from Se atoms at NP surface.

SEM and XPS analysis of the obtained film show that islands with packed NPs are homogeneously distributed on the substrate and that the density could be enhanced by simply depositing higher amount of NPs. A relatively high amount of Cl arising from chloroform is also deposited on the substrate. Changing the solvent of NPs dispersion with another one that does not stick to the HOPG surface might avoid the deposition of solvent residues. Therefore, the electrospray set-up was tested with aqueous Au NPs dispersions.

2.4.3 Deposition of Au NPs dispersed in water

This type of NPs was produced by our collaborator (Neus G. Bastús) following a recipe described in Ref 18. SEM images of the film obtained by depositing of 0,7 mL of Au NPs (3×10^{12} NPs/mL) in water, reveal a quite low density of NPs. Figure 27 (a) shows some a detail of one of the droplets formed for this electrosprayed volume. In general, the droplets diameter was about 7 µm, higher than that found in the first two experiments. Different sized droplets are expected when different solvents are used; in this case water is a less volatile solvent than chloroform. In addition, the relative high pressure inside the preparation chamber with respect to the first two experiments (see annex 3) could justify the presence of bigger droplets.

Figure 27 (b) shows the result of the deposition of 5 mL of the same sample of Au NPs in water. In this case the droplets are much smaller (about 300 nm in diameter) probably because their volume is already reduced as long as they enter to the preparation chamber under spray-jet condition. This means that the size of droplets can be controlled by setting different electrospray operation regimes.

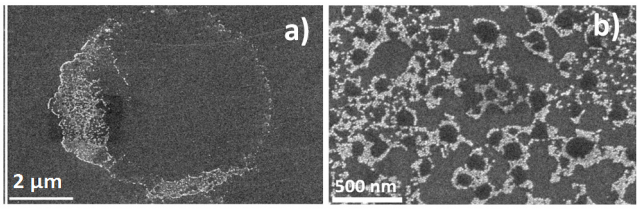

Fig 27. (a) SEM images of Au NPs electrosprayed on HOPG under drop-jet operation regime. (b) SEM image of the same sample electrosprayed under spray-jet regime.

2.4.4 Comparison between the three samples

A comparison between the different aspects of the three types of NPs individual droplets are shown in figure 29. In the case of CdSe/ZnS, NPs are distributed toward the center of the droplets while pyramidal CdSe NPs are distributed in part on the edge and in part toward the center. This is a consequence of the different stability of dispersions; CdSe/ZnS in chloroform is a more stable dispersion than pyramidal CdSe NPs in chloroform; CdSe/ZnS NPs spread homogeneously within the drop, what helps their uniform arrangement within the volume occupied by the solvent. Pyramidal CdSe NPs show a certain propensity to aggregate. However, the aggregation seems to be reduced when various drops join and force the NPs to diffuse in the available volume of chloroform (see figure 20). NP diffusion helps the self-assembly, what explains the absence of NPs layers with circular contours generated by an individual drop like the ones visible in figure 22 for CdSe/ZnS. The darker center of Au NPs droplet in figure 29 is the free space left by dried water. On the contrary to the case of CdSe/ZnS NPs sample, NPs are all deposited on the edge. This behavior has been previously explained and it is known as the “coffee rings” or the “coffee stain” effect. It occurs wherever drops containing solids forming a non-zero solvent-substrate angle (or meniscus) evaporates.

Fig 29. Droplets of electrospyed NP samples on HOPG. 300 nm reference bars.

This phenomenon was described in 1997 by Deegan and Bakajin in a detailed study of the ring-like deposit along the perimeter of a coffee drop drying on a solid surface (Ref 19). They shown that the pattern generated by the deposit is due to capillary flow induced by the differential evaporation rates across the drop: liquid evaporating from the edge is refilled by liquid from the interior and the resulting edge-ward flow can carry almost all the dispersed solid material to the edge. The evaporation flux gradient across the surface depends on the shape of the drop, being zero in the centre region and reaching its maximum value at the sharp wedge-shaped boundary. Consequently, the evaporation rate varies across the surface, but it approaches to a constant value in

those cases in which the solvent-substrate angle is near to zero. Consequently the edge-ward flow is negligible or absent in the case of polar solvent-hydrophilic substrate (or non polar solvent-hydrophilic substrate) meniscus drop shapes since in these cases the solvent tends to spread on the surface. Being the HOPG a hydrophobic substrate, the coffee rings effect is much more evident when the solvent is water.

An interesting analogy between the comparison exposed in this section and the results of a previous work showing the self-assembly of NP rings and filled spots can be done (Ref 20). A dispersion of polystyrene NPs of 100 nm in size in alcohol was spread on two different treated SiO_2 substrates, either hydrophobic or hydrophilic. By blowing the substrate with a humid nitrogen flow, NPs in alcohol are transferred into the water micro-droplets condensed on the SiO_2. After water evaporation numerous NPs coffee rings, in the case of hydrophobic substrate, or tiny spots (drops) filled by NPs, in the case of hydrophilic substrate, were formed.

Electrospray has a great potential not only for depositing NPs dispersions and liquid solvents in general, but also to investigate, in combination with XPS, the surface of NPs. In fact, taking advantage of the ligands detaching process, one can simultaneously ascertain the composition of the core, the presence of organic ligands on the NPs surface and infer the type of bounding and its strength, what open room for plenty of future experiments. In the case of CdSe/ZnS NPs it was possible to confirm the presence of TOP molecules in the NP dispersion originally composing the NP organic shell and that this type of NPs actually shows a chemical composition gradient in the core. Since the NPs ligands detach easily, they must be weakly bound. By means of electrospray the generated films are low dense. In addition, since the detaching of ligands modifies the original chemical composition of NP surface one may conclude that electrospray is not the best method for the preparation of NPs films covering wide areas. In the following an innovative deposition method that does not alter the NP surface and guaranties a high NPs density on HOPG will be presented.

2.5 Pot-deposition of CdSe pyramidal NPs

"Pot-deposition" is an innovative method experimented for the first time in the synthesis of pyramidal CdSe NP-CNT HS with the aim to reproduce the attachment of pyramidal CdSe NPs on C-sp^2 lattices on a solid substrate. It simply involves the addition of a HOPG substrate in the pot together with the other reagents before starting the synthesis of CdSe rod-like NPs. By this methodology CNTs can also be included in the pot. In this way, in a synthesis where both a dispersion of CNTs and HOPG are placed in the reagent mixture CdSe NP-CNT HS, NPs attached to the HOPG as well as "free" NPs are obtainable in the same process. After the synthesis, the HOPG substrate is carefully

isolated and washed by immersion in fresh toluene to take off all possible organic residues. Figure 30 depicts the post-synthetic treatment.

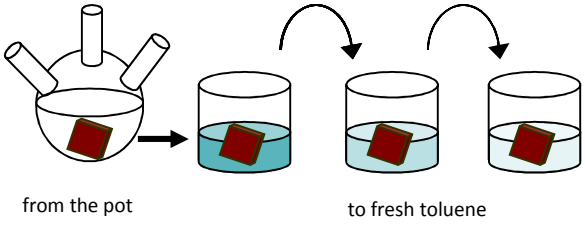

Fig 30. Post-synthetic treatment of HOPG used as substrate for pot-deposition.

Solid products composed by flakes exfoliated from the HOPG due to the mechanical shaking produced by the stirring during the synthesis are also isolated and properly washed for subsequent TEM inspection. (see chapter 6). Figure 31 shows a SEM image of a HOPG substrate covered by CdSe NPs following this methodology ((a)) and TEM images of a HOPG flake from the same synthesis ((b) and inset). As it can be observed NPs cover homogeneously the whole HOPG substrate forming compact and ordered islands. Figure 31 (b) shows a folded HOPG flake covered with pyramidal CdSe NPs. From the inset, that is a magnification of the edge of the folded flake, the way in which pyramidal CdSe NPs are attached to the flake can be observed; the hexagonal base of the pyramids is in contact with C-sp^2 lattice of graphene what confirms that the same interface between NPs and C-sp^2 generated in pyramidal CdSe NPs -CNTs HS is reproduced (Ref 21).

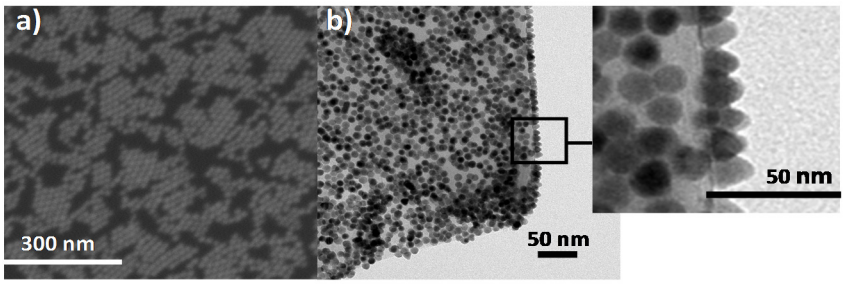

fig 31. (a) SEM image of pyramidal CdSe NPs grown on HOPG. (b and inset) TEM images of NPs grown o HOPG flakes from the same synthesis at different magnifications.

The morphology of NPs grown on HOPG by means of pot-deposition can be observed with an AFM, thing that turned out to be difficult for films of pyramidal CdSe NPs on HOPG generated by means of other deposition methods like convective assembly or Langmuir Blodgett. This is due to the massive presence of organic residues on the

surface and the poor adhesion of the NPs preventing the acquisition of clear images. However, by the pot-deposition method the samples can be easily inspected, as it is proven in figure 32, what points to a relatively strong interaction between NPs and the HOPG surface. Figure 32 (a) shows a topography AFM image sample of pyramidal CdSe NPs on HOPG obtained by pot-deposition. The measurement was performed by tapping mode in air. The morphology of the surface is clearly visible in figure 32 (b) showing the phase contrast of image (a). Figure 32 (c) is a magnification of figure 32 (b) where it is possible to observe the self-assembled NPs on the substrate forming a compact structure composed by NP hexagonal bases arranged on the substrate.

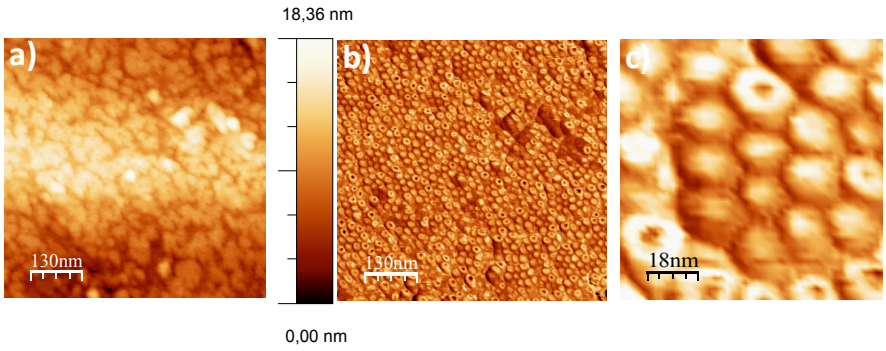

Fig 32. AFM topography image and phase contrast (a) and (b) respectively. (c) Magnification of the phase image. Tapping mode in air.

A very important property of these samples is that the organic residues on the HOPG are present in a very small amount and thus, the detected C-sp^3 and P peaks obtained by XPS analysis arise from the NP organic shell as it will be shown in the following.

Figure 33 shows a comparison between two samples presenting a low and a high NPs density as visible from SEM images (a) and (b) respectively. Figure 34 (c) depicts the C 1s spectra relative to the samples, as indicated in the figure, deconvoluted in C-sp^2 arising from the HOPG and C-sp^3 arising from organic compounds. The spectra are normalized to the signal of C-sp^2, simulating the case in which the two samples present the same amount of non-covered HOPG substrate. The fact that the C-sp^3 component is proportional to the area covered by NPs points towards a negligible contribution of organic residues from the solvents and ascertains that the C-sp^3-contribution is mainly related to the organic shell.

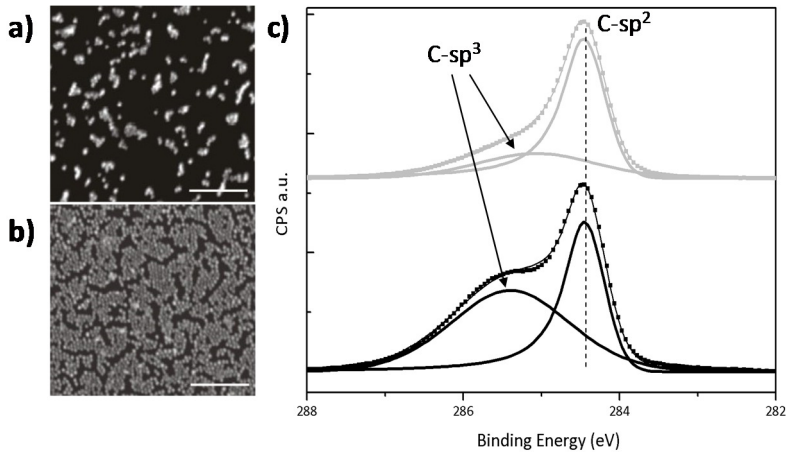

Fig 33. SEM images of samples presenting a low and a high NPs density, (a) and (b) respectively. (c) HR XPS of C 1s region relative to low (grey line) and high NPs density sample (black line). Points represent experimental data, thick lines are the components in which the spectra were deconvoluted, C-sp^2 and C-sp^3, and thin lines are the envelops.

Concerning the P, an important comparison is shown in the following. The XPS spectra of C 1s signal of an as-synthesized pyramidal CdSe NPs spincoated on SiO_2 (without purification cycles, see chapter 5) and NPs pot-deposited on HOPG from the same synthesis and washed in toluene, as described in figure 30 (grey and black lines respectively) are reported in figure 34. The spectra are normalized to the signal of Cd 4d, simulating the case in which the two samples contain the same amount of NPs. The C 1s signal from the pot-deposited NPs was deconvoluted in C-sp^2 and C-sp^3 arising from the HOPG substrate and from organic compounds respectively. In the spin-coated sample a contribution to the as-synthesized CdSe NPs C 1s signal arises from the C-sp^3 of NPs organic shell, whose intensity should be reasonably comparable to the C-sp^3 component of pot-deposited NPs (symbolically indicated with a dashed grey curve). However, as it can see, the C signal is much more prominent in this case, pointing to the presence of other organic residues in the spin-coated sample. Other contributions to C-sp^3 present in this sample arise basically from C species contained principally in TOPO, the organic medium of the synthesis and, in a much smaller amount, from free ODPA and TOP that also populate the medium of the synthesis (e.g., ODPA molecules are approximately present in a percent of 0,008% of the total amount of TOPO).

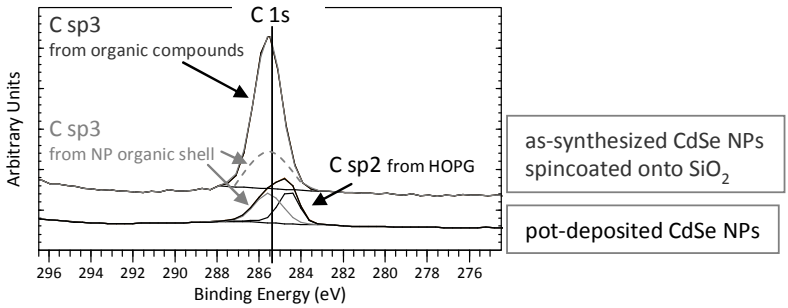

Fig 34. XPS survey relative to C 1s region of as-synthesized pyramidal CdSe NPs spincoated on SiO2 and pot-deposited NPs from the same synthesis.

Figure 35 (a) shows HR XPS spectra of the P 2p region of three samples: as-synthesized NPs spin-coated on SiO_2, NPs pot-deposited on HOPG (same samples as figure 35) and commercial CdSe Wurtzite bulk (grey, black and red lines respectively). As it was already seen above, XPS measurements detect Se LMM Auger signals interfering with the P 2p region. Normalizing the three spectra to the highest intense Se Auger peak, the intensity of the NPs spectra increases due to the superposition of the Se Auger peak and the P 2p arising from the P contained in NPs. Subtracting the CdSe bulk background from NPs spectra one obtains the P 2p signal (figure 35 (b)). The NPs samples P 2p spectra are normalized to the maximum of pot-deposited CdSe NPs signal, between 132,5 eV and 133 eV. The intensity of the as-synthesized CdSe NPs spectrum is higher and displaced toward higher BE. As proved analyzing the C 1s spectra, this sample must include P from free molecules and from organic shell. Fitting P 2p signal of as-synthesized NPs one finds a contribution centered at 133 eV, corresponding to the P 2p contribution in pot-deposited NPs (NP organic shell) and another one at 135 eV, which arises mostly from the P contained in TOPO. This shows, once again, that the contribution from organic compounds in the whole sample of pot-deposited pyramidal CdSe NPs on HOPG arise basically from the NP organic shell.

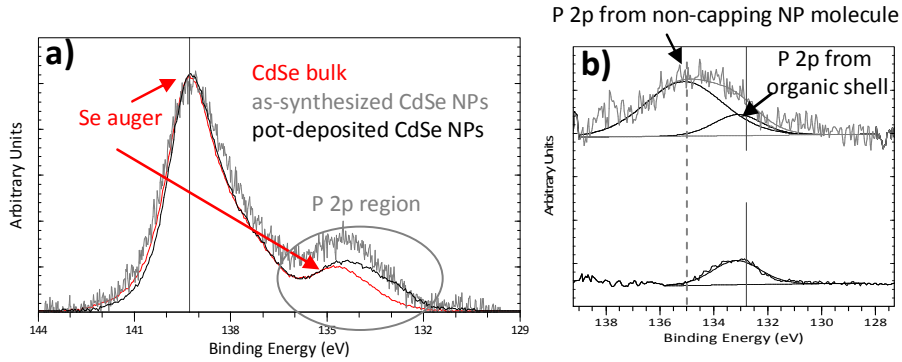

Fig 35. (a) HR XPS spectra of Se LMM auger and P 2p region of as-synthesized CdSe pyramidal spin-coated on SiO2 (grey line), CdSe pyramidal NPs (from the same synthesis) pot-deposited on HOPG (black line) and CdSe Wurzite bulk (red line). Spectra were performed with a photon energy of 1486,6 eV and an energy pass of 10 eV. (b) P 2p signals of as-synthesized CdSe pyramidal NPs spin-coated (grey line) and CdSe pyramidal NPs pot-deposited on HOPG (black line) after CdSe bulk background subtraction. P 2p contributions from TOPO and organic shell are assigned from the fits.

Another important consideration arises from the analysis of these spectra. In principle the organic shell surrounding NPs self-assembled on the HOPG includes organic ligands, which are those molecules capping NPs, anchored to the NP cores surface, and non-capping NPs molecules interacting via van der Waals. In fact, the presence of a certain amount of these non-capping NP molecules, especially between adjacent NPs is expected. The medium of the synthesis is TOPO and the organic molecules that most likely bound to Cd and Se are ODPA and TOP respectively (during the synthesis Cd-2ODPA complex is formed and Se dissolved in TOP is injected for NP nucleation, see chapter 5 for synthesis details). Hence, within the organic ligand shell, non-capping NPs molecules as TOPO and free ODPA and TOP (unbound to Cd or Se) are likely present. However, being the BE of P 2p signal arising from TOPO centred at about 135 eV and considering that no contribution to the NP organic shell P 2p signal is detected at this BE, the presence of TOPO molecules within the NP organic ligands can be neglected, in good agreement with the literature. The chemical composition of the NP organic shell will be widely discussed in the following chapters.

2.6 Comparison between the four deposition methods

NPs films produced by means of LB present show, together with the pot-deposition method, the highest NPs coverage with respect to the other methods reported here. The structure of the film is suitable to perform XPS measurements, but for the purpose of studying the interaction between CdSe NPs and C-sp^2 lattice, the presence of traces of the sub-phase would perturb the resulting information. Regarding the convective assembly films, even if the NP coverage can be quite high, the presence of organic residues on the substrate could also mislead the XPS analysis. Organic residues are not recommended in XPS since they could act as insulator layer, generating undesired effects as charge accumulations under X-ray exposition. These charge effects can damage the samples and consequently perturb the results of the measurements and in the long run, cause problems to the UHV system maintenance, reason why samples containing such large organic amount cannot be used as model samples for an extensive XPS experimentation.

In general, electrospray could be a very good option to study the surface properties of NPs films if the coverage is largely increased, what allows for the detection of higher

XPS element signals and, in our case, if the NP surface keeps unaltered. Hence, since the poor NP density and the technical problem of the organic ligands detaching process are not solved, other alternative deposition method has to be considered.

As observed by means of AFM and XPS, just a relative small amount of organic residue from the synthesis are detected in the so-called “pot-deposited” samples. This kind of films contains organic compounds basically only from the NP organic shell. This makes these samples perfect not only to study the interaction between C-sp^2 and CdSe NPs, but also to study NPs in a great detail from the point of view of the surface chemistry. In fact, thanks to the high, homogeneous, and dense distribution of NPs on the substrate and thanks to the high purity of the sample, (compared to that obtained with other method) XPS and STM measurements have actually gave reliable and reproducible results, as it will be presented along the next chapters.

References

1) G. Schmid, D.V. Talapin, and E.V. Shevchenko, Nanoparticles: From Theory to Application, ed. G. Schmid, Wiley - VCH Verlag, Weinheim 2004
2) I. Langmuir, *J. Am. Chem. Soc*., **38**, 2221 (1916)
3) K.B. Blodgett, *J. Am. Chem. Soc*., **56**, 495 (1934)
4) Vesna T. Aleksandrović, CoPt3 Nanoparticles: Ligand Exchange and Film Preparation. Dissertation, University of Hamburg, (2006)
5) A.S. Dimitrov and K. Nagayama, *Langmuir*, **12**, 1303, (1996)
6) B.G. Prevo and O.D. Velev, *Langmuir*, **20**, 2099 (2004)
7) W.W. Yu, L. Qu, W.Guo, and X. Peng, *Chem. Mater*., **15**, 2854 (2003)
8) M.I. Bodnarchuk, M.V. Kovalenko, W. Heiss, and D.V. Talapin J. *Am. Chem. Soc*., **132**,15124 (2010)
9) E.V. Shevchenko et al, *J. Am. Chem. Soc*., **130**, 3274 (2008)
10) J. B Fenn, M Mann, C. K Meng, S.F. Wong, C.M. Whitehouse, *Science*, **246**, 64, (2007)
11) G. Taylor, *Proc. Roy. Soc. London. Ser. A*, **280**, 1382 (1964)
12) G. J. Van Berkel, F. M. Zhou, *Analytical Chemistry*, **67**, 2916 (1995)
13) (a) P. Kebarle, UH Verkerk, *Mass Spectrom Rev*, **28**, 898 (2009). (b) K.Y. Li, H. Tu, A.K Ray, *Langmuir* , **21**, 3786 (2005)
14) C.J. Satterley et al, *Nanotechnology*, **18,** 455304 (2007)
15) J.N. O'Shea et al *Nanotechnology*, **18,** 035707 (2007)
16) Y. Yin & A. P. Alivisatos, *Nature*, **437,** 664 (2005)
17) J.F. Moulder, W.F. Stickle, P.E. Sobol, K.D. Bomben, Handbook of XPS X-ray Photoelectron Spectroncopy. Perkin-Elmer Corporation
18) H. Lange et al, *Langmuir*, **28**, 8862 (2012)
19) R.D. Deegan et al, *Nature*, **389**, 6653 (1997)
20) Y. Cai and Bi-min Zhang Newby, *J. Phys. Chem*., **130**, 6076 (2008)
21) A.B. Hungría et al, *Nano Res*., **1**, 89 (2008)

Chapter 3

Surface chemical characterization of rod-like and pyramidal CdSe NPs by means of XPS

3.1 Introduction

As described in chapter 1, the optical and electronic properties of semiconductor NPs strongly depend on their size, shape, core and surface chemical composition. Their properties can be tuned during the nucleation and growth processes by controlling temperature, concentrations and specially the presence of surfactants. These molecules or organic ligands, not only determine the NPs growth but also reduce the number of dangling bonds on the surface, providing surface passivation (Ref 1). Although the knowledge of the surface turns out to be critical to understand the functionality of the NPs, many issues are still the focus of intense research. For instance, the nature of the bonds between the ligands and the NP surface is, in many cases, still not clear due to the complex nature of the NPs surface and the possible chemical modification of the organic ligands during the synthetic processes or upon binding the NPs surface.

X-ray Photoelectron Spectroscopy (XPS) is a powerful technique that provides information not only about the surface chemical composition, but also about the chemical bonds with the ligands as well as within the ligands. There are several examples of XPS investigations on ligands-core NP surface interactions. For example, a study of CdSe NPs suggests that organic ligands are datively bound to the particle surface (Ref 2 and 3); however more recent studies indicate that instead of dative interactions, CdSe NPs surface terminates by bonds that present an ionic character (X-type bounds) between ligands and the core surface (Ref 4). Other investigations have been carried out on the oxidation degree and chemical nature of organic ligands in CdTe nanoparticles (Ref 5).

In this work XPS was employed to study the surface of two kinds of NPs: pyramidal and rod-like, CdSe NPs (or simply rods) directly grown on HOPG substrates by means of the pot-deposition method described in chapter 2. As already mentioned in chapter 1 the synthetic process for the production of pyramidal NPs is the same as rod-like NPs except for the injection of 3-4 µL of 1-2 dichloroethane (DCE). Here, it will be

demonstrated that the presence of DCE (or in general the presence of Cl) is responsible for those changes in the chemistry of the surface that lead to the shape transformation.

XPS measurements were performed in our laboratory (LASUAM, Autonoma University of Madrid) and also in the Helmholtz Zentrum of Berlin where high resolution (HR) XPS measurements were carried out by means of synchrotron radiation. The set of data obtained in Madrid is reported in section 3.3.1 and the set of data obtained in Berlin is reported in section 3.3.2.

In the following, a brief introduction to the XPS technique including some clarifications about the two instruments used is reported.

3.2 X-ray Photoelectron Spectroscopy (XPS)

XPS is one of the best developed spectroscopy techniques to investigate the chemical composition and electronic properties of solid surfaces. The sample is located in an ultra high vacuum chamber (UHV) and exposed to a X-ray monochromatic beam. When a sample is probed by the X-ray beam, an electron from the core-level can be removed leaving behind a hole. As this is an unstable state, the core hole can be filled by an external electron from the reservoir or by an electron from an outer level. In the first case the kinetic energy (KE) of the emitted electron, the so-called photoelectron, is wrote as

$$KE = h\nu - BE - \Phi \qquad \textbf{(equation 1)}$$

where hν is the energy of the X-ray radiation, BE is the binding energy, that is the energy of the core-level from which the electron is emitted with respect to the Fermi level of the solid, and Φ is the work function of the sample. In the second case, the electron from the outer level, moving to the lower energy level to fill the core-hole, loses an amount of energy during the transition, which is equal to the difference between the involved levels energies. The transition energy can be coupled to a second outer level electron that will be emitted from the atom if the transferred energy is greater than its level binding energy. The KE of the so-called Auger electrons can be wrote as

$$KE = BE - E(\text{first } e^- \text{ outer level}) - E(\text{second } e^- \text{ outer level}) \qquad \textbf{(equation 2)}$$

where E (first e^- outer level) is the energy level of the electron that fills the core-hole and E (second e^- outer level) is the level energy of the electron escaping from the sample. Photoelectrons and Auger electrons can be both used in XPS analysis. The processes of photoelectron and Auger generation are schematized in figure 1.

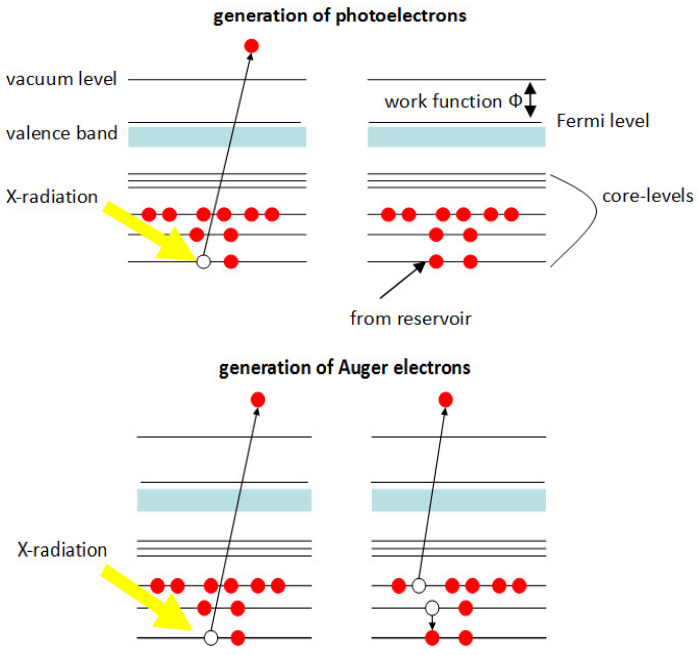

Fig 1. Scheme of the photoelectron and Auger electron generation.

The kinetic energy, KE, can be measured by using standard electron energy analyzers, and it can be used to obtain the characteristic BE of the core levels for a specific element. The obtained BE, however, is not completely determined by the chemical nature of the investigated element, in fact, the particular chemical environment can also influence the spectrum of the core-levels, inducing energy displacements of up to some eV. These are known as chemical shifts and they are used to identify the chemical state of the element under consideration. In this way, XPS analysis allows pointing out the non-equivalence of atoms due to different oxidation states or to a different chemical environment. The area under a peak is interpreted as a measure of the relative amount of the element in the sample surface.

The instrument is equipped with a detector or energy analyzer placed above the sample able to separate emitted electrons depending on the kinetic energies through an electric field. The electric field forces electrons to follow different paths according to their velocities. The type of analyzer used in these experiments is called spherical analyzer (fig 2) and consists of two concentric hemispheres set to different potentials.

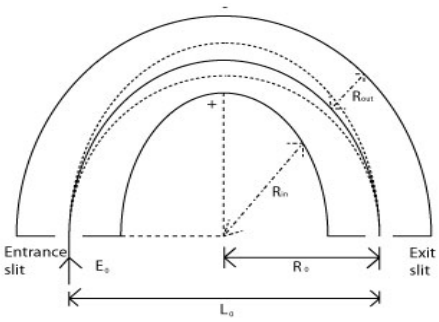

Fig 2. Scheme of a spherical analyzer. The electrons entering the analyzer through the entrance slit will follow different trajectories in the electric field of the analyzer, in such a way that only those with a particular kinetic energy can reach the exit. Changing the electric field within the analyzer allows us to investigate the number of photoemitted electrons for different kinetic energies.

XPS is a surface sensitive technique because only those electrons generated near the surface escape and are detected. It is well known that photoelectrons can be affected by inelastic collisions within the sample's atomic structure. Thus, those photoelectrons originating more than 2 nm below the surface, rather than providing direct information about the BE level from which they are extracted, they contribute to the so-called background of the measurement. This has to be underlined since the objects of this investigation consist in NPs whose size varies from 6,5 to 13,5 nm approximately. The intensity of the signals coming from the surface should be corrected to take into account the different ratio between volume and surface atoms for different sizes and shapes of NPs.

As it has already mentioned in the introduction, XPS measurements have been performed in our laboratory (section 3.3.1) and in a synchrotron facility (section 3.3.2). The radiation energy, as well as the set-up are different for the two X-ray spectrometers.

Different photon energies affect in different ways to the obtained binding energies for photoemitted and Auger electrons. While the kinetic energy of the photoemitted electrons depends linearly of the incoming photon energy, the kinetic energy of the Auger electrons remains unchanged. By transforming kinetic energies into binding energies according to equation (1), which is only valid if the electrons are photoemitted, one obtains that binding energies of photoemitted electrons do not depend on photon energy, while Auger-related peaks shift linearly in energy with the photon energy. Thus, changing the photon energy is useful in those situations in which there is an overlap of Auger and photoemission peaks. In our case this turns out to be relevant for the investigation of the P and Cl peaks. The X-ray radiation used for the experiments shown

in section 3.3.1 is generated by an Al anode which photon energy is 1486,6 eV. Using this photon energy, Auger peaks of Se are detected in the same range of binding energies as P 2p (Ref 6). On the other hand, when the X-radiation energy can be set to 620 eV such kind of Se transitions appear in a completely different range of binding energies, what allows us to obtain direct information about P.

Finally, the surface sensitivity of the XPS measurements is also known to depend on the geometry of the sample and the analyzer. As reported in the literature (Ref 7) the intensity between the element signals varies with the angle of electrons detection, while the energy position of the peaks is not affected. As figure 3 shows, XPS measurements on oxidized aluminium (Al) show that for an angle of 7,5° between detector and surface, Al 2s signal from Al metal (coming from the bulk) and Al oxidized (coming from the surface) have the same magnitude while for 51,5° the signal from oxide is hardly visible. The reason is that decreasing the exit angle of the photoemitted electrons (the angle between the surface and the electron trajectories that reach the analyzer entrance) implies that photoelectrons originated in the bulk have to travel a larger distance within the solid and, thus the likelihood of inelastic scattering increases. The intensity of the peaks corresponding to photoelectrons generated at the surface, however, is not affected. Thus, for investigation of surface species, the use of grazing geometries is advisable.

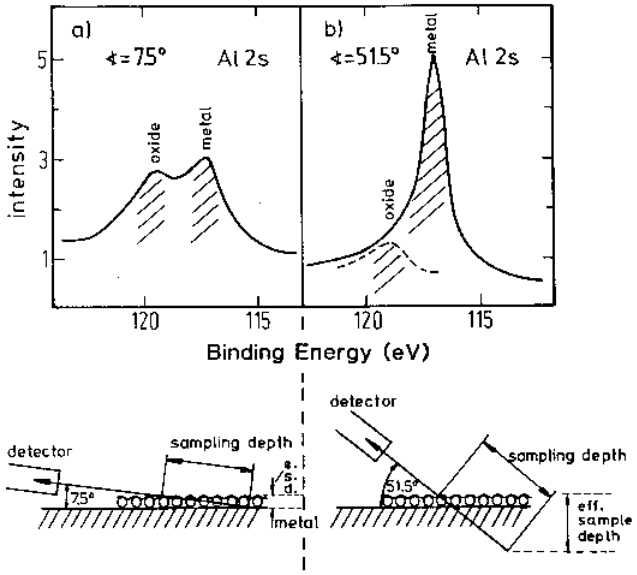

Fig 3. Surface sensitivity of XPS demonstrated by changing the electron detection for oxidized surface Al (Ref 7).

Figure 4 depicts a scheme of the geometry of XP spectrometers used. The first set of data (section 3.3.1) was obtained with a photon energy of 1486,6 eV and an angle between the substrate in which samples were deposited and the analyzer of about 60°. The second set of data (section 3.3.2) was obtained in a synchrotron facility with photon energy of 620 eV and an angle between the surface sample and the analyzer of 90°.

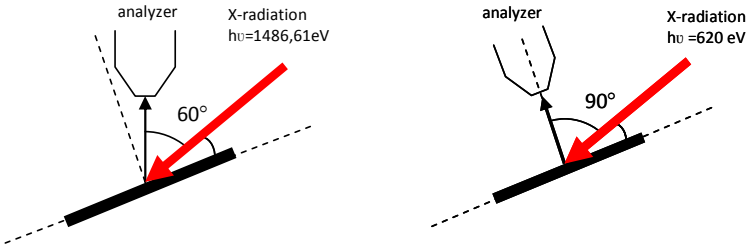

Fig 4. Scheme of the geometry of the two types of XPS employed.

3.3 Pyramids vs rod-like CdSe NPs

The presence or the absence of Cl, while CdSe NPs synthesis takes place, leads to different final NP shapes. In the presence of Cl the result of the synthesis leads to pyramidal NPs, otherwise (in absence of Cl) to rod-like NPs. Samples of pyramidal and rod-like CdSe NPs grown on HOPG by the pot-deposition method were investigated. The surface chemical changes related to the morphological change of NPs will be shown in the following sections. Synthetic processes are fully described in chapter 5. Figures 5 (a) and (b) show SEM images of pyramids and rod-like CdSe NPs grown on HOPG used as samples for XPS experiments. TEM images of free pyramids and rod-like nanoparticles obtained from the same synthesis are also shown in (c) and (d) respectively.

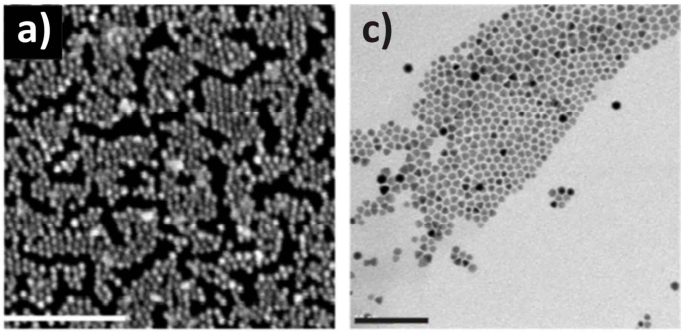

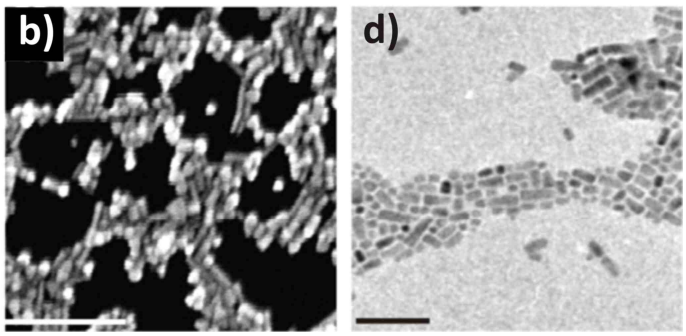

Fig 5. Comparison between pyramids and rod-like CdSe nanoparticles: SEM image of pyramids (a) and rods (b) NPs grown on HOPG by pot-deposition method, reference bar 200 nm. TEM image of pyramids (c) and rod-like (d) NPs from the same synthetic bar 100 nm.

To establish which XPS results regarding surface elements can be attributed to the differences between the surface chemical composition of pyramidal and rod-like NPs pot-deposited on HOPG, some consideration about the characteristic of the samples under study has to be done. Figure 6 depicts a scheme of pyramidal CdSe NPs pot-deposited on the HOPG, valid also for similar samples of rod-like NPs. A film of toluene left by the post synthetic treatment (indicated with a blue strip) might cover all the surface, NPs islands and non-covered HOPG. Thus, it approximately gives an equal contribution, in terms of C amount, among all the samples. NPs attached to the HOPG are composed by a CdSe core and by an organic shell as indicated in the figure. As already discussed in chapter 2, NPs organic ligands (indicated in black) and a certain amount of organic non-capping NPs molecules (indicated in red), whose presence cannot be excluded in the interstices between NPs, compose what it has been called the NP organic shell for this kind of samples. According to the XPS results reported in chapter 2, the contribution of non-capping NP molecules including TOPO, free ODPA, and physisorbed TOP on the non-covered HOPG can be neglected. This means that the P contribution in the XPS measurements arises basically from the organic shell composed mainly by ODPA related species anchored to the NPs surface (capping Cd sites) and a potential contribution of TOP (capping Se sites). Assuming that non-capping NPs molecules within the organic shell give approximately an equivalent contribution to all the samples, the differences in the P spectra of pyramids and rod-like CdSe NPs can be attributed to the differences in the organic ligands. Later on, it will be shown that similar differences found in the O signals could be attributed to differences in the organic ligands. Moreover, in chapter 4 it will be investigated the effect of annealing treatments, revealing that while the C-sp3 signal is clearly affected by gentle annealing to 80°C, removing significant amounts of Cl or oxygen requires higher energies, in good agreement with the idea that all the molecules containing such elements are mostly chemisorbed on the NP surface.

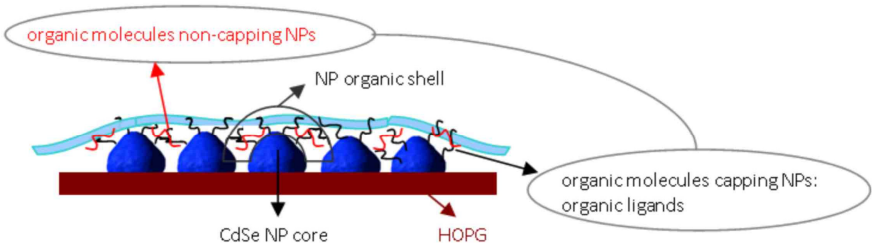

Fig 6. Scheme of CdSe NPs pot-deposited onto HOPG sample.

The hypothesis according to which non-capping NPs molecules within the organic shell give approximately an equivalent contribution to all the samples, is supported by the experimental results reported in this chapter and it will be discussed later on.

3.3.1 XPS results: photon energy of 1486,6 eV

Figure 7 (a) shows the comparison between XPS survey spectra of pyramids and rod-like NPs pot-deposited onto HOPG (black and gray line respectively). The survey shows contributions of C, coming from the substrate and organic compounds, Cd and Se from the core of NPs, P from NP organic shell, and O. The full XPS survey spectra show very similar profiles except for the Cl 2p region. In fact, as shown in the comparison between the HR spectra of the Cl 2p region of the two samples, figure 7(b), the presence of Cl at 199 eV BE is visible only in the spectrum of pyramids, which were synthesized in the presence of DCE. Thus, the first remarkable difference between the two samples is the presence of Cl in pyramids. Experimental data proving that Cl is not adsorbed onto HOPG surface will be discussed in chapter 4.

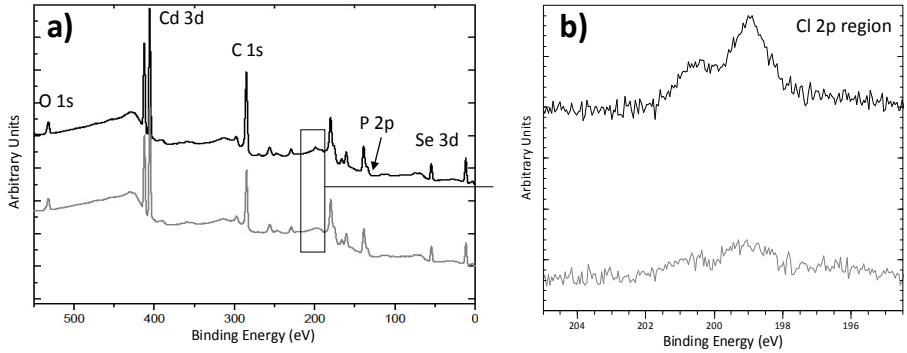

Fig 7. (a) XPS survey spectra of pyramid (black line) and rods (gray line). (b) XPS spectra corresponding to the Cl region of pyramids (black line) and rods (gray line). Spectra of (a) have been obtained with an energy pass of 50 eV and spectra of (b) with an energy pass to 10 eV.

In the following, it will be shown evidence to support the fact that Cl is chemisorbed on the surface of the NPs, which results in a modification of the organic ligand shell, while the elements that constitute the bulk of the NP cores (Cd and Se) remain basically unaffected by the presence of Cl.

Changes in elements composing the core: Se and Cd

The study of Se and Cd signals was carried out by comparison with bulk wurtzite CdSe, electronic grade (99,99%), as reference. Figure 8 depicts the survey spectra of pyramids, rod-like NPs (red line and green line respectively), and CdSe bulk (violet line). The spectra are essentially dominated by Cd and Se photoemission and Se Auger signals (see Ref 6). The only major difference is the high intensity of the C peak in the deposited samples due to contributions from the HOPG substrate and the organic molecules.

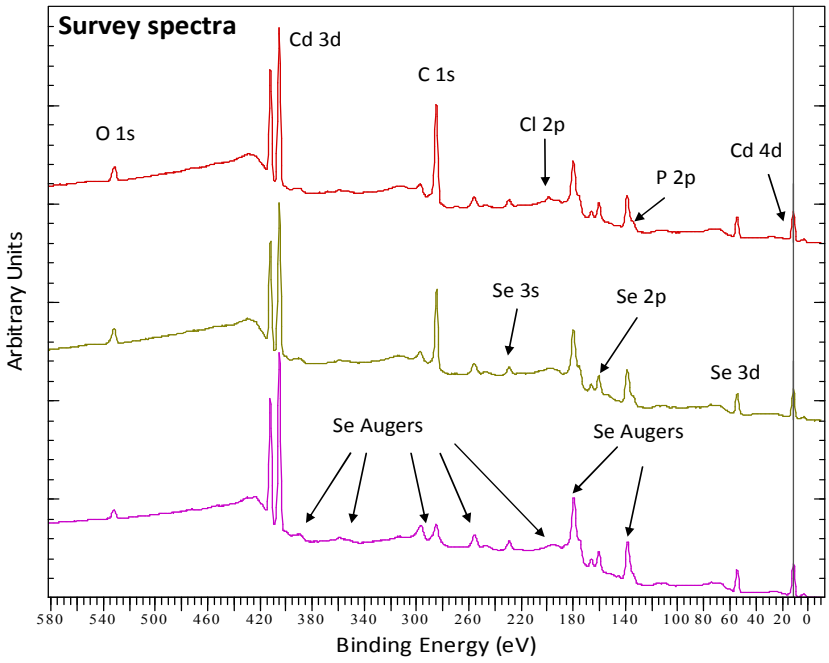

Fig 8. Survey spectra of pyramids (red line), rods (green line) and bulk CdSe (violet line). A black lin represents the BE at which all the spectra have been normalized (Cd 4d in this case). 50 eV energy pass.

Figure 9 shows the part of the survey spectra of figure 8 corresponding to the Se 3d region. The three spectra present the Se 3d peak at about 55 eV and a region between 65 and 80 eV corresponding to Se background signals. A small signal can be detected in the bulk CdSe as well as in pyramidal CdSe NPs at 60 eV approximately, ascribed to SeO_2 (Ref 8). This means that the surfaces of the crystallites in the CdSe commercial powder

are slightly oxidized in spite of the high purity degree of the samples. However, the SeO_2 signal is not present in the rod-like CdSe NPs spectrum. The lack of oxide component in the rod-like NPs demonstrates that the presence of the organic ligands effectively passivates the NP surface, protecting it efficiently against surface oxidation. As it will be discussed later, the presence of a small oxide component in the pyramid-like sample is related to the destabilizing effect that Cl has on the ligand shell of the NPs.

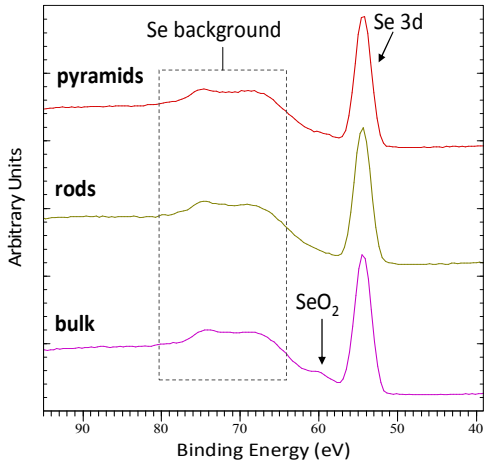

Fig 9. Part of spectra shown in figure 9 where the signals of Se Auger, Se 3d and SeO_2 are indicated.

High-resolution XPS spectra of the elements corresponding to the core of the NPs are also very similar in the three studied cases, and only small differences can be found in the width of the peak, evaluated as full width at half maximum (FWHM). Differences in the width might be related to the presence of defects in the crystal lattice, contaminants or to the different environment corresponding to the atoms at the surface. In this respect, the larger amount of surface atoms for NPs as compared to bulk CdSe powder leads to the expectation that the peaks be wider for NPs.

Figure 10 shows Se 3d spectra of pyramids, rod-like NPs, and bulk with their relative fits. Intensity ratios between the different spin-split 3d components have been taken from the literature (Ref 9). The table on the right side of the figure summarizes the FWHM of Se 3d components of the three samples. Notice that, in spite of our expectation, the difference between pyramids and rods FWHM is very small while the FWHM of bulk is much broader.

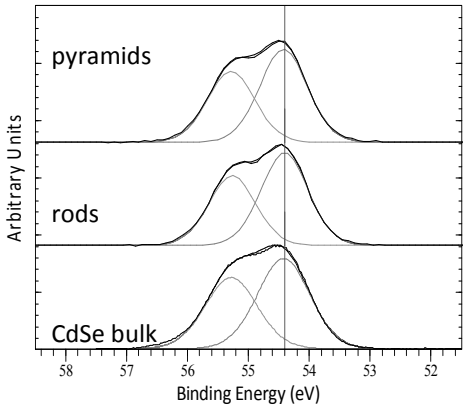

samples	FWHM (eV)
pyramids	0,91
rods	0,90
bulk	1,01

Fig 10. Se 3d deconvoluted spectra of pyramids, rods and bulk. Table on the right indicates the values of FWHM of the components. 10 eV energy pass.

Figure 11 depicts the Cd 3d spectra of pyramids, rod-like NPs, and bulk CdSe respectively. Cd 3d peaks were fitted with just one component whose relative FWHM has been reported in the table. The FWHM of Cd 3d peak of CdSe bulk appears broader with respect to pyramids and rod-like NPs similarly to what found for the Se peaks.

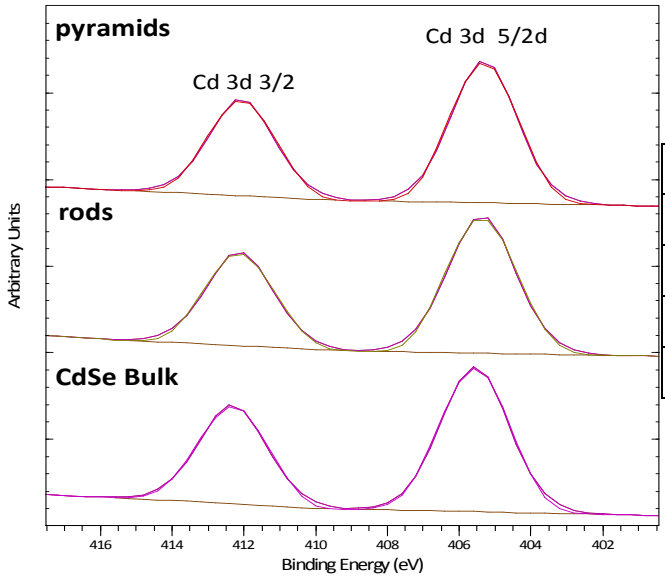

samples	FWHM (eV)
pyramids	2,15
rods	2,20
bulk	2,22

Fig 11. Spectra of Cd 3d peaks of pyramids (upper line), rods (central line), and bulk samples (lowest line) with relative fits. The table summarizes the values of FWHM found for the Gaussian functions used. 50 eV energy pass.

CdSe bulk is composed by powdered CdSe microcrystals whose purity is evaluated in 99,99%. A contribution of oxidized metal in bulk spectra is expected because surface metals are directly exposed to oxygen and not passivated by the organic ligands. But the ratio volume/surface atoms is much higher with respect to that of NPs which are nano-sized rather than micro-sized. Hence, in a XPS spectrum the contribution of surface atoms must be much higher in NPs than in bulk. The narrower peaks for NPs must thus imply that the chemical purity of the CdSe composing the NPs must be higher than that of the electronics grade CdSe. On the other hand, comparison between pyramidal and rod-like NPs does not show significant differences in the core levels of the elements present at the core of the NPs, showing that Cl probably has not been incorporated as a bulk impurity, only at the surface of the NPs.

Cl analysis

It has been thus established that Cl is incorporated in the organic shell of NPs. Some question arises to understand the nature of the bond between Cl and the NP surface. In fact, Cl atoms could be weakly bound trough Van Der Waals interactions to the organic ligands or chemisorbed to the different CdSe facets at the surface. To check whether Cl is chemically bound to the surface of pyramids, annealing treatments of the samples have been performed. Figure 12 reports the Cl 2p spectra of pyramids at demonstrating that Cl is still present after heating treatments at 150°C or 200°C for two hours. At these temperatures all those elements weakly bound to the sample are likely totally desorbed, as will be shown also in Chapter 4. These data prove that at least part of Cl is strongly interacting with the surface of pyramids.

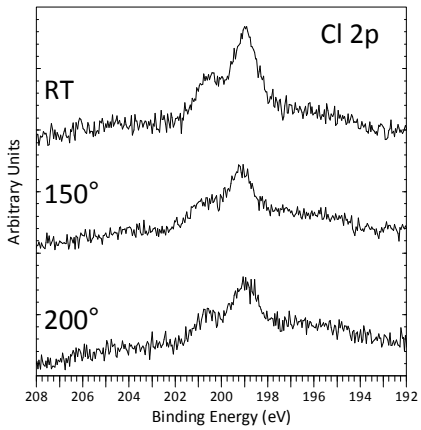

Fig 12. Cl 2p spectra of pyramids at room temperature (first line) and after the sequence of annealing 150°C (second line) and 200°C (third line). Energy pass has been set to 10 eV.

Figure 13 shows the HR Cl 2p spectrum of pyramidal NPs with relative fit. The right proportions of Cl 2p peak (1/2, 3/2) have been found in literature (see Ref 9). The spectrum is positioned at 198,95 eV and it is comparatively broad (1,27 eV) with respect to the Se 3d (0,9 eV) performed with the same energy pass (otherwise the FWHMs cannot be comparable). The strong broadening is typical in the case of elements binding to the surface due to different surface adsorption sites in the different exposed facets of the CdSe core. This consideration is valid also for P and O.

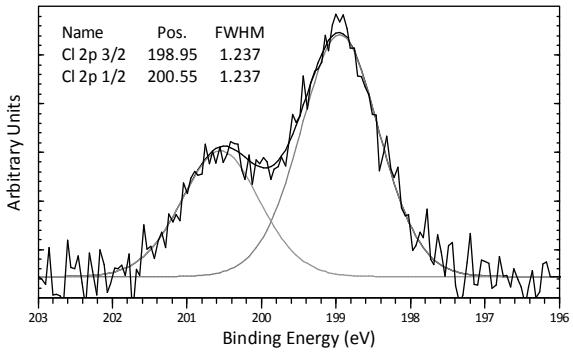

Fig 13. HR spectra of Cl 2p peak of pyramids with relative fits. FWHMs and component BE positions are indicated in the graphs. 10 eV energy pass.

The presence of Cl chemisorbed on the NPs surfaces should have important effects on the nature of the organic ligand shell. In the next section we will investigate the effect that Cl chemisorption has on the chemical nature of the organic ligand shell.

Changes in elements composing organic shell C, P and O

The organic shell for CdSe NPs consist basically of phosphorous, carbon (with sp^3 hybridization) and oxygen. Figure 14 depicts the C 1s spectra of pyramids and rod-like NPs. C 1s peaks were deconvoluted in C-sp^2 and C-sp^3 components, arising from the HOPG substrate and the organic ligands, respectively. The width of the C-sp^2 and C-sp^3 components is very different, being much wider the component corresponding to C-sp^3. This must be related to the different C-sp^3 species found in the organic ligands and possibly to the disorder at the organic shell. The position of C-sp^2, the signal arising from C atoms composing the HOPG substrate, is identical in pyramids and rods while the C-sp^3 component of pyramids is displaced 0.15 eV towards higher BE respect to the rods.

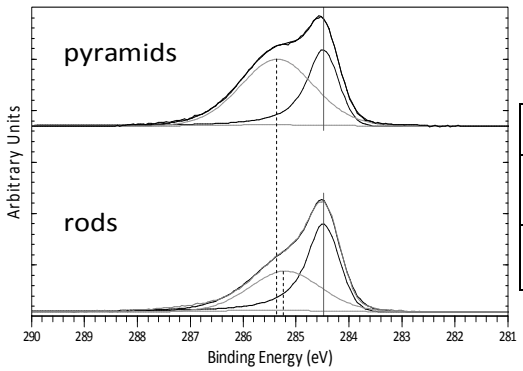

samples	C-sp^2	C-sp^3
pyramids	284,5	285,35
rods	284,5	285,20

Fig 14. HR (10 eV energy pass) C1s spectra of pyramids (first line) and rods (second line) CdSe NPs. Vertical lines indicates the centre of C-sp^2, vertical dashed lines the centre of the C-sp^3 components. The table on the right side summarizes the BE position of the components.

The signal of P, coming from the NP organic shell has to be carefully analyzed. In fact, as discussed before, for a photon energy of 1486.6 eV, the Se LMM Auger transitions appears over the same energy region as the P 2p core levels. To discern the P 2p signal coming from the nanoparticles, Se L23d8 Auger peak of CdSe bulk was subtracted to the P region spectra of pyramids and rods. This procedure might affect the experimental data but, as will be shown in Section 3.3.2, experiments carried out with different photon energies (and for which this procedure is not necessary as there is no overlap with the Auger Se peak) show exactly the same behavior.

Figure 15 shows the comparison between the P 2p spectra corresponding to pyramidal NPs (black points) and rod-like NPs (gray points) obtained as described above. The P 2p peak of pyramids is centred at 133 eV and shifted 0.5 eV towards lower BE with respect to the centre of the peak corresponding to rod-like NPs. The shape of the peak also changes. While the P 2p peak corresponding to rod-like NPs appears symmetric, that corresponding to pyramidal NPs presents a clear asymmetry. This indicates that P shows different chemical environments in pyramids and rod-like NPs.

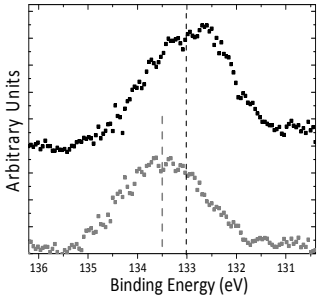

Fig 15. Comparison between pyramids (black line), rods (gray line) P signals upon Se Auger signal subtraction.

The peaks for oxygen need to be analyzed carefully. Indeed, oxygen might arise from ODPA or ODPA related species, but it may also come from a partial oxidation of the CdSe surface (as described for Se in pyramidal NPs) or other contaminants possibly adsorbed during exposure to the atmosphere (mostly water). However, from a comparison between the HR XPS O 1s spectra of CdSe bulk, CdSe NPs, and their relative fits, one of the components found in the rods O 1s spectrum could be assigned to a contribution arising from ODPA species. The detection of this component marks also a difference between the two types of NPs.

In figure 16, the O 1s spectrum corresponding to bulk CdSe was fitted with two components centred to 531,8 eV and 533,5 eV respectively. Two components for pyramids O 1s were also used, whose position are slightly shifted toward lower BE (531,6 eV and 533,3 eV respectively). The intensity ratio is however not the same as for bulk CdSe, which might be attributed to different chemical species being present at pyramidal NPs but not at the CdSe commercial powder surface, like O species contained in the organic shell.

The situation is different for rod-like NPs. Deconvolution of the O 1s spectrum in this case needs three components centred to 531,5 eV, 532,5 eV and 533,5 eV respectively. The new component at 532,5 eV must be attributed to the organic ligand shell, as any other source of oxygen should affect pyramidal and rod-like NPs alike. The central O 1s component at 532,5 eV in pyramidal NPs seems to be lost or it is small enough to be incorporated in the fit with only two components. The fact that the component centered at 533,3 eV is higher and shifted toward minor BE with respect to the highest BE component of the bulk, suggests that this component in pyramids arises from a contribution of organic ligand shell.

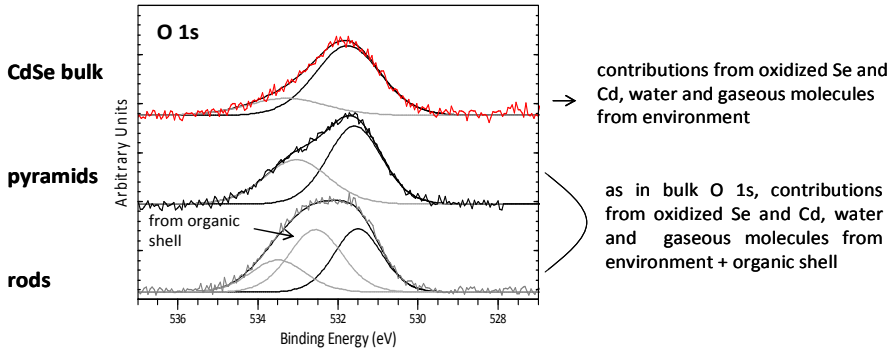

Fig 16. HR XPS O 1s spectra of CdSe bulk (red line) pyramids (black line) and rods (gray line) with relative fits. 10 eV energy pass.

Quantitative analysis

So far, it has been established that Cl is chemisorbed at the surfaces of the pyramidal NPs, thereby changing the chemical environments of the molecules composing the organic shell. There are several scenarios that would permit such chemisorption. First, if the initial ligand shell was not compact, Cl could get adsorbed at the spaces between the organic molecules. On the other hand, for very compact ligand shells, the only way in which Cl could get incorporated is by displacing some of the ligands out of the shell. Finally, if Cl adsorption was more energetically favourable on specific locations of the unit cell, the adsorption might lead to a surface reconstruction. In order to investigate such possibilities, the relative intensities of the different elements were analyzed for pyramidal and rod-like NPs.

Quantifications are computed dividing the row areas of the each peak to that of Cd, that is, it was calculated the *amount* of each element simulating the case in which both kinds of NPs contain the same amount of Cd.

Table 1 resumes the values obtained for pyramids and rod-like NPs. The errors associated were computed as the % of the standard deviation respect to the area of the signals. The amounts of C-sp3, P and O differ from pyramids to rods, being smalle for pyramids than for rods. An interesting data is the one concerning the proportion between Cd and Se. Rods seem to show a high amount of Se with respect to pyramids. Since pyramid and rod-like NP cores have to give the same contribution of Cd and Se one could attribute this difference to the morphology of the surface exposed to X-radiation. This result must however be taken with caution, since NPs surface is capped by organic ligands, and Cd and Se passivated or non-passivated by ligands will give a more or less attenuated XPS signals. Therefore the differences in the ratio Cd/Se cannot be univocally related to a different surface Cd/Se ratio and, thus to a different surface stoichiometry.

Elements	**Amount per Cd unit Pyramids**	**Error %**	**Amount per Cd unit Rods**	**Error %**
C-sp^3	0,375	3,8	0,279	3,1
Cd 3d	1	0,6	1	1,1
Se 3d	0,118	6,9	0,128	7,3
O 1s	0,122	5,1	0,172	4,8
P 2p	0,018	15,2	0,021	13,8

Cl 2p	0,036	7,1		

Tables 1. Values of the amount of elements per Cd unit for pyramids and rod-like CdSe NPs.

Table 2 summarizes the BE of the maximum of the element signals. The calibration was performed by taking a BE of 284.5 eV for C-sp^2. BE positions of Cd and Se (core elements of NPs) are the same for pyramids and rods. Pyramids C-sp^3 is shifted 0.15 eV toward higher BE with respect to rods. The maximum of pyramids P 2p is shifted 0.8 eV with respect to the maximum of rods P 2p signal (while the Δ eV between the centre of the two signals is 0,5 eV). Pyramids O 1s signal is shifted about 1 eV toward minor BE respect to rods O 1s signal.

Elements	BE positions Pyramids (eV)	BE positions Rods (eV)
HOPG	284,5	284,5
C-sp^3	285,35	285,22
Cd 3d 5/2	405,56	405,56
Se 3d 5/2	54,46	54,46
O 1s	531,67	532,25
P 2p	132,72	133,5
Cl 2p	198,96	

Table 2. BE of the maximum of all the signals.

Concluding, the results shown in this section prove that:

- the presence of Cl chemically bound to the NPs was detected in pyramids.

- Between rods and pyramids, the elements composing the organic shell differ in relative amount and in BE.

Hence, the process of shape modification from rods to pyramids is accompanied by modifications of the CdSe NP surface (core surface and organic ligands). This means that, at least, part of the Cl atoms is chemically bound to the NP surface inducing a reorganization of the surface elements what leads to the detection of differences in the XPS signals in terms of BE, shape and relative amount of the different elements.

3.3.2. Synchrotron results: photon energy of 620 eV

In the previous section it was shown that Cl is being incorporated in the organic shell of CdSe NPs, thereby changing the chemical nature of such layer. We have however found problems with the analysis of several of the interesting peaks corresponding to the elements at the NP surface, since there are many Auger transitions of the Se atoms that appear at different energy ranges, very often overlapping with the peaks of interest. Moreover, for a photon energy of 1486.6 eV, the kinetic energy of the photoemitted electrons is high for a large range of binding energies, so that the contribution from the bulk is large compared to the contribution of the surface atoms. Decreasing the photon energy should allow to move towards the minimum in the universal mean-free path curve, thereby enhancing the intensity corresponding to surface elements. For these reasons experiments at the synchrotron facility BESSY, using a photon energy of 620 eV were performed.

Four types of samples were investigated: pyramidal and rod-like CdSe NPs grown on HOPG by the pot-deposition method produced in two different laboratories; the chemical laboratory at IMDEA Nanoscience and the laboratories of the Institute of Physical Chemistry at the University of Hamburg.

Figure 17 shows the samples of CdSe NPs pot-deposited on HOPG used in HR XPS experiments. Figure 17 (b) and (d) reports the samples produced in Madrid and figure 17 (a) and (c) the samples produced in Hamburg; “H samples” and “M samples” stand for samples produced in Hamburg and samples produced in Madrid, respectively. This terminology will be used in throughout this chapter.

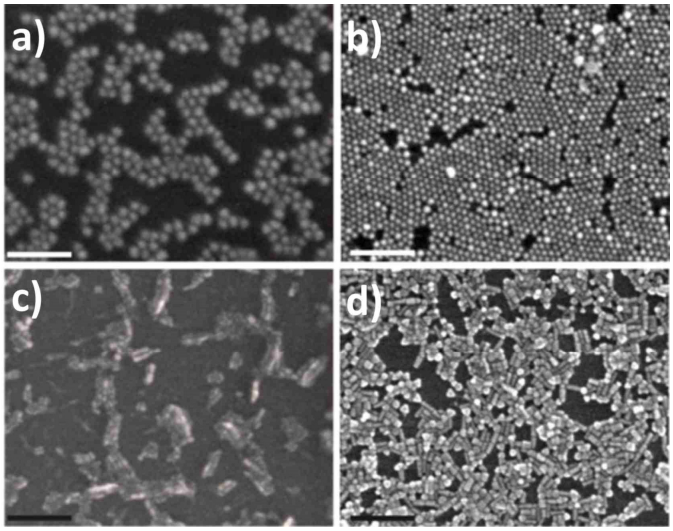

Fig 17. Pyramids and rod-like CdSe NPs pot-deposited onto HOPG produced in Hamburg "H samples" (a) and (c). Pyramids and rods CdSe NPs pot-deposited on HOPG produced in Madrid "M samples" (b) and (d). Bar reference size in (a) and (b) is 100 nm, in (c) and (d) is 200 nm.

It has to be pointed out that the samples were produced in different laboratories using the same recipes and following the same post-synthetic treatments. The direct comparison will give information about the reproducibility of the results obtained in section 3.3.1 and more in general to the reproducibility of these kinds of samples.

Core elements analysis; Se and Cd

As expected, no significant differences were found for the elements that constitute the core of the NPs, Se (Figure 18) and Cd (Figure 19). Binding energies and peak shapes remains basically the same, and only the width of the peaks is different due to the more monochromatic nature of the synchrotron X-ray beam. As for the experiments carried out for with a photon energy of 1486,6 eV, the width of the Cd peaks seems to decrease slightly (about 0.1 eV) from the rod-like to the pyramidal NPs spectra.

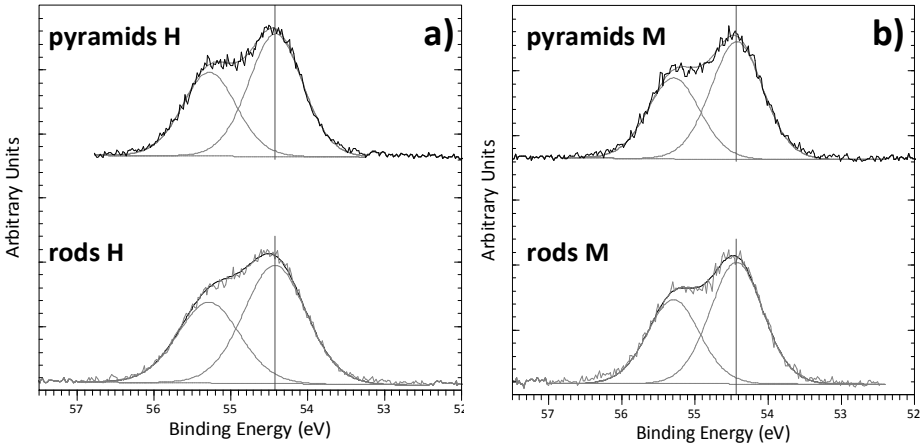

Fig 18. Se 3d HR spectra of H samples (a) and M samples (b).

Figure 19 shows HR Cd 3d spectra of the samples with the relative fits. The values of FWHM and the BE position are indicated in the graphs. In the case of Cd, the data concerning the FWHM of the peaks prove that Cd signals in rods are actually broader than that of pyramids for both H and M samples confirming the results reported in section 3.3.1.

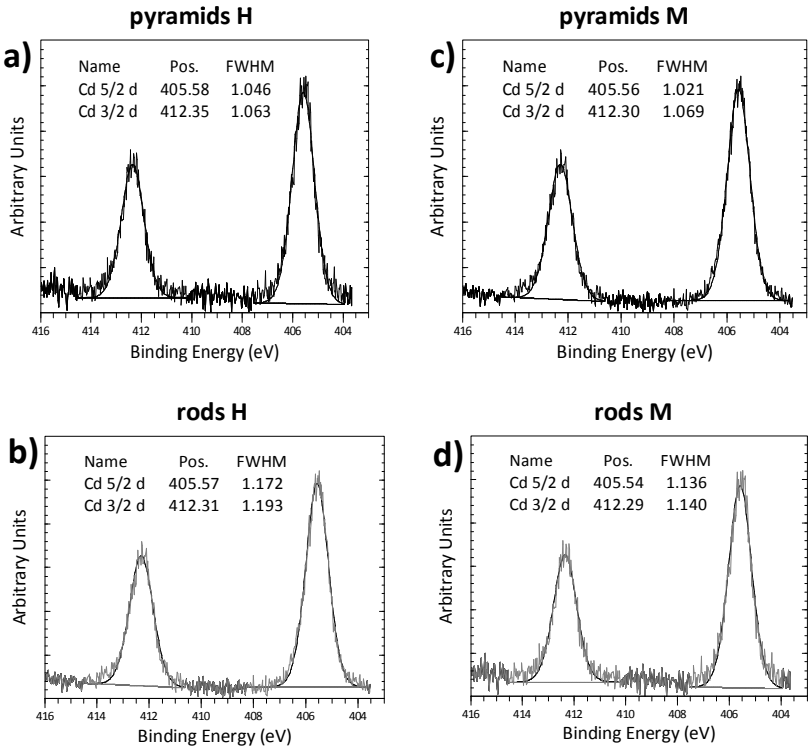

Figure 19. HR Cd 3d spectra of pyramids H (a), rods H (b), pyramids M (c) and rods M (d) with the relative fits. BE positions and FWHM are indicate in the graphs.

Cl analysis

The Cl spectra in pyramidal NPs do not change in any noticeable way, apart from the lower peak widths. Figure 20 shows Cl 2p peaks of pyramids H and pyramids M ((a) and (b) respectively). BE positions shown in the graphs are essentially the same for both signals and for Cl 2p spectrum in section 3.3.1.

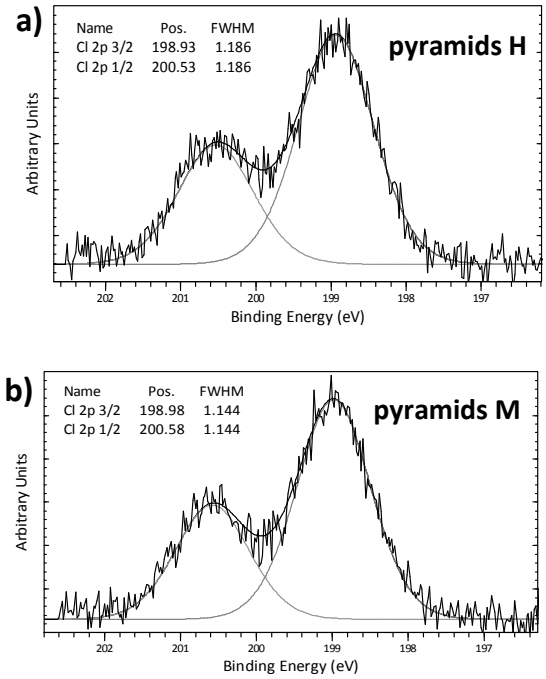

Fig 20. Spectra of Cl 2p peak of pyramids H (a), pyramids M (b) with relative fits. FWHMs and BE positions are indicated in the graphs.

Analysis of the P signal

The main new contributions arising from the use of synchrotron radiation spectra when compared to the experiments performed with a photon energy of 1486,6 have to do with the spectra concerning the organic shell. In particular, the P peak, which is now directly observable without the need to undergo the normalizing procedure, can be decomposed into different components. The identification of such components, as it will be further shown, is the key to understand the role of Cl on the modification of the organic ligand shell. Moreover, in the following chapter this knowledge will be used to understand the modification that Cl causes in the interaction to carbonaceous surfaces.

Figure 21 (a) and (c) shows HR spectra of P 2p signal of pyramids and rods H and figure 21 (b) and (d) show the P 2p spectra relative to pyramids and rods M. P 2p signals were deconvoluted in two P 2p peaks; one at lower BE (black lines couple) and one at higher BE (grey lines couple) which proportions (2p 1/2 and 3/2) were found in the literature (see Ref 9). The reasons for this choice are the following:

- P 2p spectra of rods in both cases (H and M) appear rather symmetric. Hence, having to use the correct asymmetric shape for a single P 2p component, it is necessary to perform the fit with at least two of them.

- The overall width of the P 2p peaks of figure 22 are very similar for rods and pyramids, suggesting that also pyramids will require two components to fit.

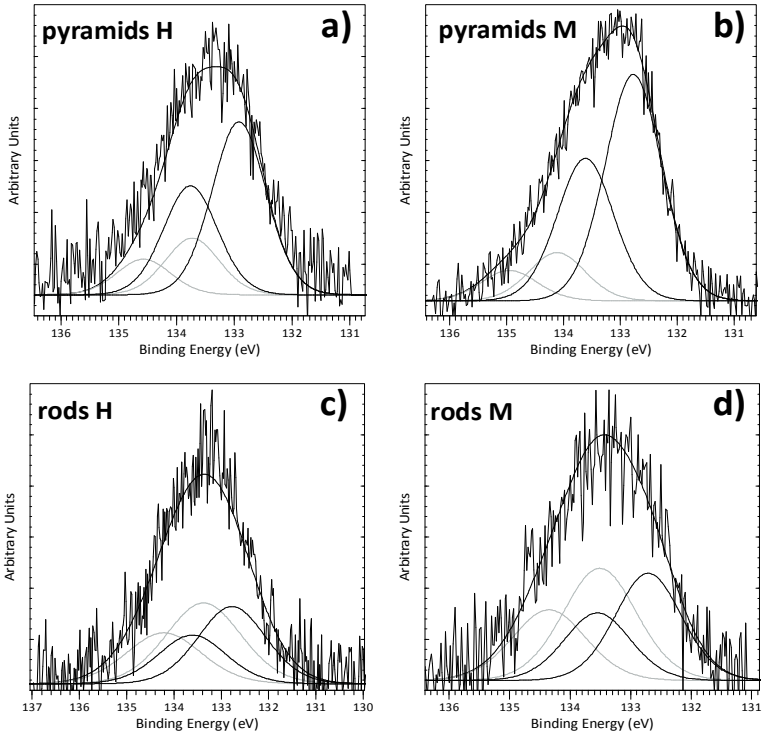

Fig 21. HR XPS spectra of P 2p signals of pyramids and rods H (a) and (c) and pyramids and rods M (b) and (d) and their relative fits.

The main conclusion of this analysis is that, while the phosphorous signal at the rod-like NPs can be understood as arising from two components equally populated, for pyramidal ones, the component at higher binding energy is strongly suppressed and slightly shifted towards higher binding energies. Table 5 summarizes the positions of the highest and the lowest BE P 2p 3/2 components. In both cases, for H and M samples, the energy separation between these two components (Δ BE) is larger in pyramids than in rods. The relative weights were found as the percent of P 2p peak intensity corresponding to each component. The relative weights of the two P 2p components and the maximum of the spectra are reported in the table 6.

samples	P 2p 3/2 BE (eV)		Δ BE (eV)
	highest BE	lowest BE	
pyramids H	133,73	132,92	0,81
rods H	133,38	132,78	0,6
pyramids M	134,11	132,77	1,34
rods M	133,51	132,71	0,8

Table 5. P 2p 3/2 BE position and Δ eV between the two components of spectra shown in figure 22.

samples	% highest BE P 2p	% lowest BE P 2p	spectra max (eV)
pyramids H	24,68	75,31	133,2
rods H	53,78	46,22	133,4
pyramids M	17,63	82,37	132,9
rods M	53,8	46,2	133,4

Table 6. Weights of P 2p components and BE position of the maximum of the spectra.

The high reproducibility of these data can be considered as an experimental prove of the hypothesis introduced in section 3.3 according to which non-capping NPs molecules composing the organic shell give approximately an equivalent contribution to all the samples. In fact, if the contribution of these molecules changed from sample to sample, the P 2p spectra of pyramidal H and M (or rods H and M) samples would not be in such a good agreement.

Furthermore, the change in the symmetry between P 2p spectra of pyramids and rods samples reported in this section is analogous to that found between pyramids and rods P 2p spectra reported in section 3.3.1. Figure 23 shows a comparison between the P 2p spectra of M samples and the samples analyzed in section 3.3.1 (figure 15). Notice the very good agreement of these results despite of the fact that they belong to

different samples and the spectra of figure 23 (b) were obtained subtracting the Se Auger signal superposed to the P 2p signals.

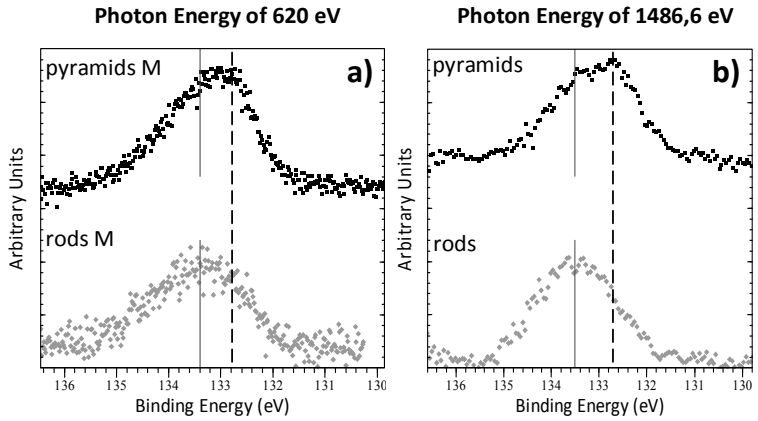

Fig 23. Comparison between P 2p spectra of M samples measured in synchrotron facility (a) and P 2p spectra of samples reported in section 3.3.1 (b). The black lines indicates the maximum of rods spectra.

Discussion

In the following it has been summarized the main experimental findings of this chapter:

1. Cl not only mediates the shape transformation by changing the reaction media, but it actually gets incorporated into the organic shell, forming strong bonds with the CdSe surface.

2. The photoemission peak corresponding to the P 2p core level is different is in binding energy and shape for rod-like and pyramidal NPs. While for rod-like NPs there seem to be two different chemical environments for the phosphorous atoms, the effect of Cl seems to eliminate one of them corresponding to the highest BE species. Similarly, for the O 1s spectra one component unequivocally ascribed to the organic shell of rod-like NPs is strongly suppressed in the spectra of pyramidal NPs.

3. C-sp^3 component is shifted toward higher BE in pyramids what reinforces the hypothesis according to which Cl is present at the NP organic shell inducing slight different chemical environments of C organic species.

Previous studies of CdSe NPs synthesized in the presence of ODPA, TOP and TOPO, have shown that the organic ligands are mainly composed of ODPA related species (Ref 10 and 11) in the form of phosphonates (Ref 12). Moreover, quantitative NMR studies of CdSe rod-like NPs showed that the organic ligands are composed of a mixture of the

so-called ODPA anhydrides, and single deprotonated ODPA (ODPA-) in a 45/55 mass ratio (Ref 13). Other authors rather claim that the organic ligands are composed by a mixture of the double deprotonated specie (ODPA2-) and anhydrides (Ref 14). The presence of TOP molecules capping NP is considered negligible since the binding energy to the Se sites is supposed to be lower than that of ODPA species bound to Cd sites. It thus natural to attribute the two components found in the P 2p peak to either deprotonated ODPA or ODPA anhydrides.

Figure 26 depicts a scheme of a neutral ODPA molecule compared to anhydrides and one of the types of deprotonated ODPA, the $ODPA^{2-}$.

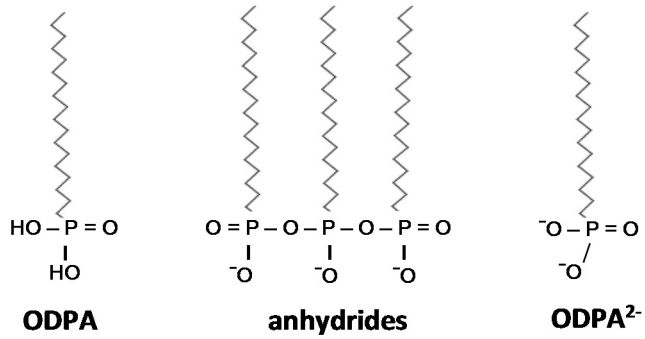

Fig 26. Comparison between neutral ODPA, anhydrides and $ODPA^{2-}$

According to the references cited above and, as already mentioned several times in this work, the phosphonate groups of ODPA species work as metal coordinating groups binding to electron-poor metal atoms (Cd in this case) providing electrons at the NPs surface. In other words, phosphonate groups of ODPA species bind to the Cd atoms via O. Considering the geometry of ODPA anhydrides (figure 26), their presence at the NP surface may be sterically impeded by the presence of Cl. This means that Cl bound to adjacent (or close) Cd atoms inhibits the anchoring of anhydrides since the O at the phosphonate groups head do not find available Cd atoms. $ODPA^{2-}$, on the other hand, can bind via two or three oxygen atoms to the surface, generating a rather strong bond, and is less sterically demanding than the anhydrides. Moreover, anhydrides form only after long reaction times, while ODPA and Cl are present in the solution from the NP nucleation, what may indicate that positions occupied for Cl are no longer available for anhydrides. Finally, Cl could also hinder the anhydride formation reaction. Any of these processes might explain the absence of anhydrides on the surfaces of the pyramidal NPs. It can be therefore attributed the component at larger binding energy to ODPA anhydrides, since its intensity decreases when Cl is present.

The absence of anhydrides might also be the origin of the shape transformation from rods to pyramids. The equilibrium shape of CdSe crystals is similar to the pyramidal morphology, and only the presence of the ligands with long alkyl chains steers the growth of rod-like NPs and stabilize anisotropic NPs. (Ref 15). The presence of ODPA anhydrides (a rather bulky ligand) may confer high stabilization to rod-like NPs impeding the shape transformation from rods to pyramids. Thus, since Cl prevents the adsorption of anhydrides, this might let the NPs relax towards their minimum energy configuration, i.e. that of a pyramidal NP.

CdSe NPs used for these XPS investigations are not subjected to the standard NP purification process usually followed for the preparation of NPs in solution, in fact, after the synthesis, the NPs pot-deposited on HOPG substrates, are just washed in several toluene baths. This washing procedure is definitely a softer treatment compared to NP purification cycles that include also the use of methanol for organic residues removal. Hence, the presence of non-capping molecules cannot be excluded. The means that the P 2p signals have to contain contributions from all the organic shell, including organic ligands and non-capping NP molecules. Since the energy position of the lowest BE P 2p component corresponds closely to that obtained for TOP molecules, detached from CdSe/ZnS NPs during the electrospray deposition (132,86 eV, see chapter 2), a certain contribution from TOP molecules non capping NPs is expected.

According to what it has said above, the highest BE P 2p component can be assigned prevalently to ODPA anhydrides and the lowest BE component to deprotonated ODPA species with a certain contribution of TOP molecules non-capping NP. Finally, the central O 1s component found in rods, which must be attributed to the organic ligands, can be assigned to the ODPA anhydrides. In fact, this component is absent or small enough to be incorporated in the fit of the pyramids O 1s spectrum. This reflects, similarly to the case of the highest P 2p BE component, the lost in ODPA anhydrides contribution in pyramids. As it has been suggested, the component cantered at 533,3 eV in pyramids may arise from a contribution of organic ligands, thus it might be related to the other type of ODPA related ligands, than to the deprotonated ODPA.species.

3.5 Conclusions

In this chapter it has been investigated by XPS the chemical composition of the surfaces of CdSe NPs with different shapes, rod-like and pyramidal. Both surfaces are (partially) covered with ODPA related organic ligands, which affect in dramatic ways the final morphology of the NPs. Thus, if the process is carried out in the absence of any chlorinated co-solvent, both deprotonated ODPA and ODPA anhydride species co-exists on the surface, and the resulting morphology is that of a rod. On the other hand, when the growth is carried out in the presence of DCE, Cl gets incorporated into the organic

shell, and prevents the adsorption of anhydrides, which renders the NPs pyramidal in shape. As it will be demostrated in the following chapters, gaining control over the chemical composition of the surface will allow to engineer different properties of the NPs, such as for example, the adhesion to C-sp2 surfaces, like CNTs, graphene, or HOPG.

References

1) X. H. Ji, D. Copenhaver, C. Sichmeller, X. G. Peng, *J. Am. Chem. Soc.*, **130**, 5726 (2008)
2) J.E. Bowen-Katari, V. L. Colvin, A. P. Alivisatos, *J. Phys*. *Chem*., **98**, 4109 (1994)
3) L.R. Becerra, C. B. Murray, R. G. Griffin, M. G. Bawendi, *J. Chem. Phys.*, **100**, 3297 (1994)
4) J. S. Owen, J. Park, P. Trudeau, A. P. Alivisatos. J. Am. Chem. Soc., 2008.
5) H. Borchert et al, *J. Phys.Chem. B*, **107**, 7454 (2003)
6) P. Weightman, E. D. Roberts and C. E. Johnson, *J. Phys. C: Solid State Phys*., **8**, L301 (1975)
7) S. Hufner, Photoelectron Spectroscopy principle and application. Springer-Verlag Berlin Heidelberg (2003)
8) M Shenasa, S. Sainkar, D. Lichtman *J. Electron Spectrosc. Relat. Phemon.*, **40**, 329 (1986)
9) J.F. Moulder, W.F. Stickle, P.E. Sobol, K.D. Bomben, Handbook of XPS X-ray Photoelectron Spectroncopy. Perkin-Elmer Corporation
10) Z.A Peng, X. Peng, *J. J. Am. Chem. Soc*., **124**, 3343 (2002)
11) H. Liu, J.S. Owen, A.P. Alivisatos, *J. Am. Chem. Soc*., **129**, 305 (2007)
12) J.S. Owen, J. Park, P.E. Trudeau, A.P. Alivisatos, *J. Am. Chem. Soc*., **130**, 12279 (2008)
13) R. Gomes et al. *J. Phys. Chem. Lett*., **2**, 145 (2011)
14) A. J Morris-Cohen, M.D. Donakowski, K. E. Knowles, E.A. Weiss, J. Phys. Chem. C, **114**, 897 (2010)
15) Z. A. Peng and X. Peng, J. Am. Chem. Soc., **123**, 1389 (2001)

Chapter 4

Adhesion of pyramidal CdSe NPs to carbonaceous surfaces and heating treatments

4.1 Introduction

The experiments shown in chapter 3 have demonstrated that the addition of DCE to the reaction media in which rod-like CdSe NPs grow leads to a significant modification of the organic shell, and to a change in the shape of the NPs. As the interaction between the CdSe NPs and solid surfaces is mediated by the ligand shell, significant differences in the efficiency of CdSe NPs decorating C-sp^2 surfaces might be expected. In the first part of this chapter, a combination of SEM and XPS measurements performed on pot-deposited NPs on HOPG with different coverage degrees are shown, demonstrating that the amount of Cl adsorbed on the NPs is related to the adhesion of NPs on HOPG and to the polydispersity degree of the samples. In the second part of this chapter, a combined study of STM and XPS on those samples presenting high coverage is reported. These experiments were carried out with the purpose of analyzing in detail the morphology of the samples and the modification of NPs upon heating treatments.

4.2 Cl per NPs versus coverage

SEM characterization

After the synthesis of pyramidal CdSe NPs pot-deposited on HOPG, the samples were observed by means of a SEM. These measurements allow for a general characterization of the NP arrangements on the HOPG surface and of the coverage. It was observed that the NPs assemble in hexagonal compact islands. However, the island size and the NP coverage differ from sample to sample. The samples analyzed in this section are shown in **fig**ure 1. SEM images of the samples are shown from (a) to (e) in order of decreasing degree of coverage, determined as the fraction of area covered by NPs in the images; 96%, 72%, 68%, 35% and 10% ± 10% The average sizes of the NPs, previously estimated from statistical measurements on TEM images, also differs among the samples, varying from 6,2 ± 0,8 nm for the smallest NPs to 13,0 ± 1,5 nm for the biggest NPs.

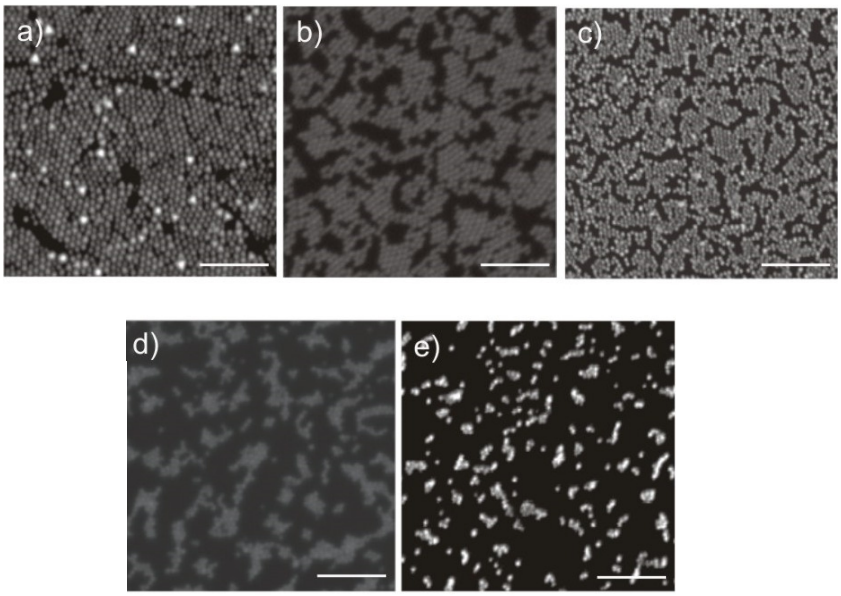

Fig 1. SEM images of pyramidal CdSe NPs grown on HOPG from a) to e) in order of decreasing coverage degree. 400 nm reference bar

Different degrees of coverage indicate different tendencies of the NPs to stick on HOPG surface, since growth temperatures and times are equal. A first explanation is that the different degree of adhesion might be related to NPs size. In fact, the interaction with the substrate is expected to be stronger for larger NPs. If this was the only explanation, larger NPs will always adsorb on HOPG faster than smaller NPs. This expectation is however not supported by our experimental observations as it will be shown along this chapter.

Apart from the NPs size, the nature of the organic ligand shell as a factor that might influence the interaction between the NPs and the C-sp^2 surface, thereby affecting the coverage. In order to identify the parameters that determine the degree of coverage, the surface chemistry of several samples presenting different coverage degree was investigated by means of XPS.

XPS results

Figure 2 (a) shows the survey spectra relative to samples corresponding to a)-e) in Figure 1, in order of decreasing coverage degree and normalized to the signal of Cd 3d. Such normalization is intended to give us information about the chemical composition of the organic shell per Cd atom, and thus, eliminate the effect that the coverage will

have on the intensities of the elements composing both the shell and the core of the NPs.

All the peaks related to the elements expected to be found in both the organic shell (namely O, C, Cl and P) and NP cores (Cd and Se) are observed. The most obvious differences among the spectra are the intensities of several peaks. As the coverage of the sample increases, the intensities of O 1s and C 1s decrease, while that of Cl 2p increases (see Figure 2 (b)). Some differences can also be found in the P 2p signal, but they are not easy to observe due to the overlap with the Se Auger peak described in the previous chapter.

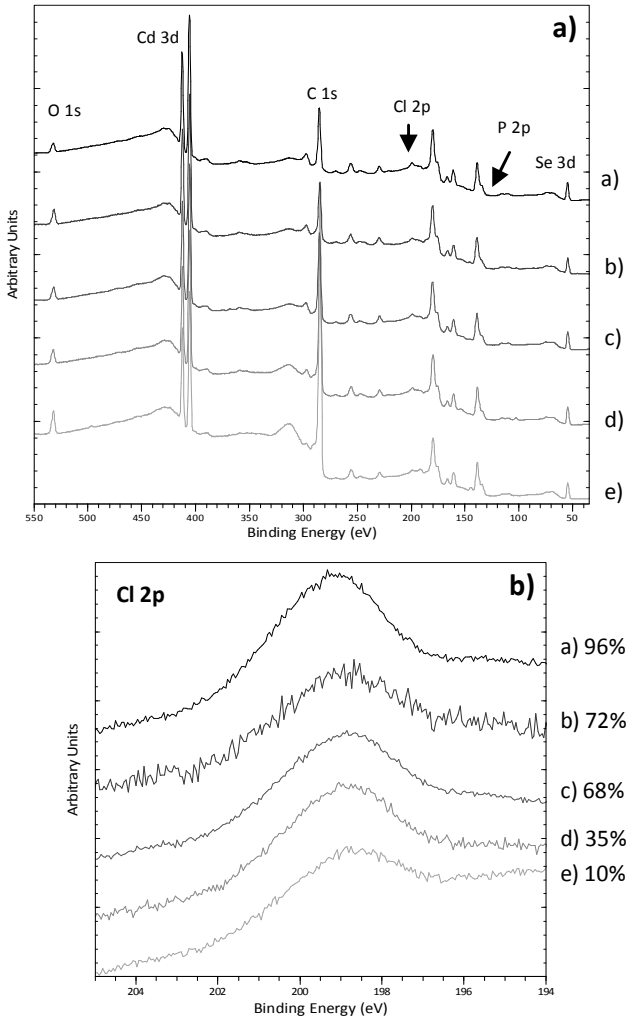

Fig 2. (a) XPS Survey spectra of samples shown in figure 1 indicated with the same labels. (b) Cl 2p regions. In (a) and (b) the spectra have been normalized to the signal of Cd 3d. hv = 1486.61 eV and energy pass = 50 eV. The coverage degrees are indicated in the figure.

The analysis of these results will start by discussing the correlation between coverage and the presence of Cl. In order to correctly interpret these data some observations have to be done. If the signal of Cl 2p arose from Cl atoms adsorbed on the HOPG substrate, a higher Cl intensity for samples with a low NPs coverage would be expected. On the other hand, if the amount of Cl adsorbed by NPs was the same for all the five samples, the Cl 2p intensity normalized to the amount of Cd would remain constant with the coverage (assuming equal NP size; the effect of the size will be addressed later). Thus, the fact that the signal of Cl normalized to Cd increases with increasing coverage seems to imply that a different amounts of Cl in the shell leads to samples with different coverage.

In order to obtain a quantitative measure of the concentration of Cl in the organic shell, the following considerations are in order. The average NP size among the five samples varies, and thus the NP surface/volume ratio, differs from sample to sample. Being Cd atoms core elements and Cl atoms mainly surface elements, the ratio Cl/Cd decreases as the surface/volume ratio decreases. To take into account this variation, the intensities of the Cl normalized to the Cd, were multiplied to the radius of the NPs. This approach simulates the case in which all the samples contain the same amount and approximately the same size of NPs and it has to be used in order to compare any other surface element signals belonging to different sized NPs. Therefore the expression:

r A (surface atoms)/A (Cd 3d) **(equation 1)**

where r is the average radio of NPs among the samples and A are the areas covered by the corresponding XPS peaks, gives a measure of the amount of a surface atoms *per NP*.

Figure 3 shows the coverage, obtained from SEM images analysis, versus the surface density of Cl per NPs, extracted from the peaks reported in the inset. The errors bars relative to the Cl per NPs were found as standard deviation calculated for the peak areas. It can be observed that the coverage presents are very marked dependency with the amount of Cl in the NP shell, being larger for samples with large amounts of Cl. This demonstrates that NPs with a larger amount of Cl in the organic shell are more prone to be adsorbed on the HOPG what indicates a stronger interaction between the CdSe NPs and the C-sp^2 surfaces.

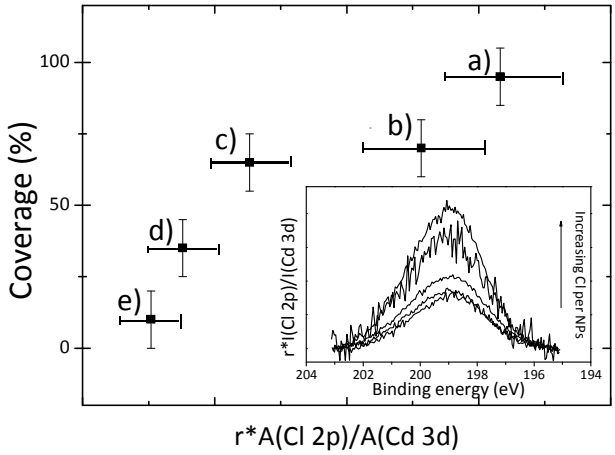

Fig 3. Coverage (in %) versus the relative quantity of Cl per NPs. The inset shows the Cl region XPS spectra of the samples normalized to the quantity of Cd and multiply to the mean radius r of the NPs for each sample. hv = 1486.61 eV and energy pass = 50 eV (Ref 1).

Comparison between a high and a low coverage sample

In order to find an explanation for the correlation between the amount of Cl and the coverage, a detailed comparison between the amount of the elements composing the organic ligands, C-sp^3, P and O per NP (see equation 1) was carried out for a high coverage (HC) and a low coverage (LC) sample (figure 1 (c) and 1 (e) respectively).

Figure 4 represents the C 1s HR spectra per NP of the samples where the grey and black lines correspond to the LC and HC respectively normalized to the Cd 3d intensity. As described above, the overall intensity of the C 1s peaks is larger for the LC sample. The spectra were deconvoluted in two components, one corresponding to C-sp^2 from the substrate and another one for the C-sp^3 from the organic compounds at the shell. The LC sample shows a higher C-sp^2 component as expected for those samples presenting larger free non-covered HOPG surface, due to the normalization to the Cd signal. It is more interesting to notice that the LC sample presents also a higher C-sp^3 component that might indicate a decrease in the ODPA-related density in the organic shell.

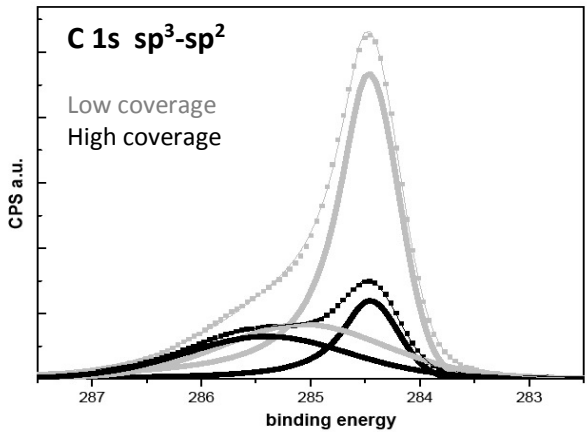

Fig 4. (a) XPS HR of C 1s region relative to low covered (grey line) and HC sample (black line). Points represent experimental data, thick lines are the components in which the spectra were deconvoluted, C-sp^2 and C-sp^3, and thin lines are the envelops. (b) C-sp^3 contributions of the samples. hv = 1486.61 eV and energy pass = 10 eV.

To attribute the different amount of C-sp^3 to the absence of ODPA related species, one needs to verify whether the amount of P and O per NP follows the same tendency as C-sp^3. The P 2p XPS peaks were extracted with the same method discussed in chapters 2 and 3 and compared. Figure 5 (a) shows XPS HR spectra of P 2p region of LC and HC samples (gray and black lines respectively) and bulk wurtzite CdSe sample (light gray line). The spectra are normalized to the highest Auger LMM peak. Being Se and Cd both core elements, normalizing to the Se or to Cd peak is equivalent. The area under the bulk CdSe spectrum is marked to better distinguish the Auger Se peak. The higher contribution of P in the LC sample is clearly visible pointing to a denser organic shell for the LC sample.

Furthermore, the same tendency of C-sp3 species and P was observed for O. In fact the intensity of O 1s per NPs for the LC samples is higher than that of the HC sample as visible in the HR spectrum shown in figure 5 (b).

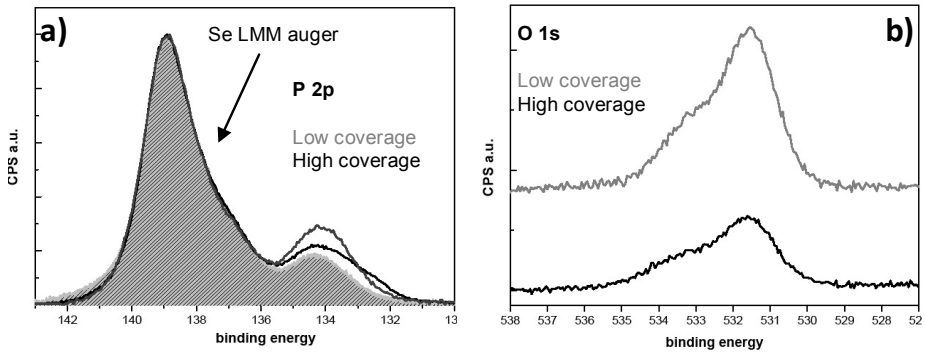

Fig 5. (a) Comparison between the P 2p region XPS HR spectra of LC (grey line) and HC samples (black line Bulk Wurtzite CdSe (light gray line) of the same region, whose area has been marked in light gray, is als depicted. (b) Comparison between the O 1s region XPS HR spectra of LC (grey line) and high covered sample (black line). hv = 1486.61 eV and energy pass = 10 eV.

The data relative to the amount of elements per NP are summarized in table 1 where the amount of Cd 3d was set to 1. P 2p areas were obtained (as in chapter 3 section 3.3.1) subtracting CdSe bulk Se LMM Auger from the NPs P 2p spectra. Concerning the data of table 1 one states that the LC sample presents

-a higher amount of C-sp^3 species, P and O per NPs, that is, a denser organic shell, hence a higher amount of organic ligands

-a lower amount of Cl, as already demonstrated above.

elements	HC		LC	
	amount per NP	error %	amount per NP	error %
C-sp^3	0,375	3,8	0,641	4,5
Cd 3d	1	0,6	1	0,8
Se 3d	0,118	6,9	0,120	7,6
O 1s	0,122	5,1	0,275	4
P 2p	0,018	15,2	0,030	12,6
Cl 2p	0,035	7,1	0,016	8

Table 1. Amount of elements per NP resulting from XPS quantification analysis.

All these results are in good agreement with the picture described in Chapter 3, according to which the incorporation of Cl into the ligand shell leads to a decrease in the amount of ODPA related species (especially ODPA anhydrides). This trend was also observed for intermediate coverages. In table 2, a comparison between the ratio

amount of Cl (per NP) / amount of P (per NP)

evaluated for similar samples presenting different coverage degrees; 88%, 56% and 48% ± 10% (same method used in section 4.1) is reported. The spectra were obtained in synchrotron facility what allows direct information about the P, the element contained exclusively in the organic shell. Notice that the use of the different experimental setup leads to differences in the intensity ratios, which cannot then be directly compared with the values previously reported in this section. From 48% to 88% the ratio Cl/P per NPs increases showing a sort of anticorrelation between organic ligands and coverage degree.

samples	Cl/P per NPs
88%	1,5
56%	1,4
48%	0,7

Table 2. Ratio between the amounts of Cl and P per NPs determined by synchrotron-based XPS experiments.

With all these ingredients, it can be now understood the role of Cl in promoting the adsorption of CdSe NPs to carbonaceous surfaces. The incorporation of Cl atoms leads to a displacement of ODPA species and may prevent the anchoring of ODPA anhydrides. Therefore, a higher amount of Cl leads to a further displacement of ligands. This situation where long alkyl-chain molecules are removed from the NPs surface favors the direct contact between the NPs and the C-sp^2 surface. Furthermore, the complete substitution of ODPA-related species at the base of the pyramids might facilitate the direct contact between the base of NPs and the C-sp^2 lattice as depicted in figure 6. This would also be in agreement with previous investigations of pyramidal CdSe NP-CNTs hybrid system by means of high-resolution transmission electron microscopy (HRTEM). While the lateral distances between adjacent NPs attached to CNTs were easily seen, no measurable distance between NPs and the CNT walls was observed (Ref 2).

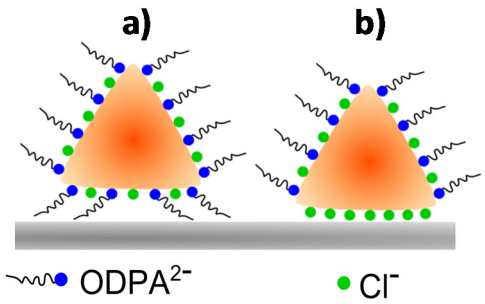

Fig 6. Scheme of NPs attachment in presence of different amounts of Cl (Ref 1).

Role of polydispersity

Notice that the Cl/P ratio for samples with 88% and 56% shown in table 2 is very close despite the quite high difference in NPs density (see table 2). This suggests that the fraction of ODPA-related species per NPs is not the only parameter that determines the coverage degree. One of these other parameters could be the polydispersity of NPs. It has been already shown that the NPs are not only adsorbed on the HOPG surface, but also they are assembled in ordered islands. Moreover, the assembly turns out to be size-selective. This is demonstrated in Figure 7 (a), which shows a SEM images of sample with bimodal distribution of NP sizes (a particular case of polydispersity). Clearly, if NPs present various size populations, they will arrange into ordered islands sorted out by the size of NPs. In this case, NPs have to find other NPs with similar sizes, what might decrease the probability that they self-assemble. Moreover, islands composed of NPs with different sizes cannot "coalesce", so that there will be a certain empty substrate left between them, thereby reducing the density of NPs on HOPG (figure 7 (b)).

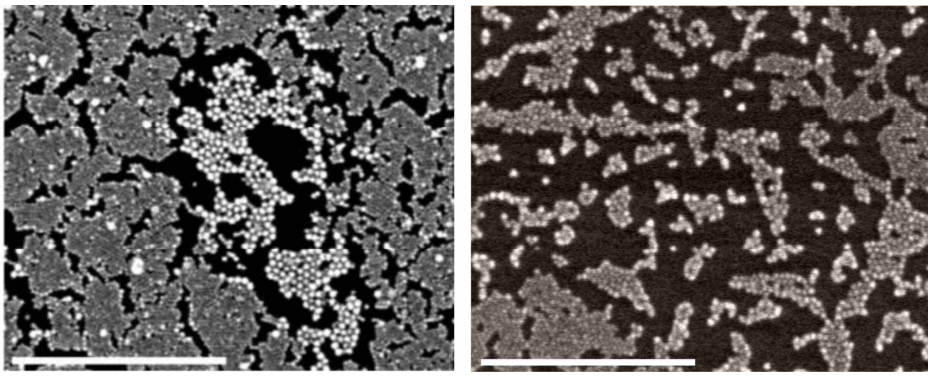

Fig 7. SEM images of two samples where islands of pyramidal CdSe NPs belonging to different populations have self-assemble on HOPG. 500 nm reference bars

Notice that the coverage of the larger NPs is not larger than that of the smaller ones, and in this particular case it is actually smaller. In general, the study of several samples of HOPG covered with NPs with very different sizes does not show a trend towards the adsorption of the larger NP size as it has been said in section 4.2.

From the results discussed in this section it can be said that, while the presence of Cl in the organic shell leads to a more effective sticking of the NPs on the HOPG surface, the size homogeneity also affects the coverage by enabling the formation of long-range ordered islands

The excess of Cl with respect to P

According to the previous discussion, one could naïvely expect that the most efficient deposition of NPs should be that in which all the ODPA derivatives are completely removed from the shell, which would then be composed only of atomic Cl. It was thus investigated the morphology of samples with large Cl/P ratios (1.9 and 2.2 respectively). The results are shown in figure 8. The SEM image reveals that, even though the coverage is still rather high, the presence of rather large crystallites (up to 150 nm in diameter) hinders the ordering and, thus, the homogeneous coverage of the sample. It thus appears that adding Cl over a certain limit does not necessarily help the process, but rather hinders it due to the formation of large aggregates and the increase in the polydispersity of the sample.

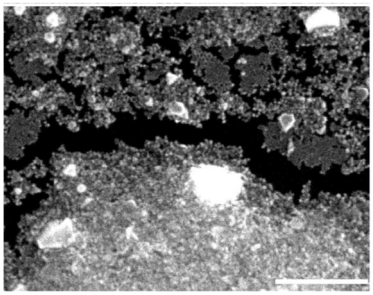

Fig 8. SEM images of samples presenting micro-sized CdSe. 300 nm reference bar.

The larger polydispersity in samples with a large Cl/P ratio can be understood through the following considerations. As it was explained in chapter 1 during the synthesis of NPs, in particular during the intra-particle ripening phase, the monomers diffuse along the surface of the NP nucleus during the process of shape stabilization. When the amount of Cl is high and the organic ODPA related species are scarce, a larger portion of the NP surface is bare CdSe, which must enhance the mobility of atomic monomers (Cd and Se) at the NP surface. If some of these atoms are allowed to separate from the main CdSe nucleus, a gradient of Cd and Se atomic concentration

between the inner and the outer diffusion sphere (see chapter 1) would be rapidly generated causing an outward atomic monomers flux. This would generate the conditions for the inter-particle or Ostwald ripening: smaller CdSe NPs, are less stable and likely release Cd and Se atoms in solution that diffuse and deposit on bigger NPs increasing the resulting polydispersity of the sample. In the case of the samples analyzed in this work, a strong inter-particle ripening occurred for those samples presenting the highest observed Cl/P ratio.

The previous discussion points to an optimum Cl/P ratio in which the NPs show the highest tendency to cover the HOPG substrate. While for low amounts of Cl the interaction between the NPs and the HOPG is weak, leading to a weak tendency for the NPs to remain adsorbed on HOPG, under Cl excess, the NPs show a high polydispersity preventing efficient self-assembly and attachment. Concluding, an overview of the quality of the samples that includes the degree of polydispersity and the density of CdSe NPs on the HOPG versus the Cl/P ratio is proposed in figure 9.

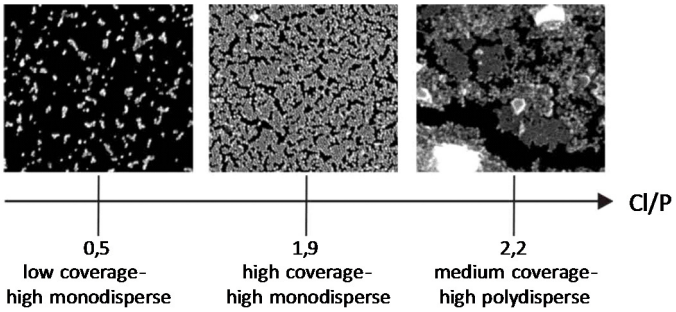

Fig 9. Overview of the quality of the samples with respect to the Cl/P ratio.

It has to be pointed out that the same tendency was found for the samples measured in synchrotron facility both in Cl/P ratio and monodispersity/coverage vs Cl/P. This confirms the reliability and reproducibility of the results.

4.3 Heating treatments; STM and XPS results

Hitherto, all the structural data has been obtained by SEM or TEM. Carrying out STM experiments would be useful as it would not necessarily require transfers from the microscopy to the spectroscopy experimental setup. Such transfers are not desirable since the sample is exposed to atmospheric conditions, thereby promoting the aging of the samples.

The aim of the experiments shown in this section was to study the previous samples by means of STM. As it will be discussed later, the samples have to be gently heated prior to any STM experiment. Complementary XPS experiments allow us to identify the effect of the annealing process as that of desorbing organic material out of the ligand shell. But heating treatments are able not only to improve the quality of the images, but also to modify the morphology of the NPs, by a process of intra-particle ripening. The modifications caused by thermal treatments were observed by means of the results obtained in synchrotron facility with the purpose of seeking a link between the change in the morphology and the change in the surface chemistry of the NPs on HOPG.

STM measurements: a brief introduction

Scanning Tunneling Microscopy (STM) is a surface technique widely used to obtain atomic-scale images of metal surfaces, molecules and in relatively recent times nano-objects (NO) like CNTs and NPs adsorbed on a metal substrate (Ref 3 and 4). A fixed bias voltage is applied between a very sharp conductive tip (nearly single atom tip) and a conductive sample. When the tip is brought sufficiently close to the sample (a few angstroms) electrons start to cross the energy barrier that separates the tip and the sample by means of the quantum effect known as tunneling. The generated tunnel current depends on the applied bias voltage and on the distance between the tip and the substrate. Hence, at a fixed bias it rapidly varies as response of the variations in the distance between the tip and the sample. In STM constant current mode (CCM) operation the tunnel current is set and kept at a constant value by means of a feedback circuit. Therefore in CCM, when the tip is scanned over the surface, vertical displacements of the tip occur in order to maintain the current at the set value. The resulting information produces an image which contrast reflects the topography of the density of electronic states of the surface atoms, which in turn is related to the morphology of the sample. During STM measurements interaction forces between the tip and the samples develop. These forces could be able to manipulate the objects deposited on the surface. For the purpose of our experiments, any manipulation of NPs from the tip had to be avoided. In fact, this interaction forces could provoke the rupture of the NPs assembly. Empirically, it was noted that a high coverage is a basic property for NPs to be measured minimizing the undesired effects of the tip-NPs interaction forces, probably thanks to the stability of NPs within the layer packing. STM experiments on pyramidal CdSe LB films were also performed, but despite the high coverage, a high level of noise seemed to be ineludible, a fact that will be discussed in further detail later on.

Since the early STM works on semiconductor NPs, the concept of the double barrier tunnel junction (DBTJ) was introduced (Ref 5) to describe the system STM tip-Nano-Object-substrate, different from the single barrier tunnel junction (SBTJ) describing

STM-tip-substrate configuration. The scheme shown in figure 10 represents a generic case (without regard to the eventual band gap of the NP) of this configuration).

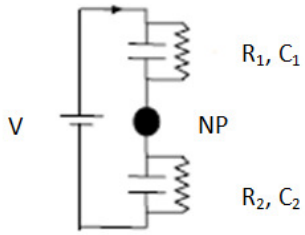

Fig 10. Schematic diagram of the DBTJ configurations.

V is the bias voltage between the tip and the substrate, R1, C1 and R2, C2 are resistance and capacitance of the first and the second barriers respectively, which in this case correspond to the tunnelling barrier from the tip across the vacuum gap and upper organic shell and into the semiconducting NP, while the second barrier corresponds to the tunnelling barrier from the NP into the HOPG substrate across the remaining shell at the interface (see figure 11). Improving the conductance through the DBTJ and therefore the STM images requires finding methods to decrease both tunnelling barriers.

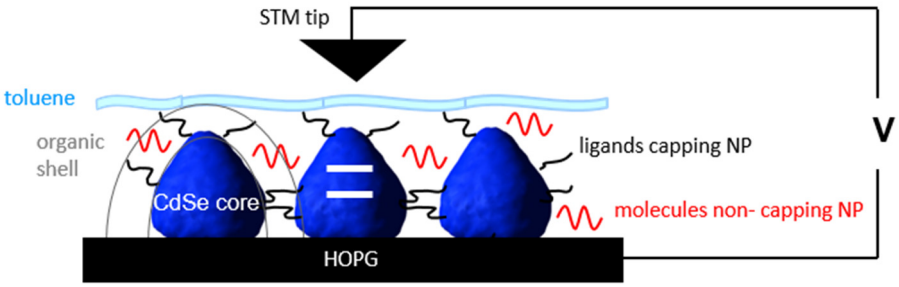

Fig 11. Scheme of CdSe pyramidal NPs pot-deposited on HOPG in a STM measurement. Toluene layer from post-synthetic treatments, HOPG substrate, NP cores and organic shell are shown. NP band gap is indicated with white lines.

As it was already discussed, the incorporation of Cl into the surface already helps in decreasing the ligands density in the organic shell. It was however helpful to treat the sample with annealing procedures which can both eliminate weakly physisorbed molecules (for relatively mild temperatures) and desorb whole ligand molecules (for higher temperatures). According to our experiments, when a sample of pyramidal CdSe NPs pot-deposited on HOPG is exposed to a series of annealing treatments at different temperatures (150°, 200°C and 400°C) the amount of C species arising from organic

materials (C-sp3) decreases with increasing annealing temperature. This was demonstrated by analyzing the XPS spectra of C 1s per NPs deconvoluted in C-sp^2 from the substrate and C-sp^3 from the organic layer as shown in figure 12.

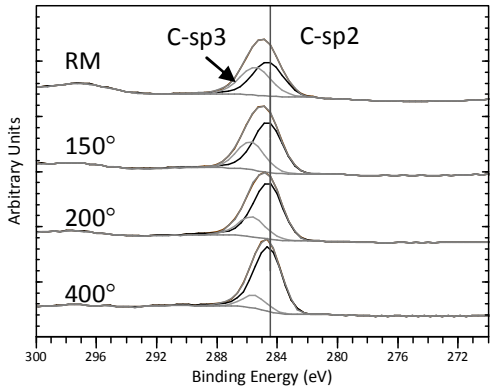

Fig 12. Reduction of C-sp^3 species from the organic layer upon annealing treatments. hv = 1486.61 eV and energy pass = 50 eV.

The lower tunneling barrier, i.e. that between the core of the NP and the HOPG surface, which is composed by the remnants of the organic ligands at the interface, is already significantly narrowed by the use of the pot-deposition method. As demonstrated in section 4.2, the NPs original ODPA-related ligands are displaced from the base of NPs by Cl atoms favoring a closer contact between NPs and HOPG. This might be the reason why high-coverage pot-deposited samples can be measured easier than LB samples despite equivalent annealings.

To conclude, the expectation of using the STM to characterize the morphology of these samples requires finding new methods to reduce the two tunnel junctions associated with the process of tunneling. While for the upper tunneling barrier the annealing procedures should decrease the thickness of the organic shell, thereby narrowing the barrier, for the lower barrier one expects that pot-deposited samples, in which the organic shell is already significantly rarified due to the action of Cl, should be already small enough so as to be negligible compared to the upper one. As it will be shown in the following section, the expectations are fulfilled and indeed STM images can be clearly obtained for pot-deposited samples annealed to at least 150°C.

STM results

All the STM experiments shown in the following were performed in CCM mode. The samples of pyramidal CdSe NPs pot-deposited on HOPG chosen for STM experiments were previously measured by means of SEM to check the quality in terms of NP

coverage and monodispersity after the synthetic process. Figure 13 (a) and (b) shows the SEM images of the two samples used for STM experiments performed at room temperature on the sample (a) and at low temperature (about 80 K) on (b). The samples present difference NP sizes (12,7 ± 1,5 nm for (a) and 10,1 nm ± 0,9 for (b)) evaluated by means of TEM analysis. The type of NP arrangement on the HOPG is similar, NP islands assembled in hexagonal close-packed arrays in both cases.

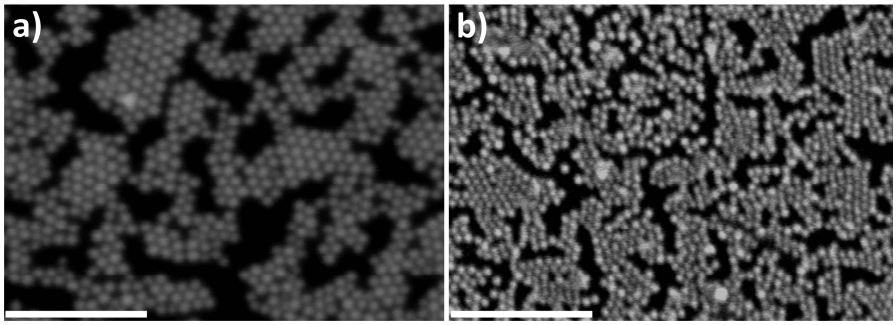

Fig 13. SEM images of the samples used for STM experiment performed at RT (a) and 80 K (b). 200 nn reference bar.

Figure 14 (a) shows a STM image taken at RT after a heating treatment at 150°C during two hours (sample (a) in figure 13). Despite the low probability of tunnel events, this image presents a very good quality. Similarly to the SEM image, the assembly of NPs into hexagonal close-packed arrays is clearly visible and darker areas corresponding to non-covered HOPG are perfectly discernible. These free HOPG areas do not present a significant amount of organic residues, as discussed in chapter 2, where it was demonstrated that the organic contribution came basically from the NP organic shell. Figure 14 (b) shows a STM image taken at about 80 K relative to the sample (b) in figure 13 after the same annealing treatment. Also in this case, the STM image reflects the same morphology of the NPs visible in the SEM image. The hexagonal close-packed arrays is appreciable, the contours of the NPs cores are even clearer visible compared to figure 14 (a). This point to the fact that the measurements performed at temperatures close to 80 K improve the quality of the STM results, probably due to the reduction of the noise provoked by the thermal disorder. Other than that no significant differences were found between the images recorded at RT and 80 K, and from now on they will used indistinctly.

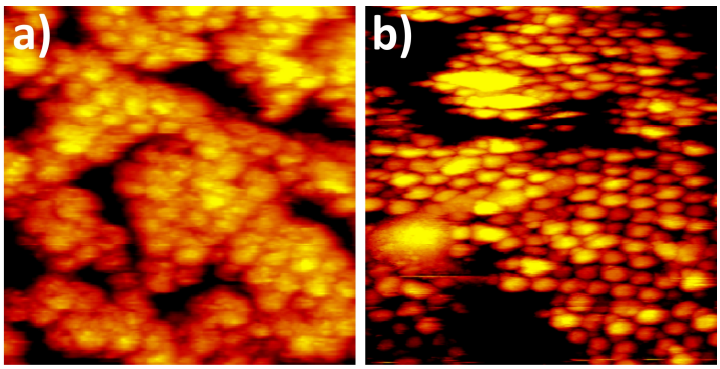

Fig 14. 200x200nm STM images of CdSe NPs on HOPG after 150°C annealing treatment. (a) RT, V = 5 .7 V, I = 1 nA. (b) 80 k, V=3.7, I=0.15 nA. (b).

Figure 15 (a) shows a STM image taken after a second annealing treatment, up to 200°C during two hours, of the sample depicted in figures 13 (b) and figure 14 (b). Notice that the hexagonal close-packed arrays on the HOPG and the NP core contours are more appreciable than those after the first annealing. In fact, the hexagonal bases of the pyramids start to be visible what proves that the STM images are reflecting the actual morphology of the NPs. This aspect has to be emphasized since in STM measurements the correspondence between the density of the electronic states and the actual morphology of the samples is not generally guaranteed, overall for such kind of objects for which the generation of the tunnel current turns out to be the result of a complex series of low probability events. The scan line shown in figure 16 (b) (grey line) gives the profile of the NP layer with respect to the substrate after the second annealing (the line scans are also indicated with green lines on the relative STM images at the right of the graphs). From the line profile the average height of the NPs can be evaluated as 11 ± 1 nm. This value is about 4 nm lower that of NPs after the first annealing, as visible from the comparison with the black line in the graph. The NPs loose about the 25% in height after the second annealing. Figure 15 (c) shows an analogous comparison regarding the shape of the NPs. The bases of the pyramids seem to be on the average slightly larger.

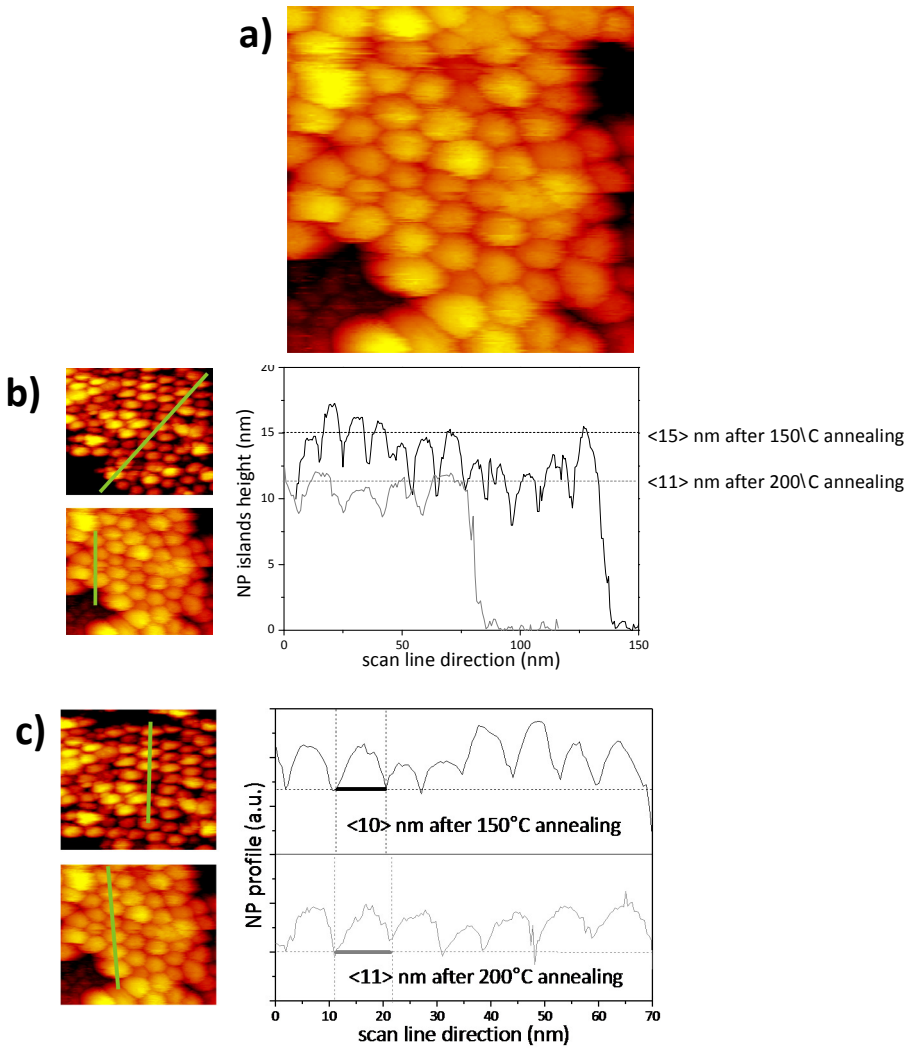

Fig 15. (a) 100x100nm STM image after 200°C annealing treatment. V = 5 eV, I = 0.3 nA. (b) Comparison between the NP islands line profiles of the same sample after 150°C and 200°C, black and grey lines respectively. (c) Analogous comparison as (b) between the NP line profiles. Line scans are indicated with a green line on the relative STM images on the right of the graphs.

Figure 16 (a) shows a STM image taken at room temperature after 400°C annealing treatment of the sample shown in Figures 13 (a) and 14 (a). The contour of NP cores is imaged more sharply, which could be related with a sharper tip. However, NP islands appear very different after such a hard annealing. From the scan lines shown in figure 16 (b) the average height of the NPs is about 7 ± 2 nm, approximately a 40% lower than that of same NPs after the first annealing as visible from the comparison with the black

line in the graph. Notice that after annealing to 400°C, the shape of the NP tops seems to be more rounded and the gap between the NPs has apparently vanished, although these two properties might also be attributed to experimental limitations (shape of the STM tip). The most important modification is related to the polydispersity of the sample. While the size of the NPs before the first annealing was rather homogeneous, after 400°C annealing the size of the NPs varies from 27 to 14 nm in diameter presenting a higher polydispersity degree. This is observable from the graph shown in figure 16 (c) where the NP profile after 150°C and 400°C annealing treatments (black line and grey line respectively) are compared. The change in the morphology of the NP islands could be related to a NP-NP mass transfer via an Ostwald ripening process on the surface.

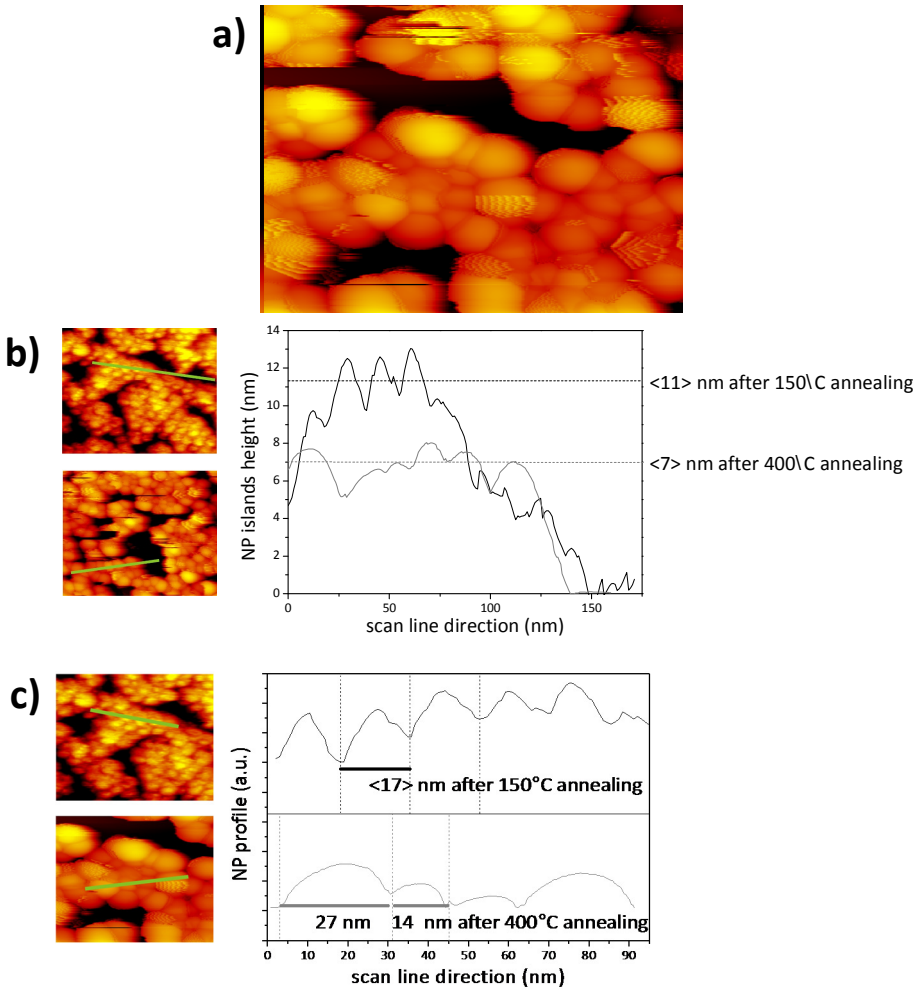

Fig 16. (a) 200x110 nm STM image after 400°C annealing treatment. RT, V = 4,1 eV, I = 1,9 nA. (b) Comparison between the NP islands line profiles of the same sample after 150°C and 400°C, black and gray line respectively. (c) Analogous comparison as (b) between the NP line profiles. Line scans are indicated with a green line on the relative STM images on the right of the graphs.

Discussion

The results of the STM experiments indicate that the NP morphology changes as consequence of thermal treatments. In particular, STM measurements taken after exposing the sample at 200°C reveal that the height of the NPs is reduced while the bases of the pyramids are slightly smaller. It seems that NPs experience a shape relaxation via an intra-particle ripening; some atoms from the top of the pyramids move toward the bases. After 400°C an increase in the polydispersity of the NPs is observed. This suggests that once the NPs are in direct contact, due to an enlargement of the bases till the NPs coalescence, a NP-NP mass transfer via inter-particle ripening (Ostwald ripening) could be activated. From the atomistic point of view, an Ostwald ripening process involves the possibility that atoms detach from the surface of the NPs, diffuse over the substrate, and get properly reattached to another NP. In this particular case, the atoms composing the CdSe cores can transfer from a NP to another directly from the bases of the pyramids. Concluding, an overview of the mass transfer process via intra-particles ripening first, and inter-particles ripening after, is illustrated in figure 17. STM images of the NPs after 150°C, 200°C and 400°C annealing treatments are shown in (a), (b) and (c) respectively, and a graphical simulation of the NP shape modification versus the temperature is depicted above the relative STM images. Notice that the hexagonal bases of the NPs is perfectly visible in (b), what points to the fact that STM measurements are reflecting the real morphology of the NPs that preserved the pyramidal shape after 200°C annealing treatment.

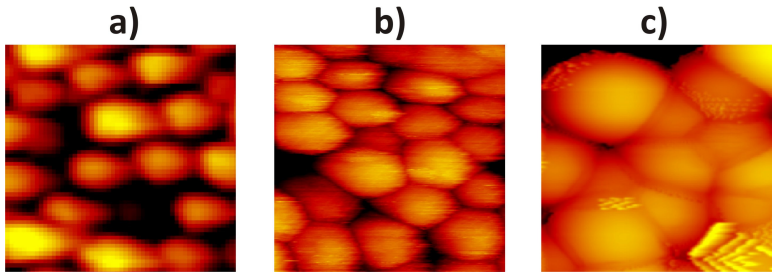

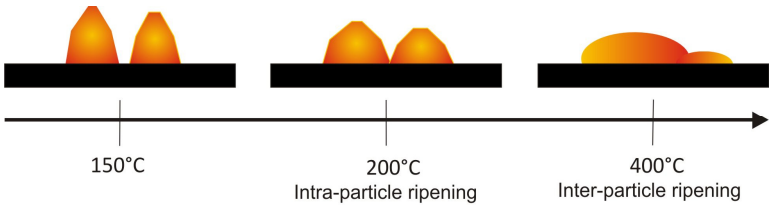

Fig 17. 50x50 nm STM images of CdSe NPs pot-deposited on HOPG after 150°C, 200°C and 400°C annealing treatments. (a) 80 k, V = 3,7 eV, I = 0,6 nA, (b) 80 k, V = 6,5 eV, I = 0,3 nA, (c) RT, ,V = 4,1 eV, I = 1,9 nA. Below each STM images, an overview of the NP shape modification versus the temperature is depicted; when the sample is heated till 200°C, an inter-particle ripening is observed. The bases of the pyramids enlarge and NPs coalesce. When the sample is heated till 400°C, a mass transfer from the bases of NPs via inter-particle ripening is activated. This causes bigger NPs grow at expenses of littler ones.

High resolution XPS annealing analysis

Several examples in literature have shown that the size distribution of epitaxial semiconductor NPs grown on semiconducting surfaces suffers severe modifications upon thermal treatments (see chapter 1). In the experiments discussed here the NPs were not grown by typical metals and semiconductors growth methods (MBE, chemical deposition) but synthesized via wet-chemistry procedures. Therefore, their surfaces are covered by the organic ligand shell. It thus appears reasonable to expect that any process of mass transport must be linked with changes in the chemical properties of the NP surfaces upon annealing treatments. To observe these changes the HR XPS spectra of the element composing the NP organic shell were analyzed.

To study the surface chemical changes related to the shape modification of the NPs subjected to thermal treatments, a similar sample of pyramidal CdSe NPs pot-deposited on HOPG was exposed to a series of annealing and the relative amount of the various surface species after each treatment were obtained. The experiments were performed in synchrotron facility allowing for a more detailed analysis of the chemical composition of the shell, especially the presence of P. The series of annealing, 80°C, 150°C, 200°C and 250°C during one hour and HR XPS measurements were performed in situ.

Figure 18 shows the C 1s HR XPS peaks normalized to the amount of Cd for the sample without any annealing treatment and after 80°C and 200°C annealing treatments. Due to the broad signals detected in these experiments, the C 1s peaks were deconvoluted in C-sp^2 from the substrate (black lines) and C-sp^3 (a) and (b) from the organic compounds (grey lines). According to ODPA XPS investigations (Ref 6 and 7) the lowest BE C-sp^3 component, C-sp3 (a), can be assigned to alkyl chains, C-H, C-C species, and the highest BE C-sp^3 component, C-sp3 (b), to C-P species. As expected, the C-sp^3 components loose intensity upon every annealing treatment. However, the most

interesting result is the behavior of the C-sp^2 from the substrate. After 80°C, the contribution from the HOPG increases; this can be explained by assuming that the C-sp^2 species are more exposed to the X-radiation upon the desorption of organic compounds physisorbed on the sample that shield the substrate. Surprisingly, however, after exposing the sample at higher temperature, the signal from the substrate decreases. This apparently strange behavior can be related to the hypothesized NP shape relaxation discussed above. In fact, a reasonable explanation for the lower contribution of photoelectrons from the HOPG is that the enlarged bases of NPs occupy a higher portion of the substrate leading to a shielding of the HOPG. Since the density of NPs attached on the HOPG does not change with annealing treatments, this would confirm what was found in STM experiments, that is, upon the exposition to certain temperature, a sort of NP shape relaxation via intra-particle ripening is activated.

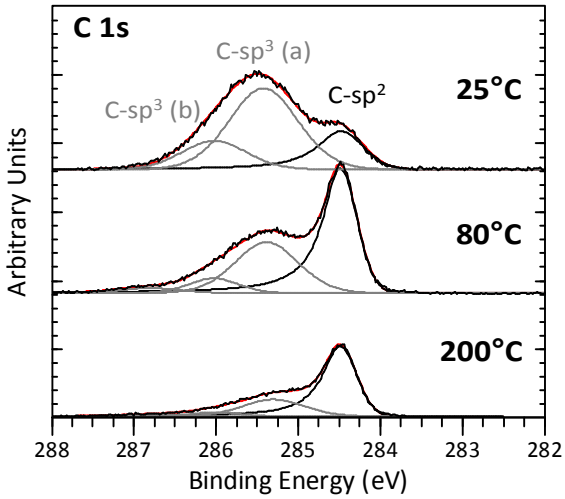

Fig 18. HR XPS of C 1s signals normalized to the amount of Cd and relative fits at RT and after exposing the sample to 80°C and 200°C. hv = 620 eV and energy pass = 20 eV.

Figure 19 shows the P 2p, Cl 2p and O 1s HR XPS peaks normalized to the amount of Cd ((a), (b), (c) respectively) at room temperature and after 80°C and 200°C annealing treatments. As it has already been shown in chapter 3, the P 2p peaks presents two components indicated as P 2p (a) and P 2p (b) (grey and black lines respectively) in figure 19 (a). The intensity of P 2p peaks decreases with the temperature, meaning that the P composing the organic shell desorbs gradually upon annealing treatments, as in the case of C-sp^3 components. In figure 19 (b) the Cl 2p peaks show a different behavior. After the first annealing (80°C) the intensity of the Cl increases. This means that the partial desorption of the organic shell lives the surface of NP cores more exposed to the

X-radiation. This increases the contribution of photoelectrons from Cl atomic-ligands. After higher temperature exposition, the Cl 2p intensity decreases meaning that the energy needed for the desorption of the Cl was than achieved. In figure 19 (c) the O 1s deconvoluted in two components, O 1s (a) and O 1s (b) (see chapter 3), shows a similar behavior of Cl 2p. After the first annealing the intensity increases, in particular that of the highest BE component, O 1s (b). Similarly to the case of Cl, these O species could be directly bound to the NP core surface, thus more exposed to the X-ray radiation after the partial desorption of the organic shell. After 200°C, the intensity decreases meaning that the energy needed for these O species to desorb was achieved.

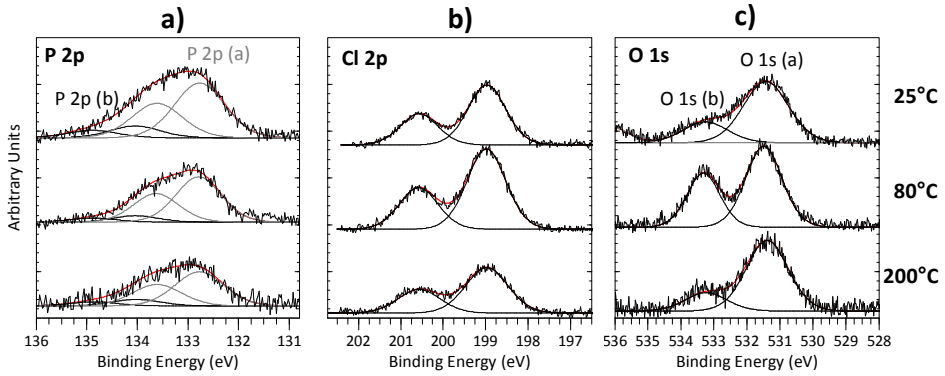

Fig 19. HR XPS of P 2p, Cl 2p and O 1s signals normalized to the amount of Cd ((a), (b) and (c) respectively) and relative fits at room temperature and after 80°C and 200°C annealing treatments. hv = 620 eV and energy pass = 20 eV.

To study the evolution of all the elements versus the temperature, the ratio between the changes in the intensity after each annealing and the total change in intensity from 80°C to 250°C was found according to the equation

$$I(T) - If \,/\, Io - If \qquad \textbf{equation 2}$$

where I(T) is the intensity (raw areas normalized to the Cd) of the peaks at the various temperatures of annealing, Io is the intensity of the peak after the 80°C annealing and If is the intensity after the final annealing at 250°C. These ratios were finally plotted versus the temperature to compare the tendency of the desorption increments relative to the total desorption for all the elements. The errors were found according to the statistical propagation of the row areas standard deviations. Figure 20 shows the plots of the desorption increments for the total C-sp3, that is, for the sum of the intensity of the C organic components (see Figure 18), O(a), C-sp2, O(b) and Cl as indicated in the plot. Despite the quite high errors, the plots clearly shows two distinct tendencies; while C-sp3 and O(a) decrease relatively slowly from 80°C to 150°C but quite strongly

from 150°C to 200°C, C-sp2, O(b) and Cl decrease more monotonically, that is, without steps, from 80Cº to 250Cº.

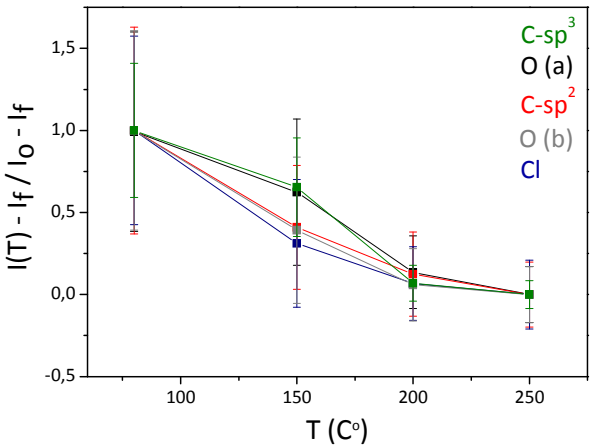

Fig 20. Desorption increments relative to the total desorption (from 80Cº to 250Cº) of ,C-sp³, O(a), C-sp², O(b) and Cl versus temperature.

As it has been already found, Cl from atomic ligands (Cl-Cd) and O (b) from deprotonated ODPA ligands (O-Cd within the possible O species) are species directly bound to the NP core surface. C-sp^2 follows a similar tendency as Cl and O (b) what suggests that the decrease in the intensity of the substrate signal is related to the desorption of the likely strongest species interacting with the NPs.

The other species that are not directly bound to the NP core surface, C-sp^3 (from alkyl chains species) and O (a) follow a different tendency meaning probably that the types of interaction are different with respect to the Cl-Cd and O-Cd bonds.

The same analysis was done for P (a) and P (b) which plots are shown in figure 21. As expected, P follows a tendency more similar to C-sp^3 and O (a) than that of O (b) and Cl reflecting, also in this case, the different types of interaction with respect to Cl-Cd and O-Cd bounds.

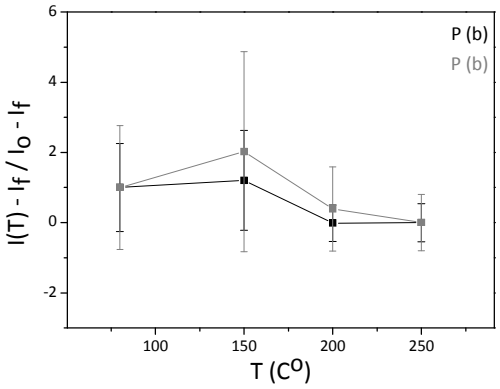

Fig 21. Desorption increments relative to the total desorption (from 80Cº to 250Cº) of ,P (a) and (b).

From all the data discussed above the following picture emerges. For low enough annealing temperatures only weakly bound species desorb, possibly organic residues from the synthesis or small molecules encapsulated in the ligand shell. This leads to a decrease in the P and C-sp^3 intensities, but all the other components become more exposed and therefore their intensities increase. From there on all the surface components become less intense with respect to the Cd 3d peak, which is explained by the desorption of ligand shell molecules. Most of the species (C-sp^3, P, O (a)) show a rather prominent decrease with the annealing to 200°C, but the two components which are attributed to tightly-bound surface species, Cl and O (b) display a more smooth behavior. This suggests a dissociative desorption process in which O atoms are being transferred to the surface, while fragments of the ODPA related species are being desorbed.

On the other hand, as it was already discussed, the evolution of the C-sp^2 intensity can be understood with the shape-relaxation processes described in the previous section. The fact that the evolution of the C-sp^2 surface follow clearly the same behaviour as Cl and O(b) indicates that it is the desorption of these species rather than the alkyl chains, what triggers the ripening processes involved in the STM observation of the previous paragraph.

Conclusions

The results shown in this chapter demonstrated that the quality of the sample of pyramidal CdSe NPs pot-deposited on HOPG in terms of NP coverage and polydispersity can be controlled by varying the amount of Cl used in the synthetic process. In fact the amount of Cl determines the displacement of the ODPA related species promoting the

adhesion of NP to the HOPG. This is further confirmed by the fact that when a certain threshold of Cl is overcome, the NPs are not enough capped during the process of growth what generates the condition for the inter-particle ripening.

A very satisfactory result achieved in this work, was to be able to measure these samples by means of STM despite the low probability of tunnel events. The possibility to observe the NP at such higher resolution allowed to observe the modification in the shape when the sample is exposed to thermal treatments. The hypothesis proposed by observing the STM results was that a relaxation of NP shape, an intra-particle ripening that makes the NP bases to enlarge at expenses of the height, takes place upon annealing treatments. Finally the analysis of the results obtained in synchrotron facility not only confirms this hypothesis by observing the decreasing of the substrate signals, but also allows to relate the intra-particle ripening to the desorption of those species directly bound to the NP core surface.

A very interesting experimental observation is that, under relatively low temperatures, the NPs get closer without losing the pyramidal shape. This property could be very useful in those applications in which a direct interaction between NPs on a substrate is required what allows for the generation a charge carriers current between NPs, e.g., in computing science, where the information carried out by the electric charges needs to be efficiently transfer.

References

1) Iacono et al, ACS nano, **7**, 2559 (2013).
2) B. Hungría et al, Nano Res., **1**, 89 (2008).
3) J. G. Hou et al, Phys. Rev. Lett., **90**, 246803 (2003).
4) T.W. Odom, J.L Huang, P. Kim, C.M. Lieber, Nature, **39**, 62 (1998).
5) D. Porath, Y. Levi, M. Tarabiah, O. Millo, Phys. Rev. B, **56**, 8929 (1997).
6) C. Viornery et al, Langmuir, **18**, 2582 (2002).
7) A.M. Puziy, O.I. Poddubnaya, A.M. Ziatdinov, Applied Surface Science, **252**,8036 (2006).

Chapter 5

General conclusions

The general conclusions of this thesis are:

1) From the synthetic point of view it has been confirmed that little variations in the amount of a chlorinated co-solvent (DCE) added during the synthesis of CdSe NPs lead to chemical and morphological changes on the NPs, modifying their shape from rod-like to pyramidal. Furthermore, if a graphitic surface is added to the synthetic mixture (such as highly oriented pyrolytic graphite (HOPG) or carbon nanotubes), once the NPs acquire the pyramidal shape they are prone to decorate graphitic surfaces in contrast to rod-like NPs, which do not show this tendency. By means of this methodology (so called pot-deposition method), ordered monolayers of CdSe NPs on HOPG can be produced.

2) Other methods to produce ordered monolayers such as Langmuir Blodgett, convective assembling and electrospray in high-vacuum conditions have been studied. Compared to the pot-deposition method these approaches produced either smaller ordered areas or leave undesired organic residues as a result of the methodology.

3) The chemical composition of the surfaces of CdSe NPs with different shapes, rod-like and pyramidal, was investigated by XPS. The results state that surfaces from both type of NPs are (partially) covered with octadecylphosphonate (ODPA) related species, namely, deprotonated ODPA and ODPA anhydride species as organic ligands (molecules bound to the NP core surfaces). The final morphology of the NPs is strongly dependent on the amount and ratio between the two types of organic ligands on the surface. If the synthetic process takes place in the absence of DCE, both deprotonated ODPA and ODPA anhydride species co-exists on the surface leading to the production of rod-like NPs. If the process takes place in the presence of the chlorinated co-solvent, Cl gets incorporated on the NP core surfaces most probably preventing the adsorption of anhydrides and leading to the production of pyramidal NPs.

4) The incorporation of Cl on the NP surface strengthens the interaction to graphitic surfaces, as demonstrated by the fact that NCs with larger amounts of Cl on their surface (determined by XPS) decorate the graphitic surfaces more efficiently than particles with a lower amount.

5) Furthermore, if a certain threshold of Cl is overcome, the resulting samples are affected by a high polydispersity as a result of severe inter-particle ripening (Ostwald ripening). Samples showing high polydispersity are not prone to distribute homogeneously on the HOPG lattices. Hence, the interaction between graphitic lattices and pyramidal CdSe NPs depends on a crucial parameter that is the amount of Cl added during the synthetic process.

6) The combined knowledge from 4) and 5) allows obtaining control over the coverage and monodispersity of CdSe NPs monolayer arrangements on graphitic surfaces.

7) The morphology of pyramidal CdSe NPs pot-deposited on HOPG was observed in detail by means of STM. The study of the NPs at such high resolution allowed to observe that upon annealing a modification in the NP shape takes place. The hypothesis proposed was that a relaxation of NP shape by means of an intra-particle ripening occurs when the sample is exposed to thermal treatments. In fact the NP bases enlarge at expenses of the height. Upon exposition to higher temperature annealing treatments NP coalesce and a NP-NP mass transfer takes place (Ostwald ripening in surface). The high resolution XPS analysis of the results obtained in a synchrotron facility on samples subjected to similar thermal treatments allowed confirming this hypothesis. Furthermore it was observed that the relaxation of the NP shape, the intra-particle ripening, is related to desorption of those species directly bound to the NP core surface.

Chapter 6

Experimental part

This chapter gives some technical information about the synthesis methods and the instruments employed.

6.1 Synthesis of nanoparticles and Hybrid System

In this work nanoparticles and hybrid systems were synthesized by means of the "hot injection method" in a Schlenk line providing N_2 or vacuum (see figure 1). The synthesis is carried out in 25 mL round bottom flasks with three necks, one connected to the line, another one connected to a thermocouple and the other one free to inject the different reactants.

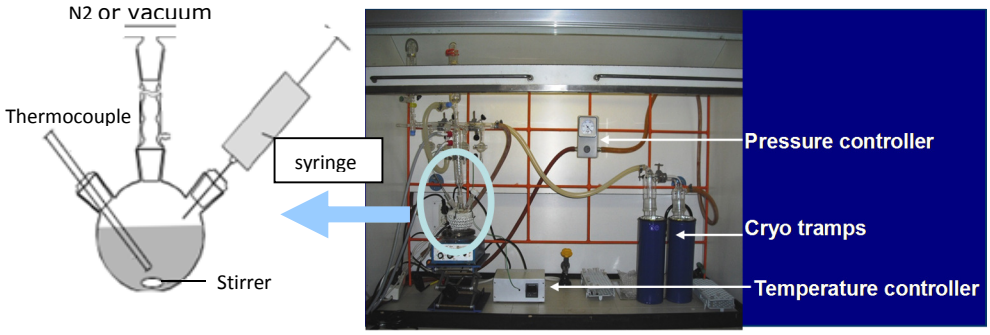

Fig. 1 Shenkle line used for hot injection synthesis La figura es mala. No se ve nada. Te mandaré una fot nueva para que la compongas. Además lo que pones del pressure controller no es tal. Eso solo es un medido Te mando la foto nueva el lunes cuando la haga en imdea.

During the synthesis the samples are kept under N_2 flow or vacuum (by means of a vacuum pump and a pressure controller), and under mechanical mixing by a stirring with a magnet. Heater mantles and thermocouples are used to set and control the temperature at any moment of the process. The cryo-tramps condense the impurities present within the line (e.g., water or solvent molecules) to avoid their presence during the reaction.

Synthesis of CdSe rod-like NPs

A mixture of 0.025g Cadmium Oxide (CdO, ChemPur), 0.14 or 0.02 g Octadecylphosphonic acid (ODPA, Alfa Aesar) and 3g of trioctylphosphine oxide (TOPO, Merck) is heated under nitrogen environment until Cd is complexed by ODPA and the solution became clear and colourless (about 270°C). 0,43 mL of a 1 M solution of selenium powder dissolved in trioctylphosphine (TOP, Sigma Aldrich)is injected at 265°C into the reaction. The temperature is quickly set to 255°C and kept for about 21 hours. The synthesis is quenched by reducing the temperature and adding 2 mL of toluene at 70°C to avoid solidification of TOPO (melting point around 50°C).

The post synthetic treatment consists on purifying the product of the synthesis by adding methanol, followed by manual shaking, and centrifuging at 14.000 rpm for three minutes. The precipitated are re-dissolve in toluene and sonicated for some minute. This process is repeated at list twice in order to get samples free from organic residues.

Synthesis of CdSe pyramidal NPs

This synthesis is the same as that of CdSe rod-like NPs except for the injection of 3 µL of dichloroethane (DCE) at 80°C after Cd complexation. The injection of DCE is performed with a Hamilton micro syringe. The procedure, including the post synthetic treatment, follows the same scheme as the synthesis of rod-like CdSe NPs.

Synthesis of pyramidal CdSe NPs attached to CNTs hybrid system (CdSe-CNTs HS)

In CdSe pyramidal NPs synthesis, before the Se@TOP injection, 3mL of sonicated CNTs dissolved in toluene are injected, whose concentration can vary according to the desired quantity of hybrid system. Upon injection under N2, the solution has to be kept under vacuum conditions (10^{-3} mbar) until the toluene evaporates. After CNTs injection the procedure follows the same steps described above.

The post synthetic treatment consists in three minutes centrifugation to generate two phases; sediment and supernatant. The sediment composed by the heaviest samples, CdSe-CNTs HS, is then re-dissolved in toluene. Several cycles of centrifugation and re-dissolution in toluene are repeated in order to obtain HS free of organic residues. The supernatant composed by CdSe pyramidal NPs is purified with the post synthetic treatment described above.

An alternative to the sedimentation of the CdSe-CNT HS by centrifugation is natural sedimentation. This method takes longer then the sedimentation with centrifugation, but the resulting HS do not present agglomerations of CNTs.

Synthesis of CdSe/ZnS colloidal nanoparticles

A mixture of 0.043 mmol of CdO (0,0056 g), 2 mmol of zinc stearate (1,2 g), 2.5 mL of oleic acid and 7.5 mL of 1-octadecne is heated till a clear solution of Cd(OA)2 and Zn(OA)2 is formed (310°C approximately). A solution of 0.2 mmol of selenium powder (0.016g) and 1,3 mmol of sulfur powder (0,044 g) both dissolved in 1 mL of TOP (Se-S@TOP) is injected into the reaction flask. After the injection, the temperature is set to 300°C. The process is quenched by cooling to room temperature and the addition of 1mL of octanothiol.

The post synthetic treatment is similar to the one described for CdSe NPs, where chloroform is used instead of toluene.

Langmuir Blodgett (LB) films

LB films were produced on a MicroTrough X-LB – multipurpose Langmuir- Blodgett from NIMA. The Hamilton glass syringe was used to spread the NPs solution on the subphase. The solution was left to evaporate before applying compression. Upon acquiring the isotherm and repetition of the procedure the sample was left to stabilize for about 2 hours before collecting the film. This was done by applying a speed of about 1 mm/min in the stepper motor. The samples were dried under vacuum.

6.2 Sample characterization

Transmission electron microscopy (TEM)

The samples presented in this work have been observed with a JEOL 1010 operating at an accelerating voltage of 100 kV belonging to the servicio interdepartamental de investigacion (SIDI) of Autonoma University of Madrid.

Scanning electron microscopy (SEM)

The instrument employed in this work is a SEM Philips XL30 connected with an analyzer EDAX DX4i with a spatial resolution of about 10 nm belonging to SIDI.

Atomic force microscopy (AFM):

AFM is a microscopy technique in which the images are formed from the interactions between a silicon or silicon nitride tip mounted on a cantilever and a sample surface. When the tip is brought into proximity of a sample surface, Van Der Waals, capillary, and electrostatic forces between the tip and the sample lead to a deflection of the cantilever which is converted into an electrical signal.

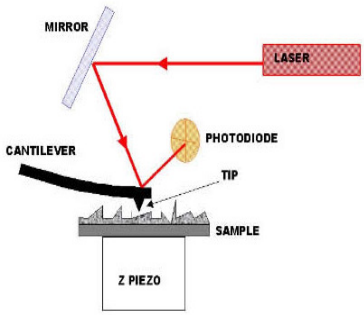

Fig. 2 Scheme of an AFM operation

When the deflection of the cantilever is used as feedback signal, the so-called "contact mode", the tip is fiscally in contact with the surface. There are also dynamic modes where the cantilever vibrates, and its oscillation is measured rather than the static deflection of the tip. These modes are usually called "tapping modes". In these dynamic modes, a set point amplitude is chosen, and the height is adjusted to match this amplitude trough the feedback system. The cantilever oscillation response changes with different interactions of the tip. It is possible to record the different cantilever vibration phases while a topography measurement is being performed. The resulting data form an image called simply "phase". It is common to interpret variations in the phase as variations in hardness of the sample, that is, the contrast in a phase image represents different materials.

The instrument used in this work is an AFM JPK Nanowizard belonging to IMDEA Nanoscience.

Ultra High Vacuum system (UHV): XPS and STM

The ultra high vacuum system (UHV) is composed by three main chambers, *preparation*, STM and XPS chambers, connected to their own independent vacuum pump systems able to maintain a pressure that normally do not overcome the range of 10^{-10} mbar. A system of valves allows connecting or isolating the chambers. A picture of the UHV system is shown in figure 3.

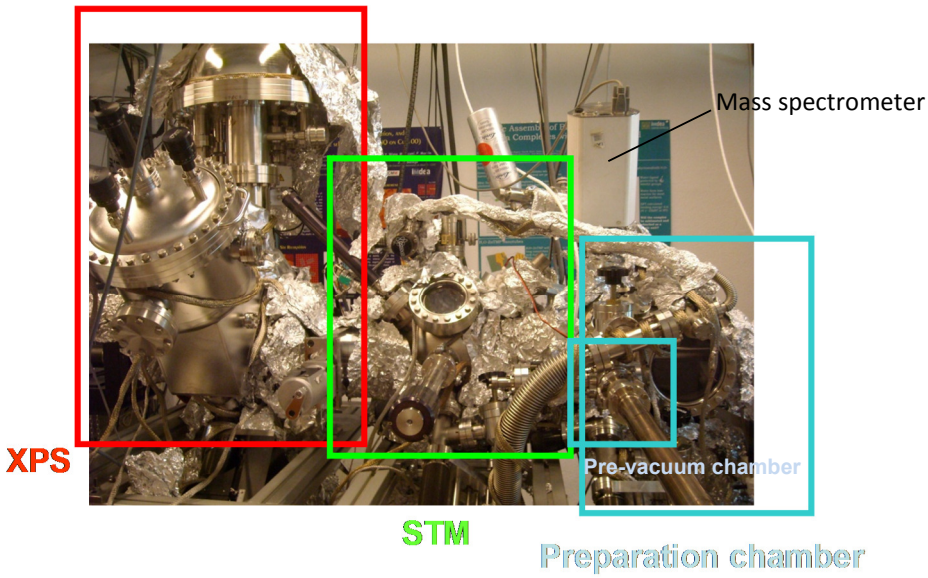

Fig 3. Picture of the UHV system employed in this work composed by preparation, STM and XPS chambers.

The samples are mounted on metallic holders (usually tantalum or tungsten) suitable to be handled by means of manipulators and transference bars manageable from the outside, so that the samples can be moved from a chamber to another one within the system. The preparation chamber, indicated with a blue square in the picture, is equipped with a littler chamber, connected to an independent vacuum pump system, the pre-vacuum chamber. The pre-vacuum and the main preparation chambers are connected (or isolated) throw a valve. In a normal procedure, the sample mounted on its holder is inserted in the pre-vacuum chamber at ambient pressure, stored until the pressure reaches a value between the range of 10^{-7} and 10^{-8} mbar and further transferred to the main preparation chamber at UHV environment. Samples cleaning procedures previous to XPS and STM measurements (if necessary), and annealing treatments. All the chambers are equipped with pressure controllers (gages) and the preparation chamber is also provided with a mass spectrometer (indicated in figure 3) to check the chemical composition of the chamber during cleaning procedures (e.g., the argon flux) and/or detect eventual leaks that can affect the maintenance of UHV environment of the all system. The preparation chamber was employed for the electrospray depositions (see chapter 2) where the HOPG substrates were placed and the flux of elements entering to the chamber to be deposited onto the substrate was checked with the mass spectrometer.

For STM measurements, the sample is moved to the STM chamber (indicated with a green square in figure 3) and placed facing inward to the microscope block as shown in

figure 4. The picture shows the interior of the STM chamber through one of the windows of the system. The STM block where the sample is placed, and the *parking* where the samples can be stored are visible in figure 4. Once the sample is placed in the microscope block, the STM tip (not visible because it is inside the block) moves toward the surface by means of a piezoelectric mechanism. The tip approaches the surface until a tunnel current between tip and sample is generated, than the surface scanning can be started.

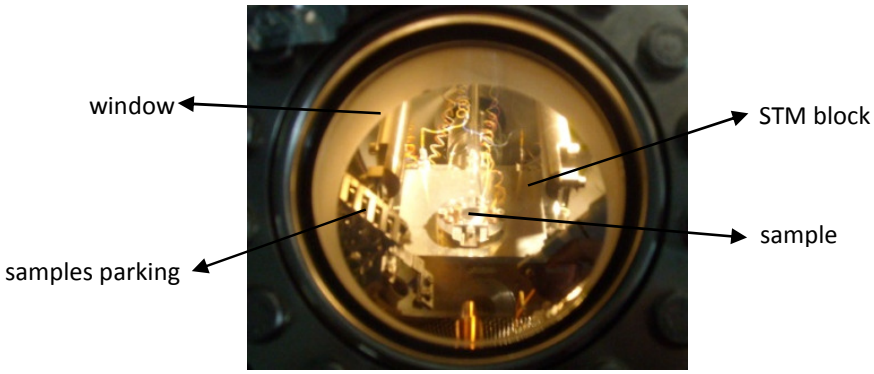

Fig 4. View of the interior of the STM chamber

The microscope is equipped with a liquid nitrogen cooling system so that STM measurements can be performed within a range between 80 K to room temperature. The software uses for STM investigation is STM image analysis version 2.0.3.1. from SPECS.

The sample can be moved to the XPS chamber (red square in figure 3) for XPS measurements. The scheme of the parts composing the XPS is shown in figure 5. The X-ray can be generated by an Al or Ag anodes placed in the X-ray source equipped with a cooling system. In the XPS experiments performed in this chamber the Al anode generating a photon energy of 1486,6 eV was used. X-rays are deflected toward a monochromator placed in another UHV chamber as shown in figure 5. The resulting radiation is then directed to the sample inside the XPS chamber. The electrons emitted from the sample are detected by an analyzer type PHIBOS 150 from SPECS.

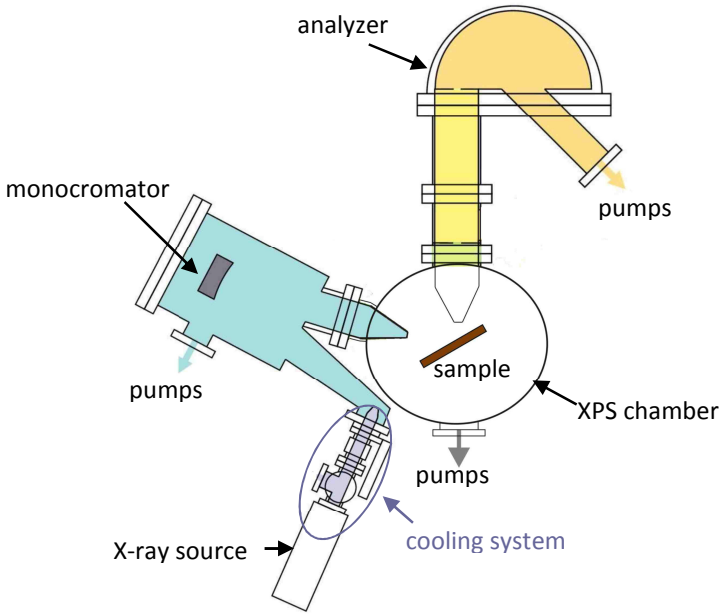

Fig 5. Scheme of the XPS components

The software used for XPS analysis is CASA XPS version 2.3 provided by SPECS.

6.3 Electrospray set-up

The electrospray is composed by several parts, as shown in figure 6. The syringe is the liquid reservoir connected to a capillary where the solution is transported to the high voltage tip, called also electrospray emitters. With the axis manipulator the high voltage tip can be micro positioned in front of the entrance capillary. Due to the effects produced by the application of a potential, generally a few KeV between the high voltage tip and the capillary entrance (indicated as Δ eV in the inset of figure 6), an electrically charged spray of the solution is generated. Capillary entrance and all the stages are grounded (the electrical connections are schematically indicated in the inset of figure 6). At atmosphere pressure (about 10^3 mbar) the spray passes throw the entrance capillary to the first stage, the space between the first and the second flange (see figure 6), where the pressure is lowered by a vacuum pump till the range of 10^2 mbar. The second flange presents a central conical aperture of 0,4 mm through which the spray passes to the second stage (between the second and the third flange), where, by means of another vacuum pump, the pressure is lowered till the range of 10^{-1} mbar. Through the conical aperture of 0,6 mm at the third flange, the spray passes to the third pumped stage where the pressure is in the range of 10^{-3} mbar. Finally the spray enters

to the preparation chamber through the exit flange, which has an axial aperture of 1mm, where the pressure is in the range of 10^{-6} mbar and deposited onto a previously lined up substrate. The preparation chamber can be isolated with a slide valve (indicated as a red circle in figure 6) and the pressure re-established at the regime value.

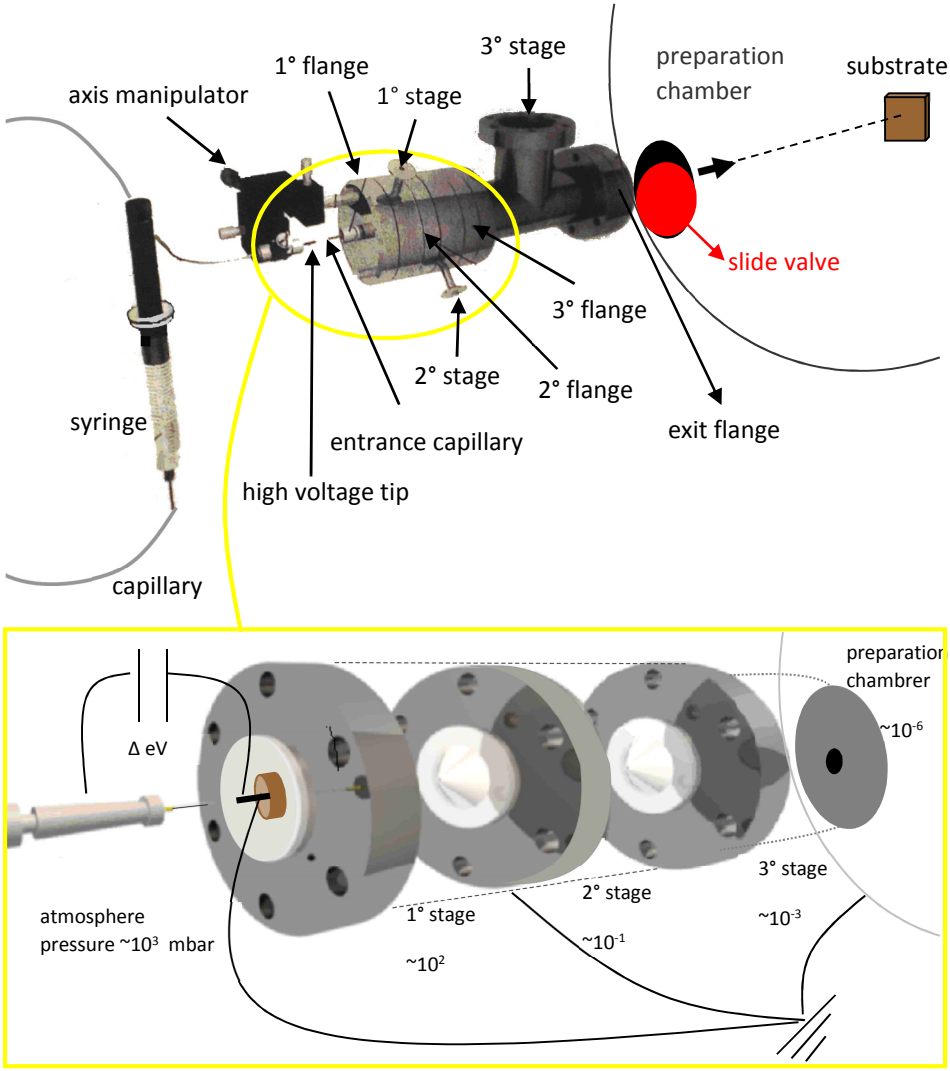

Fig 6. scheme of the electrospray set-up

The order of magnitude of the pressures reported here are relative to the first two experiments shown in chapter 2 (CdSe pyramidal and CdSe/ZnS NPs in chloroform). For the third experiment (Au NPs in water) the exit flange was removed to maximize the electrospray flux. The values of the pressures relative to this third experiment are reported in annex 3.

Electrospray allignment

To line up the instrument a window flange has to replace the first flange in order to let a fixed light beam, indicated with a red arrow in figure 7, traveling through the different stages to an empty sample holder placed in the preparation chamber. The position of the sample holder is changed until a reflection of the beam produced by the sample holder is visible through one of the different windows of the preparation chamber.

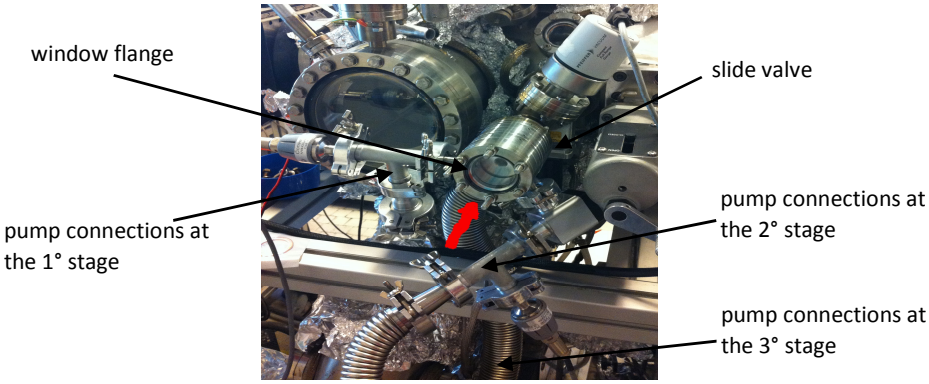

Fig 7. Electrospray set-up for the allignment

Figure 7 shows the electrospray with the window flange mounted for the allignment. The slide valve and the three pump connections at first, second and third stages are indicated in the figure. Once the position of the sample holder is found, X, Y and Z coordinates are registered and used in the experiments. The removal of the window flange and the assembly of the first flange to perform the depositions are needed and this procedure can affect the allignment of the instrument. Hence, an alternative line up was tested.

When the instrument is completely mounted, a laser fixed in front of the capillary entrance is turned on. The laser beam can be adjusted with a micro-positioning system right in the direction of the capillary entrance. The laser beam passes through the stages and joins the preparation chamber. When a light spot is visible on the centre of the

sample holder, the electrospray is lined up. Figure 8 (a) shows the capillary entrance under laser exposition (symbolically indicated with a violet arrow). The pump connections at the three stages are indicated in the figure as well as the high voltage tip holder at the already assembled micro-manipulator axis. The micro-manipulator axis is previously calibrated so that, once the instrument is lined up, the high voltage tip can be directly positioned in front of the entrance capillary, thing that is impossible to do by using the first line up method described above.

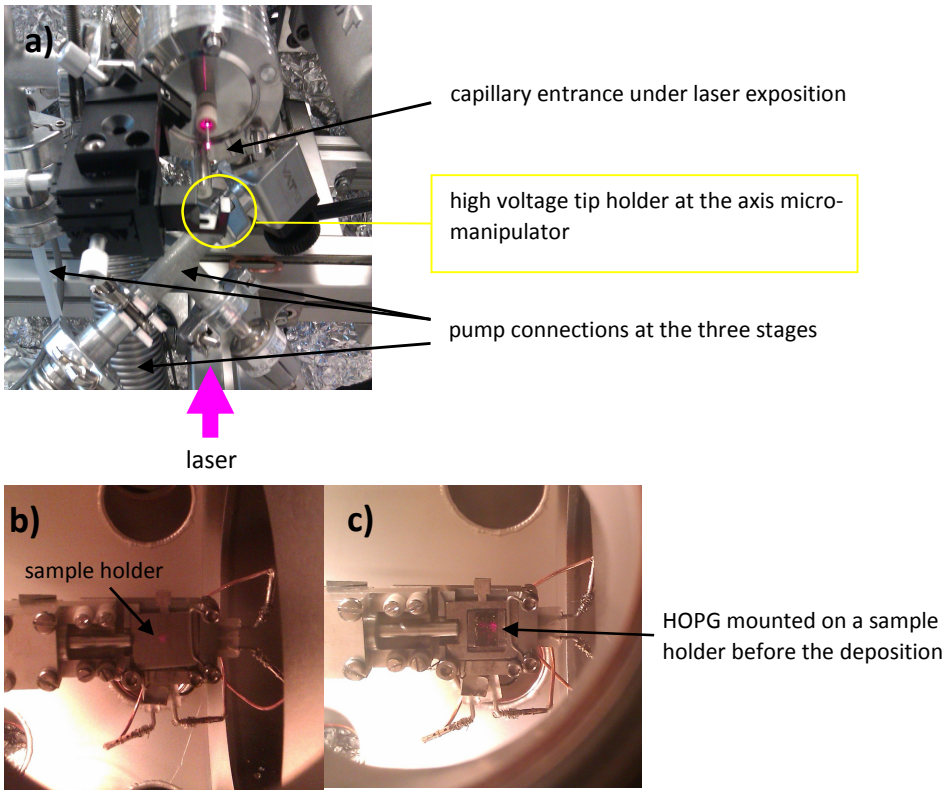

Fig 8. Allignment of the electrospray by using a laser (a). Sample holder inside the preparation chamber centred to the direction of the laser beam (b). HOPG substrate lined-up with the laser beam (c).

The electrospray is alligned the when the laser red spot is centred to the sample holder (figure 8 (b)). The laser red spot could be also identified directly on the HOPG (figure 8 (b)). In this case, the line-up could be performed just before the deposition, which involves just the assembly of the high voltage tip, connected to the liquid reservoir, on its holder. This method not only allows a high precise line up without

handling the instrument, but also does not involve the ventilation of the pumps, procedure that takes quite a lot time.

Electrospray calibration

After the allignment, the electrospray has to be calibrated. As indicated by the producer, a solution of fluorescent molecules was electrosprayed onto a SiO_2 substrate. Figure 9 shows the images of the fluorescence microscope used to characterize the sample after depositing a solution of a fluorescent molecule (DiOC18) in chloroform during 20 seconds at a set voltage of 2 KeV. The molecules were deposited proving that the set-up of the system was correct.

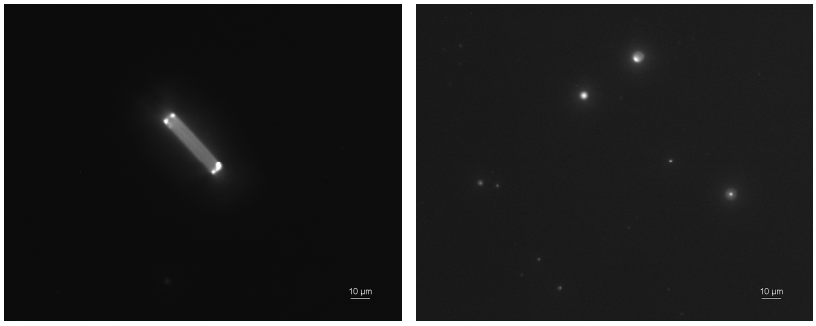

Fig. 9. Fluorescence microscope images of DiOC18 molecules deposited on SiO^2 substrate by means of electrospray for calibration.

Annexes

1 Calculation of CdSe dispersion concentration used in convective assembling

The concentration of the suspension of NPs was calculated from Lambert-Beer law $A = \varepsilon C L$, where A is the absorbance at the peak position of the first exciton peak, C is the molar concentration (mol/L) of the NP suspension, L is the path length (cm) of the suspension that the crosses (fixed at 1 cm) and ε is the extinction coefficient per mole of NP suspension (L/mol cm). The extinction coefficient ε for CdSe NPs has been tabulated in the literature, such as the ones for CdS, CdTe NPs (see chapter 2, Ref 7). These values have been obtained empirically for colloidal CdSe NPs up to 8.5 nm in diameter. The figure shows the UV-Vis spectrum from which absorbance at the first exciton peak position (670 nm) was extracted.

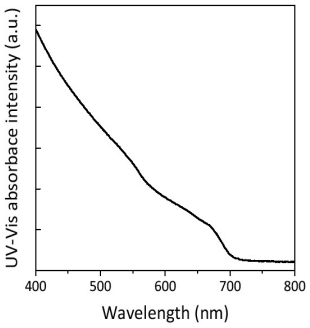

Fig 1. Absorbance spectrum of the suspension of pyramid CdSe NPs in toluene used in convective assembly depositio The wavelength of the first exciton absorption peak is 67 nm.

Approximating pyramidal to spherical NP shape, the concentration of the suspension was estimated to be 320 µmol/L. This concentration was used for the second experiment and smaller concentrations were done by dilution. The Absorbance spectrum was recorded with Variant Cary 60 spectrophotometer belonging to Imdea Nanoscience.

2 Comparison between convective assembling of CdSe NPs using different dispersion concentrations

Figure 1 shows the pictures of HOPG dipped in the three dispersion of CdSe NPs with concentrations 320 µmol/L (a), 32 µmol/L (b) and 3,2 µmol/L (c) at the beginning of convective assembly deposition.

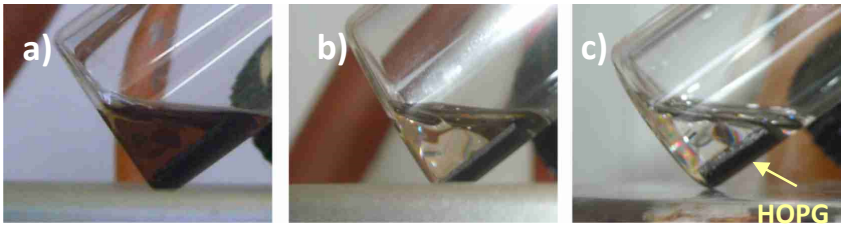

Fig 1 (a) Pictures of HOPG substrates dipped in a suspension of 320 µmol/L (a), 32 µmol/L (b) and 3.2 µmol/L (b) of pyramidal CdSe NPs. The deposition angle was 35° for the three experiments. The vials were kept at atmosphere pressure and at room temperature for one day.

Figure 2 shows SEM images of the obtained NPs films. The coverage decreases by increasing the suspension concentration. In figures 2(a) and 2(b) the direction of the solvent evaporation is visible and indicated as a blue arrow.

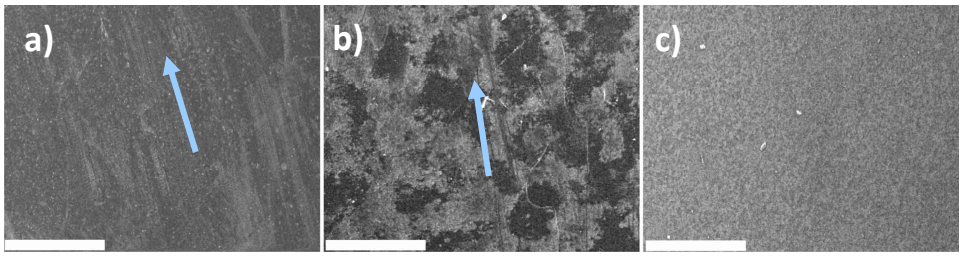

Fig 2. SEM images of convective assembling films generated by the evaporation of suspension of 320 µmol/L (a), 32 µmol/L (b) and 3,2 µmol/L of pyramidal CdSe NPs (c). 500 µm reference bar.

3 Electrospray experiment details

Pyramid CdSe NPs in chloroform

The optimized configuration leading to a drop-jet electrospray operating regime includes the following values:

Vc = 2,7 kV

distance d about 10 mm

syringe rate compression = 1 mL per hour.

These three parameters were kept during the deposition process. However, pressure fluctuations from 4·10-6mbar to 8·10-6mbar usually occurred, forcing the interruption of the experiment because of capillary entrance obstructions. The values of the pressures are summarized in table 1. The preparation chamber pressure corresponds to an average value.

Pressure (mbar)	
1 Stage	$7{,}6 \cdot 10^{2}$
2 Stage	$1{,}2 \cdot 10^{-1}$
3 Stage	$9{,}0 \cdot 10^{-3}$
preparation chamber	$< 6\ 10^{-6} >$

Table 1. Pressure values

CdSe/ZnS NPs dispersed in chloroform

The preparation chamber pressure did not overcome the values of $3.5 \cdot 10^{-6}$ mbar. The flux, whose intensity can be qualitatively evaluated by checking the intensity of chloroform related peaks, was lower than that generated in the deposition of CdSe pyramidal NPs in chloroform, what may be related to a denser capping ligand shell of CdSe/ZnS NPs. The optimized parameters leading to a drop-jet operation regime are:

Vc = 2,12 kV

distance d about 7-10 mm

syringe rate compression = 1 mL per hour

The values of first, second and third stage pressure before starting the deposition were basically the same as the ones shown in table 1, while preparation chamber pressure average during the deposition was $3{,}3 \cdot 10^{-6}$ mbar, lower than the first experiment.

Deposition of Au NPs dispersed in water

For this experiment the set up was changed: the last flange with an aperture of 1 mm that leads to the main chamber (see figure 19) was removed. Hence, the preparation chamber pressure was higher than in the other experiments. The allignment of the electrospray was optimized with the use of a laser (see chapter 5). The goal was to increase the amount of electrospray flux toward the center of the substrate. Two electrospray operating regimes, drops-jet and cone-jet, have been tasted.

Drops-jet operating regime

The favorable empirical parameters configuration for this type of deposition ended up being:

The optimized parameters leading to a drop-jet operation regime are in this case are:

Vc = 2,4 kV

distance d about 10 mm

syringe rate compression = 0.6 mL per hour

The three parameters were kept during the deposition. In total, about 0,7 mL of Au NPs (3. 10^{12} NPs/mL) in water were deposited in the reported experiment. The values of the pressure are summarized in table 2 where the preparation chamber pressure corresponds to an average value.

Pressure mbar	
1 Stage	$1{,}3 \cdot 10^{1}$
2 Stage	$3{,}8 \cdot 10^{-2}$
3 Stage	$3{,}1 \cdot 10^{-4}$
preparation chamber	$< 3 \cdot 10^{-5} >$

Table 2. Pressure values

Spray-jet operating regime

To establish the spray-jet operating regime the parameters were changed and set as summarized below;

Vc = 2,85 kV

distance d about 5 mm

syringe rate compression = 4 mL per hour.

Pressure values for the first, second and third stages were basically the same as the ones indicated in table 2, while the preparation chamber pressure was in average

$2{,}7 \cdot 10^{-5}$mbar, lower than in the case of drop-jet regime. In total, 5 mL of Au NPs ($3. 10^{12}$ NPs/mL) in water were deposited.

List of publication

Fabiola Iacono, Cristina Palencia, Leonor de la Cueva, Michaela Meyns, Luigi Terracciano, Antje Vollmer, María José de la Mata, Christian Klinke, José M. Gallego, Beatriz H. Juárez, and Roberto Otero , Interfacing Quantum Dots and Graphitic Surfaces with Cl Atomic Ligands, ACS Nano 7, 2559 (2013)

Michaela Meyns, Fabiola Iacono, Cristina Palencia, Jan Geweke, Roberto Otero, José M. Gallego, Beatriz H. Juárez, Christian Klinke, Kinetic shape control of CdSe nanoparticles by means of halogenated compounds, ACS Nano, submitted.

Fabiola Iacono, José María Gallego, Antje Vollmer, Beatriz H. Juárez and Roberto Otero, Triggering Ostwald Ripening Processes for CdSe Quantum Dots Deposited on HOPG by controlled Ligand Desorption in Vacuum, in preparation.

Acknowledgment

A number of people have contributed, in different ways, to the realization of this thesis, and my sincere gratitude goes to them.

I want to thank Beatriz and Roberto, for given me the opportunity to do many experiences and learn all I needed to carry out this work. Santi and Leonor, for their help in observing and producing many of the samples shown in this thesis.

I would like to thank Massimo Palma, for his example of serious and honest guidance in scientific issues.

My gratitude also goes to my good friends Cecilia, Belen, Jose and Tere, for their great support and the funniest moments spent in this amazing city.

Thanks to Rita, Giovanni and Ester, for being always on my side.

Thanks a lot, guys.